

Recent progress with observations and models to characterize the magnetic fields from star-forming cores to protostellar disks

Anaëlle Maury^{1,2,*}, Patrick Hennebelle¹ and Josep Miquel Girart^{3,4}

¹CEA/DRF/IRFU Astrophysics department, Paris-Saclay University, UMR AIM, Gif-sur-Yvette, France

²Harvard-Smithsonian Center for Astrophysics, Cambridge, USA

³Institut de Ciències de l'Espai (ICE), CSIC, Can Magrans s/n, E-08193 Cerdanyola del Vallès, Catalonia, Spain

⁴Institut d'Estudis Espacials de Catalunya (IEEC), E-08034 Barcelona, Catalonia, Spain

Correspondence*:

CEA/DRF/IRFU/DAP, Orme des Merisiers batiment 709, 91191 Gif-sur-Yvette, France

anaelle.maury@cea.fr

ABSTRACT

In this review paper, we aim at providing a global outlook on the progresses made in the recent years to characterize the role of magnetic fields during the embedded phases of the star formation process. Thanks to the development of observational capabilities and the parallel progress in numerical models capturing most of the important physics at work during star formation, it has recently become possible to confront detailed predictions of magnetized models to observational properties of the youngest protostars. We provide an overview of the most important consequences when adding magnetic fields to state-of-the-art models of protostellar formation, emphasizing their role to shape the resulting star(s) and their disk(s). We discuss the importance of magnetic field coupling to set the efficiency of magnetic processes, and provide a review of observational works putting constraints on the two main agents responsible for the coupling in star-forming cores: dust grains and ionized gas. We recall the physical processes and observational methods allowing to trace the magnetic field topology and its intensity in embedded protostars, and review the main steps, success and limitations in comparing real observations to synthetic observations

from the non-ideal MHD models. Finally, we discuss the main threads of observational evidence that suggest a key role of magnetic fields for star and disk formation, and propose a scenario solving the angular momentum for star formation, also highlighting the remaining tensions that exist between models and observations.

Keywords: Star formation, magnetic fields, protostars, MHD modeling, polarization

1 INTRODUCTION

The formation of stars takes place in filamentary molecular clouds, when the high-density interstellar medium partly collapses and fragments into bound starless dense cores. Depending on their properties, such cores can undergo further collapse to form a protostar that will accrete its circumstellar material (evolving through the Class 0, I, II and later stages) until reaching the main sequence. Class 0 protostars are the first (proto)stellar objects, observed only $t \lesssim 5 \times 10^4$ yr (André et al., 1993, 2000; Evans et al., 2009; Maury et al., 2011) after their formation, while most of their mass is still in the form of a dense core/envelope collapsing onto the central protostellar embryo. Embedded Class 0 and Class I

protostars are also accreting objects, as most of the final stellar mass is assembled during those short phases. During this accretion phase, the circumstellar gas must redistribute most of its initial angular momentum outward or else centrifugal forces will soon balance gravity and prevent inflow, accretion, and the growth of the star. This long-standing “angular momentum problem” was estimated to be quite severe (Bodenheimer, 1995). Comparing observations of the specific angular momentum J/M in star-forming clouds prior to contraction ($J/M \sim 10^{21} \text{ cm}^2 \text{ s}^{-1}$, Goodman et al. 1993) to the angular momentum contained in a typical solar-type star ($J/M \sim 10^{15} \text{ cm}^2 \text{ s}^{-1}$) indicates that, during the brief accretion phase, the gas must transfer all but 1 millionth of its initial angular momentum out of the accretion flow (Belloche, 2013). Exactly how the circumstellar mass contained in a star-forming core is transferred to the forming star, but not its associated angular momentum, has been an active field of research in modern astronomy.

Wherever we have the means of observing them, magnetic fields are detected on nearly all scales and across the full spectrum of astrophysical environments: from our own Earth (Russell, 1991) to stars (Donati and Landstreet, 2009), the Milky Way (Wielebinski, 2005) and cosmological structures (Kunze, 2013). As regards star-formation processes, magnetic fields provide a mechanism for launching and collimating outflows winds and jets (Blandford and Payne, 1982), which are routinely observed around young stellar objects (YSOs), and magnetic fields of typical strengths 10–100 μG are threading nearly all star-forming clouds (Crutcher, 2012). Therefore, it is now widely accepted that most star-forming cores are magnetized to some level. However, it is only recently that the role of these magnetic fields could be investigated in details.

Indeed, in the past decade, numerical models of star formation have been gradually including most of the physical ingredients for a detailed description of protostellar evolution in the presence of magnetic fields, such as resistive MHD, radiative transfer

and chemical networks, at all the relevant scales. Moreover, observational capabilities resolving the internal environment of star-forming cores, e.g., interferometry at (sub)millimeter wavelengths, have started to produce detailed maps of the gas and dust properties at the very small scales of protostellar cores, where material is accreted into a stellar embryo, stored in a disk, and ejected under the form of outflows and jets. The massive development of polarization capabilities on telescopes probing the cold Universe, such as on the SubMillimeter Array (SMA), then on the Atacama Large Millimeter Array (ALMA), and now also developed at the IRAM Northern Extended Millimeter Array (NOEMA), have produced sensitive observations of magnetic fields in protostellar cores with a great level of detail. These are used as tools to put unprecedented constraints on magnetic features the star-formation models should be able to reproduce (e.g. Hull and Zhang, 2019).

Hence, the simultaneous major improvements of instrumental and computational facilities have opened an era of detailed confrontation between observed protostellar properties and magnetized models predictions. Testing the detailed interplay of physics at work has allowed a major leap forward in our understanding of star and disk formation processes, and provide a new detailed scenario to describe the early stages of the formation of stars and their planetary systems. In this review, we present a synthetic description of the progresses made in the past decade regarding the properties and roles of magnetic fields in shaping young protostars, their envelopes, disks, and resulting stellar systems.

2 HOW MAGNETIC FIELD INFLUENCES GRAVITATIONAL COLLAPSE: A THEORETICAL OVERVIEW

This section is devoted to a review of the fundamental MHD processes relevant in the context of dense core collapse and disk formation.

2.1 The fluid equations

The fluid equations are as follows. ρ , P , \mathbf{v} , \mathbf{B} , and Φ_g are, respectively, gas density, pressure, velocity, magnetic field, and gravitational potential, while η_O , η_H , and η_{AD} are the Ohmic, Hall and ambipolar diffusivities.

$$\frac{\partial \rho}{\partial t} + \nabla \cdot (\rho \mathbf{v}) = 0, \quad (1)$$

is the continuity equation which describes matter conservation.

$$\begin{aligned} & \rho \left(\frac{\partial \mathbf{v}}{\partial t} + (\mathbf{v} \cdot \nabla) \mathbf{v} \right) \quad (2) \\ &= -\nabla P + \frac{1}{4\pi} (\nabla \times \mathbf{B}) \times \mathbf{B} - \rho \nabla \Phi_g \\ &= -\nabla \left(P + \frac{B^2}{8\pi} \right) + \frac{1}{4\pi} \mathbf{B} \cdot \nabla \mathbf{B} - \rho \nabla \Phi_g, \end{aligned}$$

represents the momentum conservation. We see in particular that the Lorentz force can be written as a magnetic pressure and a magnetic tension.

$$\begin{aligned} & \frac{\partial \mathbf{B}}{\partial t} = \nabla \times (\mathbf{v} \times \mathbf{B}) - \frac{c^2}{4\pi} \nabla \quad (3) \\ & \times \left\{ \eta_O \nabla \times \mathbf{B} + \eta_H (\nabla \times \mathbf{B}) \times \frac{\mathbf{B}}{B} \right. \\ & \left. + \eta_{AD} \frac{\mathbf{B}}{B} \times \left[(\nabla \times \mathbf{B}) \times \frac{\mathbf{B}}{B} \right] \right\}, \end{aligned}$$

is the Maxwell-Faraday equation. The three non-ideal MHD terms, namely the Ohm, Hall and ambipolar diffusion contributions are accounted for.

While this set of equations is complete (after the inclusion of an energy conservation equation, and an equation of state), it is nevertheless enlightening to also discuss the equation describing the conservation of angular momentum. It is obtained by combining the azimuthal component of the momentum equation with the continuity equation (see for instance Joos et al., 2012). The

equation of conservation of angular momentum is

$$\begin{aligned} & \partial_t (\rho r v_\phi) + \nabla \cdot r \left[\rho v_\phi \mathbf{v} \quad (4) \right. \\ & \left. + \left(P + \frac{B^2}{8\pi} - \frac{g^2}{8\pi G} \right) \mathbf{e}_\phi - \frac{B_\phi}{4\pi} \mathbf{B} + \frac{g_\phi}{4\pi G} \mathbf{g} \right] = 0, \end{aligned}$$

This equation reveals the existence of two torques able to transport the angular momentum, namely $-r B_\phi \mathbf{B} / 4\pi$, the magnetic torque and $r g_\phi \mathbf{g} / (4\pi G)$, the gravitational torque. These two torques are playing a fundamental role during the collapse regarding the issue of angular momentum evolution. They have a similar expression, and in particular both require a toroidal and a poloidal fields. However, there is an important difference between the two because a toroidal magnetic field, B_ϕ , can be produced in an axi-symmetric cloud, once the cloud is in rotation. On the contrary, a toroidal gravitational field, requires a non-axisymmetric density distribution such as a spiral wave.

2.2 Magnetic support and magnetic compression: the pseudo-disk

The simplest effect magnetic field has on a cloud is through magnetic pressure, which provides a support against gravity. Assuming field freezing within a cloud of radius R , threaded by magnetic field, B , we have that $\phi = \pi R^2 B$, the magnetic flux, is conserved during collapse. It is easy to calculate the ratio of magnetic over gravitational energy

$$\frac{E_{\text{mag}}}{E_{\text{grav}}} \propto \frac{R^3 B^2}{GM^2/R} \propto \frac{1}{G} \left(\frac{\phi}{M} \right)^2. \quad (5)$$

Equation 5 shows that the energy ratio stays constant, as long as spherical symmetry is maintained and that it is proportional to ϕ/M , i.e. the ratio of the magnetic flux over the cloud mass. Obviously there is a critical value for $(M/\phi)_{\text{cri}}$ above which magnetic field is strong enough to prevent gravitational collapse. The latter is expected to be such as $(M/\phi)_{\text{cri}} \propto 1/\sqrt{G}$. A calibration has been performed by Mouschovias and Spitzer (1976)

using exact equilibrium and, it has been inferred that

$$\left(\frac{M}{\phi}\right)_{crit} = \frac{1}{\sqrt{G}} \frac{c_1 \sqrt{5}}{3\pi}, \quad (6)$$

where $c_1 \simeq 0.51$. It is then common to define μ , the mass-to-flux over critical mass-to-flux ratio. A value of $\mu = 1$ indicates that magnetic field and gravity compensate while a value of μ larger than 1, implies that magnetic field cannot prevent collapse to occur. Another commonly used closely related parameter has traditionally been called λ and uses the column density and magnetic field,

$$\lambda = 2\pi G^{1/2} \frac{\Sigma}{B}. \quad (7)$$

Due to the anisotropic nature of the magnetic field, and in particular to the fact that the Lorentz force vanishes along the field lines, a magnetized cloud does not collapse spherically but typically get flatten along the field lines. It should be stressed however that as the collapse proceeds, the field lines get strongly pinched by the differential motions, forming an hour glass shape. This has two consequences. First, it creates a magnetic pressure force, $-\partial_r(B_z^2)/8\pi$, parallel to the equatorial plane and pointing outwards. This typically slows down the collapse when magnetic field is strong enough. Second, it creates another component of the magnetic force, which is oriented along the z-axis and is equal to $-\partial_z(B_r^2)/8\pi$. However, for symmetry reasons, B_r is usually vanishing in the equatorial plane. Therefore, this force is pointing toward the mid-plane and is compressing the gas. Compared to the hydrodynamical collapse, for which the singular isothermal, $\rho = c_s^2/(2\pi Gr^2)$ is usually an acceptable approximation, particularly for low mass cores, this creates close to the equatorial plane, a density enhancement which can be as high as a factor of several. Because of its shape, this thin layer is usually called a pseudo-disk. Exact solutions of this equilibrium, called the magnetized isothermal toroids, have been obtained by Li and Shu (1996), while an

approximation of the density enhancement and the dense layer thickness is presented in Hennebelle and Fromang (2008). It should be stressed that like for the singular isothermal sphere, the resulting equilibrium is unstable to collapse and thus, unless the core is magnetically dominated, the pseudo-disk collapses. Indeed, the pseudo-disk, unlike a centrifugally supported disk, is not a structure which is at mechanical equilibrium. It is essentially a collapsing envelope that has been flattened by the magnetic field effect.

It is worth stressing that the aligned configuration, i.e., magnetic field and rotation being initially parallel, which has generally been assumed in most early calculations, is somehow peculiar because in this configuration only the z-component of the field is not zero in the equatorial plane and therefore the magnetic pressure is squeezing the gas along the z-axis. If magnetic field and rotation are initially misaligned, the magnetic field lines get twisted by rotation and the radial field does not vanish anymore in the equatorial plane. This has as effect to somehow thicken the pseudo-disk (Hennebelle and Ciardi, 2009; Hirano et al., 2020).

2.3 Magnetic Braking

The magnetic braking acts through the magnetic torque $-rB_\phi\mathbf{B}$. Since it is a local quantity, it is not straightforward to anticipate its role, and it is enlightening to investigate some of its key properties thanks to simple cases, as proposed by Mouschovias and Paleologou (1980) and more recently by Joos et al. (2012) and Hirano et al. (2020).

2.3.1 Aligned rotator

Let us first consider a cloud of mass M , density ρ_c , radius R_c , and half-height Z , surrounded by an external medium of density ρ_{ext} . The cloud is initially in rotation at a speed, Ω , and for simplicity the magnetic field \mathbf{B} is considered uniform and parallel to the rotation axis. The magnetic braking timescale, $\tau_{||}$, is estimated as the time needed for a torsional Alfvén wave to transfer the initial angular momentum of the cloud to the external medium

(Mouschovias, 1979):

$$\rho_{\text{ext}} v_{\text{A,ext}} \tau_{\parallel} \sim \rho_c Z. \quad (8)$$

The Alfvén speed in the external medium is given by $v_{\text{A,ext}} = B/\sqrt{4\pi\rho_{\text{ext}}}$, the mass of the core is $M \sim 2\pi\rho_c R_c^2 Z$, while the magnetic flux is $\Phi_B \sim \pi R_c^2 B$. This leads to

$$\tau_{\parallel} \sim \left(\frac{\pi}{\rho_{\text{ext}}}\right)^{1/2} \frac{M}{\Phi_B}. \quad (9)$$

Therefore the magnetic braking timescale depends on the cloud environment through the density of the external medium, ρ_{ext} . This emphasizes that magnetic braking represents a transfer of angular momentum between a faster rotating cloud and a slowly rotating surrounding medium.

However, as discussed above, in a collapsing cloud, the magnetic field lines are strongly bent and therefore in Eq. (8), one should take into account that as the Alfvén waves propagate away from the clouds, the field lines are fanning out. Moreover, at equilibrium the field lines are likely in corotation, otherwise, the field toroidal component will be further growing. This leads to modify Eq. (8) as

$$\Omega R_0^2 \pi R_0^2 \rho_{\text{ext}} v_{\text{A,ext}} \tau_{\parallel,fo} \sim \Omega R_c^2 \pi R_c^2 \rho_c Z, \quad (10)$$

where R_0 is the typical distance between the field lines and the rotation axis, in the external medium. We thus obtain the magnetic braking time for the case of fan-out, $\tau_{\parallel,fo}$, which is given by

$$\tau_{\parallel,fo} = \frac{\rho_c}{\rho_{\text{ext}}} \frac{Z}{v_{\text{A,ext}}} \left(\frac{R_c}{R_0}\right)^4. \quad (11)$$

It is similar to Eq. (8), apart from the term $(R_c/R_0)^4$, whose origin is twofold. First, because the field lines fan-out, the volume of the external medium swept by the Alfvén waves is larger by $(R_0/R_c)^2$ than when the field lines are straight. Second, because it is assumed that the field lines are in co-rotation, the fluid elements which are attached to the field lines have a specific angular

momentum that increases like R_0^2 . This altogether leads to another factor $(R_0/R_c)^2$.

Combining Eq. (11) with the expressions of the mass, $M \sim 2\pi\rho_c R_c^2 Z$, the magnetic flux of the core $\Phi_B \sim \pi R_0^2 B_{\text{ext}} = \pi R_c^2 B_c$, and the expression for $v_{\text{A,ext}}$, we obtain (see, e.g. Mouschovias and Morton, 1985),

$$\tau_{\parallel,fo} = \left(\frac{\pi}{\rho_{\text{ext}}}\right)^{1/2} \frac{M}{\Phi_B} \left(\frac{R_c}{R_0}\right)^2. \quad (12)$$

Compared to the magnetic braking time with straight lines, the magnetic braking timescale is thus significantly reduced since in a collapsing core $R_c \ll R_0$ and $(R_c/R_0)^2$ is expected to be a small number.

2.3.2 Perpendicular rotator ($\alpha = 90^\circ$)

In the case of a perpendicular rotator, i.e., if magnetic field lines are initially perpendicular to the rotation axis, the braking timescale corresponds to the time it takes for the Alfvén waves to reach R_\perp , the radius at which the angular momentum of the external medium is equal to the initial angular momentum of the cloud. The Alfvén waves propagate in the equatorial plane and sweep a cylinder of half-height Z and radius R_\perp , thus

$$\rho_{\text{ext}}(R_\perp^4 - R_c^4) \sim \rho_c R_c^4. \quad (13)$$

Considering that the magnetic field is such that $B(r) \propto r^{-1}$, so that $v_{\text{A}}(r) = v_{\text{A}}(R_c) \times R_c/r$, the magnetic braking time is then

$$\tau_\perp = \int_{R_c}^{R_\perp} \frac{dr}{v_{\text{A}}(r)} = \frac{1}{2} \frac{R_c}{v_{\text{A}}(R_c)} \left[\left(1 + \frac{\rho_c}{\rho_{\text{ext}}}\right)^{1/2} - 1 \right], \quad (14)$$

which leads to

$$\tau_\perp \sim 2 \left(\frac{\pi}{\rho_c}\right)^{1/2} \frac{M}{\Phi_B}. \quad (15)$$

Comparing the braking timescales between the aligned configuration with straight field lines and

the perpendicular rotator, Eq. (9) and (15) gives

$$\frac{\tau_{\parallel}}{\tau_{\perp}} = \frac{1}{2} \left(\frac{\rho_c}{\rho_{\text{ext}}} \right)^{1/2}. \quad (16)$$

Since $\rho_c \gg \rho_{\text{ext}}$, magnetic braking is found to be more efficient in the perpendicular case. However, when taking into account the fact that field lines are fanning out, the term $(R_c/R_0)^2$ must be taken into account. As an illustrative example, let us assume that the density follows the singular isothermal sphere, i.e. $\rho_{\text{ext}}(R_0) \propto R_0^{-2}$, and $\rho_c(R_c) \propto R_c^{-2}$. With Eqs. (12) and (15), we obtain

$$\frac{\tau_{\parallel,fo}}{\tau_{\perp}} = \frac{R_c}{R_0}. \quad (17)$$

Since $R_c/R_0 \ll 1$, the magnetic braking time is thus shorter in an aligned rotator than in a perpendicular one provided the field lines are fanning out.

Numerical simulations of misaligned collapsing cores have been performed by Matsumoto and Tomisaka (2004), Joos et al. (2012), Tsukamoto et al. (2018) and Hirano et al. (2020) where analysis of the angular momentum distribution through the core were also performed. The reported results have been in apparent contradiction. While Matsumoto and Tomisaka (2004) and Tsukamoto et al. (2018) concluded that the angular momentum in the core was higher in the aligned configuration than in the perpendicular one, Joos et al. (2012) and Hirano et al. (2020) concluded the opposite. The origin of this apparent contradiction lays on the different timescale that are being probed in these studies. Matsumoto and Tomisaka (2004) and Tsukamoto et al. (2018) analyse their simulations at a relatively early time, that is to say before any disk forms. They also analyse the angular momentum within very dense material. However, Joos et al. (2012) and Hirano et al. (2020) investigate later times, after a disk has formed and looked at the angular momentum distribution through the core. The most likely explanation is that at early times and for the densest material, the field lines have not been strongly stretched and thus the braking time is

shorter in the perpendicular configuration than in the parallel one. However, as time goes on, the material that falls in the central region, say the star/disk material, was initially located further away and thus the corresponding field lines are more and more bent leading to a stronger braking.

3 THE FORMATION OF CENTRIFUGALLY SUPPORTED DISKS

In recent years, most of the efforts regarding the collapse of dense cores has been devoted to the study of disk formation. This has appeared to be a complex topic, which in particular relies on the assumptions made regarding the microphysics. Here we follow a progressive approach starting from the basics.

3.1 What is the origin of angular momentum in star formation models?

The very first question to be asked when discussing rotationally supported disks is obviously what is the value of angular momentum to be considered and where it comes from. Traditionally the working assumption has been that angular momentum was inherited from large scales and that it was conserved, at least to some degree, during the collapse. While this picture is widely accepted, it should be stressed that, in fact, it partly relies on the underlying assumption that the collapsing cloud is axisymmetric, in which case the distinction between radial and azimuthal velocity fields can be made rigorously. Moreover, observationally infall and rotational motions can be made easily. However, in the general case, clouds are not axisymmetric and this has important consequences. First, while angular momentum is still conserved with respect to the center of mass, the latter is usually not a relevant point because it is not the collapse center. Moreover, the star that forms is not attached to the center of mass, but its position moves as it evolves, creating small offsets between the global center of mass of the envelope+star system, and the star itself. Therefore, angular momentum is not a conserved

quantity with respect to the star. From the inertial forces, a torque is actually operating. This implies that angular momentum may not necessarily need to be inherited from the large scales. Indeed, Verliat et al. (2020) investigated the collapse of a non-axisymmetric cloud which initially had no motion and therefore no angular momentum. They show that in this configuration, disks would form as well.

In the rest of the section, we will not consider this scenario further, but it will be discussed later in this review.

3.2 Disk formation in hydrodynamical models

Let us consider a rotating and axisymmetric cloud without magnetic field. In such circumstance, angular momentum is a conserved quantity. Let M_* be the stellar mass and j , the fluid particle specific angular momentum. The centrifugal radius, r_d , is such that centrifugal and gravitational forces compensate each other, leading to

$$r_d = \frac{j^2}{GM_*}, \quad (18)$$

which clearly shows that disk formation is directly related to angular momentum distribution.

Let us consider a cloud with a density profile initially proportional to $1/r^2$ (e.g. Shu, 1977) leading to a mass, $M(R_0)$, within radius R_0 , such that $M(R_0) \propto R_0$. On the other-hand, the specific angular momentum is given by $j(R_0) = R_0^2\Omega$. Therefore, we get $j(R_0) \propto M(R_0)^2$. The centrifugal radius for a fluid particle initially located in R_0 can therefore be expressed as $r_d = j(R_0)^2/(GM(R_0)) \propto M(R_0)^3$ (Terebey et al., 1984). On the other hand, considering a uniform density, $M(R_0) \propto R_0^3$ and $j \propto M(R_0)^{2/3}$ which gives $r_d \propto M(R_0)^{1/3}$. If for simplicity a constant accretion rate is assumed, the disk is found to grow like t^3 when the density is initially in r^{-2} and to grow like $t^{1/3}$ when it is uniform.

From these two examples, it is seen that the angular momentum distribution sensitively

determines the disk radius. To get a quantitative estimate useful for reference, let ρ_0 be the cloud density, and Ω_0 the angular rotation velocity. For a fluid particle initially located at radius R_0 , the centrifugal radius is given by

$$r_{d,\text{hydro}} \simeq \frac{\Omega_0^2 R_0^4}{4\pi/3\rho_0 R_0^3 G} = 3\beta R_0 \quad (19)$$

$$= 106 \text{ AU} \frac{\beta}{0.02} \left(\frac{M}{0.1 M_\odot} \right)^{1/3} \left(\frac{\rho_0}{10^{-18} \text{ g cm}^{-3}} \right)^{-1/3},$$

where $\beta = R_0^3 \Omega_0^2 / 3GM$ is the ratio of rotational over gravitational energy. Note that observationally, cores have been initially inferred to have a typical $\beta \simeq 0.02$ (Goodman et al., 1993; Belloche, 2013), which is the value used for reference.

3.3 Disk formation in ideal MHD models

The first collapse calculations, which have been performed with a magnetic field, assumed to be parallel to the rotation axis (e.g. Allen et al., 2003; Galli et al., 2006; Price and Bate, 2007; Hennebelle and Fromang, 2008; Mellon and Li, 2008). A surprising conclusion has been that even with relatively modest magnetic fields, typically corresponding to μ as high as 5-10, the disk formation was nearly suppressed, a process which has been called catastrophic braking. The reason of this behavior can be understood by using simple orders of magnitude.

The magnetic braking and the rotation time, which are most important, are given by

$$\tau_{\text{br}} \simeq \frac{\rho v_\phi 4\pi h}{B_z B_\phi}, \quad (20)$$

$$\tau_{\text{rot}} \simeq \frac{2\pi r}{v_\phi}, \quad (21)$$

where h is the scale height of the disk. If the rotation time is longer than the braking time, a fluid particle may rotate a few times before it loses a significant amount of angular momentum. Since the magnetic torque is proportional to B_ϕ , we need to estimate it, which can be accomplished using the Maxwell-Faraday equation. Essentially, B_ϕ is produced by

the twisting of the poloidal magnetic field by the differential rotation. As long as ideal-MHD holds, it grows continuously with time, and we have

$$B_\phi \simeq \tau_{\text{br}} \frac{B_z v_\phi}{h}. \quad (22)$$

This leads to

$$\begin{aligned} \frac{\tau_{\text{br}}}{\tau_{\text{rot}}} &\simeq \left(\frac{M_*}{M_d} \times \frac{h}{r_d} \right)^{1/2} \frac{G^{1/2} \Sigma}{2B_z} \quad (23) \\ &\simeq \left(\frac{M_*}{M_d} \frac{h}{r_d} \right)^{1/2} \frac{\lambda_{\text{eff}}}{4\pi}, \end{aligned}$$

where we have assumed $v_\phi \simeq \sqrt{GM_*/r}$, M_* being the mass of the central star and where $M_d = \pi r_d^2 \rho h$ is the disk mass, $\Sigma = 2h\rho$, is the disk column density and $\lambda_{\text{eff}} = 2\pi G^{1/2} \Sigma / B$ is the mass to flux ratio. This shows that modest magnetic intensities corresponding to values as high as few times 4π , the magnetic braking timescale is shorter than the rotation time and therefore should prevent or severely limit the formation of centrifugally supported disk in good agreement with what has been inferred from the simulations.

3.4 Disk formation with non-ideal MHD

Since observational estimates of the typical values of μ in dense cores indicate values of a few (Crutcher, 2012), a very efficient magnetic braking capable of suppressing disk formation for most observed cores, is clearly in tension with observations. As mentioned in Sect. 2.3, misalignment between magnetic field and rotation (Joos et al., 2012; Li et al., 2013; Gray et al., 2018; Hirano et al., 2020) could help to alleviate the problem by reducing the efficiency of magnetic braking. Indeed, disk formation is reported in all studies which have considered misalignment for values of μ on the order of several, though the exact value of μ at which disk would form, varies between studies. We stress however that when a disk forms, if ideal MHD applies, the toroidal magnetic field within the disk is continuously amplified and therefore the disk quickly becomes thick and

inflated (Hennebelle and Teyssier, 2008). This emphasizes the need to consider non-ideal MHD.

A very important property of ideal MHD is that the magnetic flux through a given fluid particle is conserved. When non-ideal MHD processes are important, significant deviations from flux freezing can be produced, and this may qualitatively change the impact of magnetic braking. Two main classes of process may lead to strong departures from flux freezing. First, if the coupling between the magnetic field and the neutrals is poor and second, if the flow is strongly turbulent. Let us stress that the latter corresponds to a high magnetic Reynolds number, while the former would correspond to a low magnetic Reynolds number.

3.4.1 The possible role of turbulence

Turbulence violates the frozen-in condition of ideal MHD flows because it drives reconnection and thus, the diffusion of the magnetic field lines. Since the original proposition made by Lazarian and Vishniac (1999), this has been extensively studied and demonstrated numerically (e.g. Kowal et al., 2009; Eyink et al., 2013; Santos-Lima et al., 2021).

The role that turbulence may have on disk formation has been carefully investigated by Santos-Lima et al. (2012), Seifried et al. (2012) and Joos et al. (2013). In all these studies, it has been concluded that the efficiency of magnetic braking is reduced by turbulence, though the proposed explanations were not identical. Santos-Lima et al. (2012) emphasized the role of turbulent reconnection which transports magnetic field outwards therefore leading to a reduced magnetic torque, while Joos et al. (2013) stressed that the misalignment induced by turbulence may add up to the reconnection diffusion triggered by turbulence in reducing magnetic braking efficiency. Seifried et al. (2012) proposed that it may be the coherence of the averaged magnetic torque that is reduced by the fluctuating magnetic field, again induced by turbulence. While it is clear that reconnection diffusion is occurring in simulations which include turbulence (see Santos-Lima et al., 2013, for a discussion), it remains difficult to estimate the

respective role played by these three effects, which all concur to favor disk formation.

3.4.2 Low ionisation and high resistivities

One of the most obvious solutions to the so-called magnetic braking catastrophe is to be searched in high magnetic resistivities. This has been early proposed by Galli et al. (2006) where Ohmic dissipation was envisioned to limit magnetic braking. A long series of increasingly realistic calculations has since been performed by several authors. A comprehensive description of the various calculations performed can be found in Zhao et al. (2020).

For instance, Dapp and Basu (2010) show that when Ohmic dissipation is included in their calculation a small disk forms but not when they assume ideal MHD. This is because at small scale, the magnetic field is efficiently diffused out and therefore the braking time typically becomes longer than the rotation time. Several works have performed simulations that include ambipolar diffusion, (Dapp et al., 2012; Tomida et al., 2013, 2015; Masson et al., 2016; Zhao et al., 2016; Hennebelle et al., 2020) finding that centrifugally supported disks of few tens of AU always form. Note that on the contrary, Wurster (2016) and Lam et al. (2019) conclude that ambipolar diffusion is not sufficient to produce a disk.

Analytical arguments to predict the radius of the disks have been developed by Hennebelle et al. (2016). The effect of ambipolar diffusion, τ_{diff} , is determined by a characteristic timescale which describes how fast B_ϕ is diffused out of the disk

$$\tau_{\text{diff}} \simeq \frac{4\pi h^2}{c^2 \eta_{\text{AD}}} \frac{B_z^2 + B_\phi^2}{B_z^2} \simeq \frac{4\pi h^2}{c^2 \eta_{\text{AD}}}. \quad (24)$$

To get a stationary B_ϕ within the disk, an equilibrium between generation and diffusion must occur. Combining Eqs. (22) and (24), as well as Eq. (20) with Eq. (21) together with an estimate of

the density at the edge of the disk,

$$\rho(r) = \delta \frac{C_s^2}{2\pi G r^2} \left(1 + \frac{1}{2} \left(\frac{v_\phi(r)}{C_s} \right)^2 \right). \quad (25)$$

where δ is a coefficient on the order of a few, the following expression is inferred

$$r_{\text{ad}} \simeq 18 \text{ AU} \times \delta^{2/9} \left(\frac{\eta_{\text{AD}}}{7.16 \times 10^{18} \text{ cm}^2 \text{ s}^{-1}} \right)^{2/9} \times \left(\frac{B_z}{0.1 \text{ G}} \right)^{-4/9} \left(\frac{M_{\text{d}} + M_*}{0.1 M_\odot} \right)^{1/3}. \quad (26)$$

This expression has been compared with a broad set of MHD simulations (Hennebelle et al., 2016, 2020) and an agreement within a factor of about 2 has been inferred for the simulations in which the magnetic field is strong enough. It shows in particular that the disk size grows with the magnetic resistivity and also with the stellar mass.

The influence of the Hall effect (see Eq. 3) has been the subject of several studies. Let us first note a peculiarity of the Hall term. Flipping the sign of \mathbf{B} in Eq. (3), we see that all terms, but the Hall one, change their sign. Physically, this is because the Hall term describes the generation of the magnetic field induced by the motion of the charged particles induced by the Lorentz force. This implies that two configurations, i.e., the aligned and anti-aligned cases ($\Omega \cdot \mathbf{B} > 0$ and < 0 respectively) have to be distinguished. As a consequence, several teams have found that in the aligned configuration, the magnetic braking is enhanced and, on the contrary, it is reduced. This includes the work of Braiding and Wardle (2012) in which analytical solutions are being used, Tsukamoto et al. (2015), Wurster (2016) which perform 3D smooth particle hydrodynamical simulations and Marchand et al. (2019) which perform adaptive mesh refinement calculations. Due to these different magnetic braking efficiencies, these authors find that the disks that form in the aligned case are smaller, than the disks which form when the Hall effect is not accounted for, which are themselves smaller than the disks which form in the anti-aligned configurations. This has led to the idea

of the possible existence of a bimodal population of disks. Lee et al. (2021c) have extended the study of Hennebelle et al. (2016) to include the Hall effect, predicting disks of similar size to that inferred in the simulations. Tsukamoto et al. (2017) present calculations of misaligned configuration and conclude that the impact of anti-alignment persists, even so the differences between the 45° and 135° is significantly reduced compared to the differences between 0° and 180° .

Importantly, Zhao et al. (2020) and Zhao et al. (2021) have run 2D simulations for longer period of time and conclude that the external part of the disks formed in the anti-aligned configuration, tend to disappear, leading to a few tens of AU disks. This would suggest that the bimodal distribution could be a transient feature.

Finally, we stress that both the high resistivities and the reconnection diffusion induced by turbulence could contribute simultaneously or in different situations. For instance, if in some dense cores, the ionisation fraction is high, the resistivities could be lower and the reconnection diffusion possibly dominant. However, so far the studies which have considered in isolated dense cores, both high resistivities and turbulence, have concluded that the latter does not substantially modify the formation of disk (e.g. Hennebelle et al., 2020; Wurster and Lewis, 2020).

4 TRACING MAGNETIC FIELDS WITH PHOTONS AROUND PROTOSTARS OR AT CORE SCALES

The current perspective on magnetic fields properties in star-forming cores has been established observationally by the analysis of polarized light resulting from the interaction of the B fields with the surrounding gas molecules and dust grains. Several observational techniques have been developed: we detail them concisely here below, then describe how these measurements are used to obtain quantitative constraints from observed objects, and how the physical processes they rely on

have been implemented in radiative transfer models to produce synthetic observations.

4.1 Observational signatures of magnetic fields in protostars

Most of the observational signatures of the presence of the magnetic field in the interstellar medium are directly related with polarization. However, there are other mechanisms that can also produce polarization and are not related with the presence of magnetic fields. Here on, we focus on the magnetic fields signatures expected in molecular clouds at core's scales, the possible caveats and other sources of polarization for each case:

4.1.1 Zeeman effect

Molecular rotational lines split in submagnetic levels under the presence of a magnetic field. The frequency separation of these levels is proportional to the magnetic field strength and the magnetic dipole moment. For most molecules, the magnetic dipole moment is very small, making the Zeeman splitting undetectable, except for the maser lines (e.g., Alves et al., 2012; Crutcher and Kemball, 2019). However, molecules with an unpaired electron have relatively large magnetic moments, yielding to significant Zeeman splitting. The Zeeman molecules that are abundant in molecular clouds are OH, CN, SO, CCH and CCS. The splitting can be measured through circular polarization, but in almost all cases not in total intensity. This is because the Zeeman splitting in frequency is typically only of the order of $\text{Hz } \mu\text{G}^{-1}$ (Bel and Leroy, 1989, 1998; Shinnaga and Yamamoto, 2000; Uchida et al., 2001; Turner and Heiles, 2006; Cazzoli et al., 2017), much smaller than typical linewidths in molecular clouds for the expected magnetic field strength (\lesssim few mG). The circular polarization is proportional to the magnetic field strength component along the line-of-sight, the intensity derivative and the specific Zeeman splitting for the observed line. The molecules with hyperfine structure (CCH, CN) are more adequate to observe the Zeeman splitting because different hyperfine levels have different Zeeman splitting values. This allows to separate

the possible instrumental polarization, which does not distinguish between hyperfine lines, from the Zeeman effect. There have been several attempts to detect Zeeman effect at core scales, mostly through CN rotational transitions, but there are only a handful of detections reported in the literature (Crutcher et al., 1999; Crutcher, 1999; Levin et al., 2001; Falgarone et al., 2008; Maury et al., 2012; Pillai et al., 2016; Nakamura et al., 2019), and none at disk scales (Vlemmings et al., 2019; Harrison et al., 2021).

Caveats: This is the only method that can provide a direct estimation of the field strength along the line of sight. Nevertheless, in order to be able to derive the role of the magnetic fields at the core and disk scale, special care has to be made on where the emission of the Zeeman molecules arise. These are radical molecules, so they are chemically active and their abundances may change significantly depending on the environment conditions. Thus, in prestellar cores, CN appears to behave as other N-bearing molecules and thus survives at high densities (Hily-Blant et al., 2008). On the contrary, CCH, CCS and SO appear to deplete toward the core's center (Tafalla et al., 2006; Padovani et al., 2009b; Juárez et al., 2017; Seo et al., 2019). For massive cores, all these molecules but SO appear to be anticorrelated with the dust emission at scales of $\lesssim 0.05$ pc (Dirienzo et al., 2015; Paron et al., 2021). The distribution of these molecules in the planet-forming disk is also complex and, combined with the expected magnetic field configuration, makes the interpretation of Zeeman observations difficult (Mazzei et al., 2020).

4.1.2 Linear polarization of molecular lines

Rotational levels split into magnetic sublevels under the presence of magnetic fields. Transitions where the submagnetic level does not change will be linearly polarized, with the polarization angle parallel to the magnetic field. In the other cases, the polarization will be perpendicular to the magnetic field. In most cases, collisions do not differentiate among magnetic sublevels, so they populate the sublevels equally. That means that

the net linear polarization is zero. However, an anisotropic radiation field will generate unbalance of the sublevels, giving a partially linearly polarized emission. This process is known as the Goldreich-Kylafis (G-K) effect because it was initially developed by Goldreich and Kylafis (1981). The level of linear polarization produced by the G-K effect depends on various parameters, such as the ratio of the collisional rate to the radiative decay rate and the optical depth (Goldreich and Kylafis, 1981, 1982; Deguchi and Watson, 1984).

However, the polarization direction can be parallel or perpendicular to the magnetic field. This means that the properties of the emission (optical depth, velocity, and density gradients) should be analyzed to solve this ambiguity. Once this is done, then this technique allows obtaining the magnetic field morphology projected in the plane of the sky. Multi-transition observations of the linearly polarized lines can be used to derive the field strength (Cortes et al., 2005). The G-K has been detected in a small sample of cores (Girart et al., 2004; Lai et al., 2003a; Cortes et al., 2005, 2008; Cortés et al., 2021), in few disks (Stephens et al., 2020; Teague et al., 2021) and in some molecular outflows (Girart et al., 1999; Ching et al., 2016; Lee et al., 2018a). Differential collisions due to ambipolar diffusion could also produce polarization in the ion molecules Lankhaar and Vlemmings (2020a).

Caveats: The properties of linearly polarized emission from a molecular line produced by the G-K can be altered if there is a foreground molecular component at the same velocity (Hezareh et al., 2013). This is the Anisotropic Resonant Scattering (ARS) effect, which not only alters the properties of the linear polarization, but it leaks a fraction of this, generating circular polarization (Houde et al., 2013, 2022). There is some evidence that this may happen (Chamma et al., 2018). Sensitive observations of all Stokes parameters are needed to correct for this effect and obtain the unaltered original signature of the G-K effect. In addition, the detection of this non-Zeeman circular polarization could be used to measure the magnetic field strength (Houde et al., 2013). Molecular ions could also have

collisionally-driven linear polarization produced by ambipolar drifts (Lankhaar and Vlemmings, 2020a). The resulting polarization has an angle perpendicular to the magnetic field direction. This effect could be distinguished from G-K by using optically thin molecular ion lines.

4.1.3 Dust polarization

Since the early 1950s we know that interstellar grains are partially aligned with the magnetic fields (Davis and Greenstein, 1951). The major axis of the grains are aligned perpendicular to the magnetic field, yielding to linear polarization in the dust emission with an angle perpendicular to the magnetic field projected in the plane of the sky. There have been some proposed mechanisms that allow the grain angular momentum to align with the magnetic field (e.g. see review by Lazarian et al., 2015). Radiative torques (RATs) are thought to be the most efficient way to help grains to align with the magnetic field. Some predictions of this theory have been confirmed observationally (Alves et al., 2014; Jones et al., 2015). However, recent results with ALMA shows that at core scales RATs are not enough to explain the observed dust polarization properties (Le Gouellec et al., 2020). The dust emission appears to be polarized at significant levels ($\gtrsim 1\%$) in a significant high fraction of observed cores, and therefore it is the most used technique in the millimeter through far-IR wavelengths to study the magnetic fields at core and disk scales (e.g., Girart et al. 2009, Pattle et al. 2017, Alves et al. 2018, Sanhueza et al., 2021, and for a more complete references see Hull and Zhang, 2019 and Pattle et al., 2022).

Caveats: At disks scales, grain growth is so important that self-scattering produced by large grains appears to be the dominant polarization mechanism (e.g., Kataoka et al., 2015; Yang et al., 2017; Kirchschrager and Bertrang, 2020), although other mechanisms have also been proposed to generate polarization at disk scales (Tazaki et al., 2017; Kataoka et al., 2019; Brunngräber and Wolf, 2019). Of special interest for environments containing large grains, if feasible, is the the

alignment of these grains with magnetic fields in the Mie regime, when grains start to have a size similar to or larger than the wavelength of the incident light (Guillet et al., 2020a). At the core scales, in the densest part where the dust emission may be optically thick, especially at the shortest wavelengths, the polarization pattern may be altered or even reversed (Liu et al., 2016; Ko et al., 2020).

4.1.4 Ion to neutral velocity drift

The ionization fraction in molecular clouds is tiny, $\sim 10^{-6}$, but the ions and neutrals are well coupled. However, small kinematic differences are expected due to diffuse processes such ambipolar diffusion (Houde et al., 2000; Li and Houde, 2008; Falceta-Gonçalves et al., 2010). This effect can be observed as differences between neutrals and ions, in their line width and in the velocity maps. HCO⁺ and HCN lines with the same rotational level from their different isotopologues are ideal to test this because they have similar excitation conditions. The line width differences have been observed in several cores (Houde et al., 2000; Lai et al., 2003b). In a magnetized turbulent medium the linewidth difference should change with the length scale, which has been observed at ~ 0.1 pc scales, allowing to measure the turbulent dissipation scale and the magnetic field strength (Li and Houde, 2008; Hezareh et al., 2010, 2014). Recent observations of NH₃ and N₂H⁺, at $\lesssim 0.1$ pc scales, show that, contrarily of what is expected in AD, the ion linewidth is systematically broader than that of the neutral by 20% (Pineda et al., 2021).

Caveats: The expected velocity drift is very difficult to measure at small scales typical of inner envelopes, as the velocity offset is expected to be of the order of the best spectral resolution currently available from typical instruments and the velocity field is complex (Yen et al., 2018; Cabedo et al., 2022). The main limitation of this method is to ensure that the selected neutral and ion species trace the same gas, or are affected by optical depth effects (e.g., Pratap et al., 1997; Jørgensen et al., 2004; Girart et al., 2005; Zinchenko et al., 2009).

4.1.5 Observational techniques to infer magnetic field properties

Here, we describe the main techniques that allow to infer the magnetic field properties from observations, independently of the use of the radiative transfer tools that are described in the next subsection. The most popular technique is the Davis-Chandrasekhar-Fermi (CDF) equation (Davis and Greenstein, 1951; Chandrasekhar and Fermi, 1953) which allows estimating the magnetic field strength in the scenario of small perturbation due to the anisotropic motions (such as turbulence). The equation relates the magnetic field in the plane-of-the sky, B_{pos} with the gas density, ρ , the non-thermal velocity dispersion along the line-of-sight, δv and the dispersion of the polarization angles of in the plane of the sky, $\delta\theta$: $B_{\text{pos}} = \sqrt{4\pi\rho} \delta v / \delta\theta$ (Chandrasekhar and Fermi, 1953). There have been several works to account for the limitations of this technique, such as line-of-sight smearing or cases with large dispersion, that in general leads to an overestimation of the field strength (Ostriker et al., 2001; Heitsch et al., 2001; Falceta-Gonçalves et al., 2008; Cho and Yoo, 2016; Skalidis and Tassis, 2021; Liu et al., 2021). A more sophisticated method is the use of the structure function, which allows separating the turbulent component from the smooth variations of the polarization angles to the large scale field (Hildebrand et al., 2009; Houde et al., 2009, 2011, 2016). There are other (semi) analytical expressions that allow to evaluate the relevance of magnetic fields for the specific hour glass configuration (Ewertowski and Basu, 2013; Myers et al., 2018).

4.2 Polarized radiative transfer tools for protostellar environments

In this section, we describe how physical processes responsible for producing polarized light as a result of the interaction of magnetic fields with protostellar material are implemented in radiative transfer codes and coupled to the numerical models for star and disk formation. We focus on two codes which are widely used by the community interested in star formation: POLARIS

for dust grain alignment (Reissl et al., 2016), and PORTAL for spectral lines (Lankhaar and Vlemmings, 2020b). While a complete description of the polarization-inducing processes go beyond the scope of this review, we briefly describe them below.

4.2.1 Radiative transfer of emission from magnetically aligned grains

The three-dimensional continuum radiative transfer RT code POLARIS (Reissl et al., 2016) uses 3D models of astrophysical structures to produce synthetic maps of the polarized dust continuum emission, allowing several flavours of alignment mechanisms for the dust grains. The photon propagation within the 3D model is implemented following a Monte-Carlo photon transfer scheme. The interaction of the incoming radiation with dust grains is determined in each cell, and depends on mostly of the cross-section of extinction, the dust density. Depending on the local physical conditions such as the dust grain albedo, POLARIS either computes the scattering, or the absorption with instantaneous re-emission, then a new wavelength is calculated and the dust thermal energy of the cell is adjusted. In this computation of photon propagation and dust heating mode, POLARIS assumes that dust grains are spherical: this step thus allows to derive the dust temperature in each cell with a limited computational effort. The alignment probability of dust grains in each cell is calculated, accounting for the imperfect internal alignment and the imperfect alignment between the dust grain's angular momentum and magnetic field. Then, the anisotropy of the radiation field at any given wavelength λ is calculated in each cell which allows determining the alignment of the different dust grains due to radiative torques (RATs, see previous section). Since a distribution of dust grain sizes is considered (usually following a classical MRN, after Mathis et al. 1977, distribution consisting of power-laws of separate populations of bare spherical silicate and graphite grains), the RAT alignment in given irradiation and B-field conditions depends also on the effective grain radius

a_{align} . Dust grains larger than a_{align} are considered aligned (with a fraction depending on the high-J attractor point f_{high-J} , which can be manually set to any value between 0 and 1), and contribute to the polarization of the dust thermal emission. Several studies have used the POLARIS code to predict and confront observations of polarized dust emission, from molecular cloud conditions (Liu et al., 2021; Reissl et al., 2021) down to disk conditions (Brunngräber and Wolf, 2021). Note that a few studies have used radiative transfer tools developed in a recent past, such as Dustpol (Padovani et al., 2012; Lee et al., 2017) but here we focus on the most recent results, and hence on POLARIS because it is the most widely used RT code for dust polarization nowadays. An example of synthetic observations of the polarized dust emission, assuming different alignment conditions for the dust from the same numerical model of a collapsing core, is shown in Figure 1. Details and results of the works specifically dedicated to protostars are described in the next Section 4.3 below.

4.2.2 Radiative transfer of emission from magnetically-sensitive molecular lines

The POLARIS code can also be used to simulate the polarization of spectral lines due to the Zeeman effect, thanks to the ZRAD extension (Brauer et al., 2017). This is based on the line RT algorithm Mol3D (Ober et al., 2015), and makes use of atomic and molecular parameters such as the energy levels and transitions taken from the Leiden Atomic and Molecular Database (LAMDA), the Landé factors of the involved energy levels, the line strengths of the allowed transitions between Zeeman sublevels, and emitting radius of the molecular species. It has been used to test the robustness of Zeeman measurements to infer magnetic field strengths in molecular clouds, showing that while the gas density affects little the uncertainty of the measurements, strong variations in the LOS component of the gas velocity and of the magnetic field strength significantly impact the precision of the method (Brauer et al., 2017).

PORTAL is an adaptive three-dimensional polarized line radiative transfer model that considers the local anisotropy of the radiation field as the only alignment mechanism of molecular or atomic species to calculate the aligned molecular or atomic states. It allows simulating the polarization of photons produced from line emission through a magnetic field of arbitrary morphology. While it can be run in stand-alone mode, PORTAL can also process the outputs of 3D radiative transfer codes on regular grids. It has been used, coupled to the parallelized non-LTE 3D line radiative transfer code Line Emission Modelling Engine (LIME, Brinch and Hogerheijde 2010), to predict spectral line polarization of different molecular transitions arising from protoplanetary disks, at the ALMA wavelengths (Lankhaar et al., 2022).

4.3 Synthetic observations of B-fields from protostellar models: methods

The question of the physical processes causing the polarization of photons from star-forming structures, both from the dust and from molecular species, has been a long-standing one. Some simple analytical models assuming a quasi-perfect alignment of dust grains with magnetic field lines, for example, have been proposed in the past, and sometimes even successfully reproduced some observations (Padovani et al., 2012). The development of more detailed physical models of grain alignment have allowed more predictive studies of the polarized dust emission arising from magnetically-aligned grains, and quantitative confrontation to observations performed towards protostellar envelopes.

The combination of polarized radiative transfer, as described above, to state-of-the-art numerical models of protostellar formation can be used to compare model predictions to actual observations. The general process is quite standard. First, one selects the outputs corresponding the best to the properties of the observed object to be compared to. Usually, a numerical simulation output can be extracted as a datacube containing the gas density, the gas pressure (or equivalently the

gas temperature), the three components of the velocity field, as well as the three components of the magnetic field. These gas properties are extracted and put in a suitable format to be post-processed with a radiative transfer code, such as POLARIS. The central radiation source is modelled as a blackbody of chosen luminosity that allows to reproduce the observed bolometric luminosity of the studied object. Note that, to facilitate the propagation of photons and avoid missed photon packages from the central source due to long computational times, many authors choose to artificially empty a small central sphere of radius a few au around the sink particle, as in Valdivia et al. (2019). The radiative transfer can also include an external isotropic radiation field of strength that illuminates the external layers of the core. The dust properties are normally taken from tabulated values and in most studies assumed uniform throughout the model, with a gas-to-dust ratio of 100, and a typical composition and size distribution reproducing observations of dust in the ISM (Mathis et al., 1977; Hildebrand and Dragoon, 1995). The radiative transfer calculation is done via Monte Carlo methods or ray tracing methods. For example, the POLARIS code computes first the propagation of photons alongside the dust temperature via a MCMC analysis, and then solves the grain alignment equations, using the density, radiation field, dust grain properties and temperature, in each cell of the grid. Grain alignment can be assumed to be perfect, or to depend on local conditions, as, e.g., when assuming RAT alignment (Hoang and Lazarian, 2014). The outputs are maps of the Stokes I, Q and U from the dust thermal emission, which can be further convoluted by instrumental effects (e.g., the simobs task in CASA to simulate ALMA datasets) and compared to observations.

5 OBSERVED PROTOSTELLAR PROPERTIES

Measuring the properties of the gas, the dust, and the magnetic field in embedded protostars is cornerstone to inform the magnetized models

of star formation, test their predictions, but also understand the role of non-ideal effects in disk formation and evolution. We recall here below some key observational results which relate directly to these questions.

5.1 Dust Grains

Because they are the seeds from which planet formation processes are triggered in circumstellar disks, and because they are also key agents in the efficiency of coupling the magnetic field to the gas, characterizing dust grains is a cornerstone in building a comprehensive scenario of star formation.

In the far-IR and longer wavelengths, the opacity of astrophysical dust scales with wavelength as $\kappa_{\nu} \propto \nu^{\beta}$, where β is the emissivity spectral index of dust emission. β reflects how emissive dust grains are, and is therefore, commonly used to characterize dust grains in astrophysical structures. It is measured by comparing the relative intensity of dust thermal emission when observed at different wavelengths: indeed, if the dust emission is optically thin, the ratio of flux densities at different wavelengths only depends on β . In the diffuse interstellar medium, Planck studies have shown the dust has $\beta \sim 1.6$ (Planck collab. 2014, Juvela et al. 2015). Observational works show that significant variations in β is found at protostellar core scales, with millimetre-wavelength β values much lower than this typical value, however (Martin et al., 2012; Chen et al., 2016; Sadavoy et al., 2016; Bracco et al., 2017; Van De Putte et al., 2020).

While studies dedicated to resolving the dust properties at small radii in embedded protostars (Jørgensen et al., 2007; Kwon et al., 2009; Chiang et al., 2012; Miotello et al., 2014) started before the advent of large millimetre interferometers such as NOEMA and ALMA, the development of these two observatories has allowed a significant leap forward in this area of research. Li et al. (2017), Galametz et al. (2019), Tychoniec et al. (2020) and Bouvier et al. (2021) have measured the dust emissivity spectral index in relatively large samples

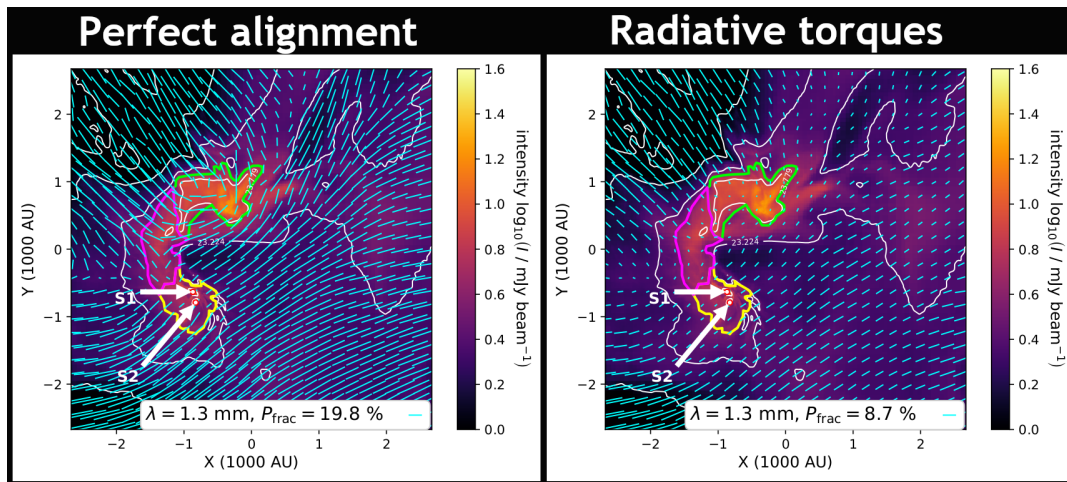


Figure 1. Synthetic maps of the 1.3 mm dust continuum emission. Overlaid are the polarization vectors rotated by 90° , obtained with POLARIS either considering perfect alignment of the dust grains (right) or RAT grain alignment (left), from Kuffmeier et al. (2020).

of embedded protostars, finding β values ranging between 0 and 2, with a majority of the protostellar dust exhibiting $\beta < 1$ at envelope radii ~ 500 au. Figure 2 shows in its left panel the observations of millimeter dust emissivity indices measured by Galametz et al. (2019) in the CALYPSO survey, finding that most protostars show significantly shallow dust emissivities at envelope radii $\sim 100 - 500$ au, with $\beta < 1$. Galametz et al. (2019) did an analysis of their interferometric data in the visibility space, allowing to also distinguish a radial evolution of the dust emissivity, with many objects showing a decrease of β with decreasing envelope radius. These observations also confirm it is the dust pertaining to the innermost envelope, and not to the unresolved disks at smaller scales, which is different from the dust typically observed in the diffuse ISM. In Class I protostars, less observations sensitive to the inner envelope regions are available: despite the poor statistics they also tend to show low dust emissivity in a majority of objects, with sometimes extremely low values ($\beta < 0.5$) at disk scales (see e.g. Harsono et al., 2018; Nakatani et al., 2020; Zhang et al., 2021).

Other effects affecting the millimetre flux could be responsible for the low dust opacities found, such as anomalous emission from spinning dust grains (Planck Collaboration et al., 2011), contamination

by non-thermal emission or the dust self-scattering (Liu et al., 2019). At the typical envelope scales, however, both the effects of optical depth and non-thermal emission are expected to be negligible at millimetre wavelengths (Tychoniec et al., 2020).

Another possible explanation for the observed difference in the dust emissivity β could stem from different dust grain composition compared to that of the diffuse ISM. For example, it has been suggested that grains with higher ratio of carbonaceous to silicate would exhibit lower β (Jones et al., 2017; Ysard et al., 2019; Zelko and Finkbeiner, 2020). Similarly, grains that are less compact and more fluffy could also be associated to low emissivity (Brunngräber and Wolf, 2021; Köhler et al., 2008). These explanations are not favoured as the unique cause for the observed low emissivities, however, because of the low values found by observations (around 0) can not be matched by current dust models, even with significant changes of composition and compactness. Indeed, laboratory studies probing different interstellar dust analogues suggest that dust emissivities < 1 at millimetre wavelengths can only be produced by grains larger than $100 \mu\text{m}$ (Demyk et al., 2017b,a; Ysard et al., 2019) in the typical physical conditions reigning in protostellar envelopes.

Another independent thread of evidence for the presence of relatively large grains in Class 0 envelopes and disks stems from polarimetric observations (Le Gouellec et al., 2019; Lee et al., 2021a) and their comparison to synthetic observations (Valdivia et al., 2019; Le Gouellec et al., 2020), performed as described in 4.3. They show that relatively large grains are required to reproduce the observed level of polarization fractions (see an example in the right panel of Figure 2). Indeed, if dust grains align following the radiative torques (RATs) theory, the radiation field in deeply embedded protostellar environments is not prone to align the small grains where polarization of the dust mm emission is routinely detected. Only synthetic observations performed with dust grain size distributions including grains up to $a_{\max} \sim 20 \mu\text{m}$ produce polarized dust emission at levels similar to those currently observed in solar-type protostars, at (sub-)millimetre wavelengths.

5.2 Fraction of ionized gas

Characterizing the ionization of the gas in the dense envelope material is critical to set constraints on the coupling of the magnetic field with the infalling-rotating envelope gas, and the role of diffusive processes, such as ambipolar diffusion or reconnection diffusion, to counteract the outward transport of angular momentum from the infalling-rotating envelope due to B-fields.

Cosmic rays (CRs), mostly relativistic protons, are the dominant source of ionization in relatively dense molecular gas where ultraviolet radiation cannot penetrate (Grenier et al., 2015). Protostars are deeply embedded sources, where the gas ionization fraction can only be inferred using indirect chemical signatures. A handful of measurements were obtained in Class 0 objects at core scales (typical densities $n_{\text{H}_2} \sim 10^4 \text{ cm}^{-3}$): they suggest typical cosmic ray ionization rates $\chi_e \sim 10^{-17} - 10^{-15} \text{ s}^{-1}$ with large uncertainties (Ceccarelli et al., 2014; Podio et al., 2014; Favre et al., 2017, 2018). In Class I protostars, only a few studies have been carried out, using the abundance of HCO^+ to estimate gas ionization from cosmic

rays in two young disks around $\xi \sim 10^{-17} \text{ s}^{-1}$, and suggest it is lower in the disk compared to the inner envelope (Harsono et al., 2021; van 't Hoff et al., 2022). Such low values may suggest it is unlikely that the accretion through the disk to the central star could be driven by magneto-rotational instabilities. In the Class 0 protostar B335, Cabedo et al. (2022) used deuteration detected in molecular line emission maps to characterize the ionization of the gas at envelope radii $\lesssim 500 \text{ au}$ (typical densities $n_{\text{H}_2} \sim 10^6 \text{ cm}^{-3}$), and found large cosmic ray ionization rate ζ between 10^{-16} and 10^{-14} s^{-1} . Such high values seem inconsistent with the fiducial value if the interstellar cosmic rays flux is responsible for the gas ionization, as it should be efficiently attenuated while penetrating into the dense cores (Padovani et al., 2018). The observations of Cabedo et al. (2022) also show the CRs ionization rate is increasing at small envelope radii, toward the central protostellar embryo. Several theoretical works have investigated the role of shocks at the protostellar surface and magnetic mirroring within the jets as efficient forges to accelerate locally low-energy cosmic rays, and their role in increasing the ionization rate of the shielded protostellar material (Padovani et al., 2015; Silsbee et al., 2018; Padovani et al., 2021; Fitz Axen et al., 2021). In B335, it seems that local acceleration of CRs, and not the penetration of interstellar CRs, may be responsible for the gas ionization at small envelope radii. This would imply that, in the inner envelope, the collapse transitions from non-ideal to a quasi-ideal MHD once the central protostar starts ionizing its surrounding gas, and very efficient magnetic braking of the rotating-infalling protostellar gas might then take place.

5.3 Gas kinematics: angular momentum and mass infall rates

The dynamical role of the magnetic field can also be assessed by careful examination of the distribution of angular momentum associated to protostellar gas, and measurement of the mass transported inwards, from envelope to disk scales (Pineda et al., 2019; Galametz et al., 2020; Yen et al.,

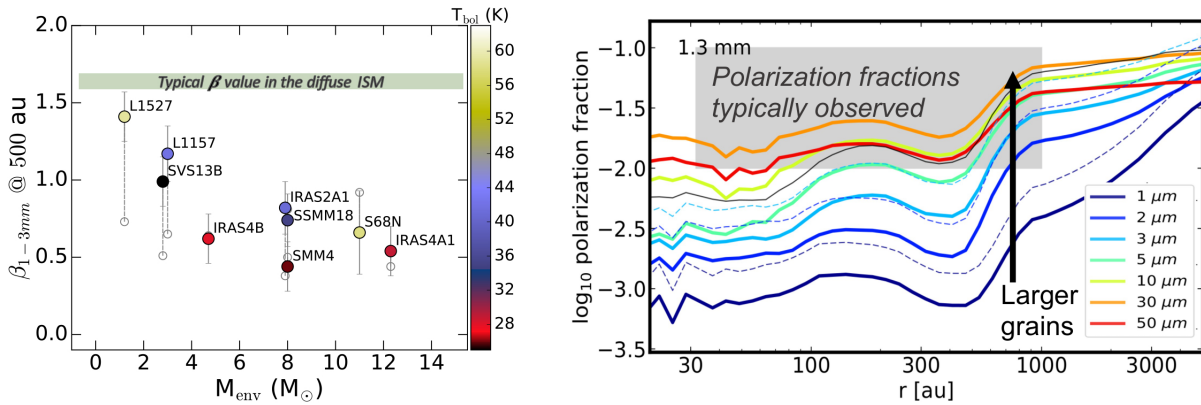


Figure 2. Left: Observed millimeter dust emissivity index in a sample of young protostars from Galametz et al. (2019). All protostellar envelopes probed at radii ~ 500 au show lower values than the progenitor diffuse ISM. Right: Radial profile of the polarization fraction from the 1.3 mm dust emission predicted from RAT alignment of dust grains in a typical low-mass protostellar envelope (Valdivia et al., 2019). Large ($> 10 \mu\text{m}$) dust grains are required to match the observations of the polarized emission (grey area).

2021b). This is not simple from an observational point of view, as the velocity field of the molecular gas is much less organized than expected from the simple monotoneous collapse of axisymmetric rotating cores in many protostars. Recent studies have revealed envelopes with complete reversal of the velocity fields, or containing multiple velocity components (Gaudel et al., 2020; Maureira et al., 2017) at radii $r < 5000$ au. Figure 3 shows a few recent examples of the detection of well-developed asymmetric features from envelopes to disk scales, which may trace preferred pathways funneling the accretion, such as streamers (Pineda et al., 2020; Chen et al., 2021) or supersonic infall along outflow cavity walls (Cabedo et al., 2021).

Mass infall rates from large to small scales are difficult to estimate, as the complex kinematics of envelopes surrounding embedded protostars produce convoluted signatures whose degeneracies can only be lifted by a joint analysis of a variety of tracers probing widely varying density conditions and spatial scales. Double-peaked profiles in spectral lines from molecular species (due to self-absorption) with a brighter blueshifted peak are sometimes used as a signpost of probable infall motions (e.g., Choi et al., 1995; Mardones et al., 1997; Evans et al., 2015; He et al., 2015; Yang et al., 2021). These profiles are used to

derive infall rates, \dot{M}_{infall} , following the expression: $\dot{M}_{\text{infall}} = (\Omega/2)V_{\text{infall}}(R_c) \mu m_{\text{H}} \langle n_{\text{H}_2} \rangle R_c^2$, where Ω is the solid angle subtended by the core center over which infall occurs, R_c is the core's radius, $V_{\text{infall}}(R_c)$ is the infall velocity at this radius and $\langle n_{\text{H}_2} \rangle$ is the core's average volume density (e.g. Beltrán et al., 2022). Surprisingly, few of these line profiles are observed towards embedded protostars at core scales (Mottram et al., 2013, 2017). Interferometric observations resolving the inner envelopes also revealed only a handful of them, for which modeling suggests typical mass infall rates $\sim 10^{-5} M_{\odot}$ per year at ~ 500 au scales in Class 0 protostars (Pineda et al., 2012; Evans et al., 2015; Su et al., 2019). Class I protostars in Ophiuchus have been surveyed with ALMA, exhibiting typical mass accretion rates a few $10^{-7} M_{\odot}$ per year (Artur de la Villarmois et al., 2019). In the well-characterized Class I protostar TMC1-A, the observed mass infall rate is measured to be larger than the value towards Ophiuchus Class I, estimated around $\sim 10^{-6} M_{\odot}$ per year. This protostar also shows a decelerating infall velocity towards small radii, and an infall velocity ~ 0.3 times smaller than the free-fall velocity yielded by the dynamical mass of the protostar (Aso et al., 2015). The accretion rates derived in high mass star forming cores are significantly larger, typically between $\sim 10^{-4}$ to

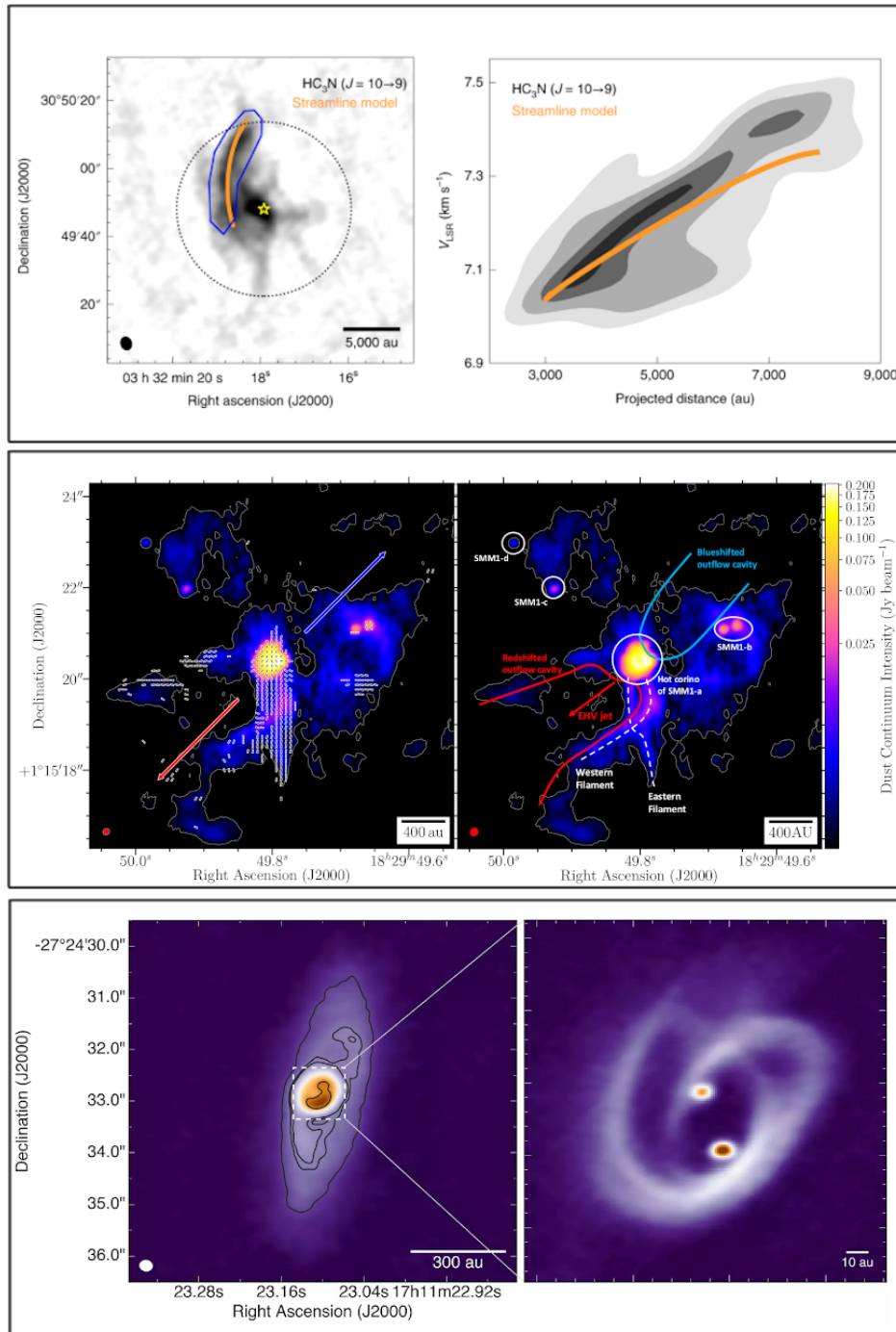


Figure 3. Streamer structures seen at different scales and towards different embedded protostars. Top: IRAS 03292+3039 in Perseus (Pineda et al., 2020). Middle: Serp-SMM1 in Serpens (Le Gouellec et al., 2019). Bottom: [BHB2007] 11 in the Pipe (Alves et al., 2019).

$10^{-2} M_{\odot}$ per year at scales of few hundred to few thousands of au (e.g., Beltrán et al., 2006; Qiu et al., 2011; Wyrowski et al., 2012; Liu et al., 2013, 2020). In the case of the G31.41+.31, high angular resolution multi-line inverse P-Cygni measurements

indicate infall acceleration at decreasing radius (Beltrán et al., 2022).

A key figure to assess the magnitude of rotational energy contained in protostellar cores, and compare these rotational motions to model predictions, is the

specific angular momentum of the gas $j_{\text{spe}} = r \times v_{\phi}$. High angular resolution observations of molecular line emission in Class 0 protostars have revealed that the gas contained in envelopes has a specific angular momentum $j_{\text{spe}} \sim 10^{20} \text{ cm}^2 \text{ s}^{-1}$ at 1000 au (Yen et al., 2015a; Tatematsu et al., 2016; Pineda et al., 2019; Gaudel et al., 2020; Heimsath et al., 2021; Hsieh et al., 2021). In the literature, it is common to find that the conservation of angular momentum in an infalling rotating envelope should produce a radial profile of rotational velocity $v_{\phi} \propto r^{-1}$, because $j_{\text{spe}} = r \times v_{\phi}$ should be constant. While if the initial rotation profile at the beginning of collapse follows a $v_{\phi} \propto r^{-1}$ relationship, this is true, it is not in most cases. Indeed, an infalling envelope initially in solid body rotation ($v_r \propto r^{-1/2}$ and $v_{\phi} \propto r$) should exhibit $j_{\text{spe}} \propto r^2$. If gas particles conserve their specific angular momentum during the collapse, the slope of the radial profile $j_{\text{spe}}(r)$ should be conserved with time as they move inwards, and protostellar envelopes should thus be observed with $j_{\text{spe}} \propto r^2$ down to the disk sizes. However, this is not what is observed. At envelope radii between 1000 and 10000 au, j_{spe} scales as a power-law with radius, $j_{\text{spe}} \propto r^n$ with $n \sim 1.6 - 1.8$. Interestingly, as pointed out by Gaudel et al. (2020), this scaling is closer to the trend expected from the dissipation cascade of Kolmogorov-like turbulence than from solid-body rotation. This may suggest that large-scale ISM turbulence or turbulence locally driven around/by protostars is actually responsible for the observed angular momentum in outer envelopes. Moreover, resolved observations have identified a break in the specific angular momentum radial profiles, from the steep outer profile $j_{\text{spe}}(r) \propto r^{1.6}$ at envelope radii $r > 1600$ au, to a quasi flat $j_{\text{spe}}(r) \sim \text{cte}$ inner profile at radii < 1600 au (Gaudel et al., 2020). If angular momentum was conserved during the collapse, it suggests that the initial angular momentum profile in these cores was, also, mostly flat and would rule out that cores are build with solid body rotation as initial conditions.

Taken altogether, these observed features suggest that a complex interplay of magnetic fields,

turbulence, and gravity are responsible for organizing the collapse along preferential directions, and that the angular momentum contained at small scales does not seem closely related to the gas flows observed at larger envelope radii.

5.4 Magnetic fields at core's scales

High angular resolution observations at (sub-)mm wavelengths show that the thermal dust emission probing the envelope-to-disk scales (~ 50 -10,000 au) is polarized at a few percent level. This has been observed both in low and high mass star forming regions (see e.g. Matthews et al., 2009; Zhang et al., 2014; Galametz et al., 2018; Hull and Zhang, 2019; Beltrán et al., 2019; Sanhueza et al., 2021; Eswaraiah et al., 2021). Considering that the polarized flux is a quantity that is prone to cancellation if the polarization angle is highly disorganized along the line of sight, observations of rather large polarization fractions suggests the magnetic field lines underlying the alignment of the protostellar dust remain at least partly organized inside star-forming cores (Le Gouellec et al., 2020). Indeed, these observations have already yielded to a large statistical sample to look for morphological trends at core scales. This is even taking into account that in many (mostly pre-ALMA) observations the detected signal was not extended enough to infer a clear, well resolved, morphology. In many dense cores, the magnetic lines are often quite organized. Indeed, the expected hourglass configuration expected in the collapse of cores threaded by a uniform magnetic field has been detected (see e.g. Schleuning, 1998; Girart et al., 2006, 2009; Qiu et al., 2014; Kandori et al., 2017; Maury et al., 2018; Beltrán et al., 2019; Redaelli et al., 2019; Kwon et al., 2019). This configuration implies that either magnetic lines efficiently resist the angular momentum due to rotation or that the latter is weak, otherwise the field lines would show a clear toroidal component. However, there are few cores where a spiral pattern suggests that the kinetic energy associated to angular momentum may dominate (Lee et al., 2019; Beuther et al., 2020; Sanhueza et al., 2021).

In some cases (Hull et al., 2017b), the observations reveal quite disorganized B-field topologies, which suggest weak-field conditions, and the possible role of turbulence or anisotropic gas flows in organizing the magnetic field lines.

Moreover, there are two interesting features that ALMA observations have revealed. One is the detection of significant polarization along the outflow cavity walls, as in some cases this is the only place where polarization is indeed detected (Le Gouellec et al., 2019; Hull et al., 2020). The other is the presence of well organized polarized filaments with the magnetic field along the filament (Le Gouellec et al., 2019; Takahashi et al., 2019; Hull et al., 2020). This may be related with accretion streamers that have been detected recently (Yen et al., 2019; Alves et al., 2020; Pineda et al., 2020), although kinematic information is needed to confirm this scenario.

(Koch et al., 2014) compiled the magnetic fields properties of 50 low and high mass protostellar cores. They propose four types of morphology (see also Koch et al., 2013): (1) magnetic field mostly aligned along the minor axis of the core, (2) magnetic field mostly aligned along the major axis of the core, (3) hourglass and quasi-radial fields, and (4) irregular shapes. This correlation was also confirmed by (Zhang et al., 2014), which also found that the magnetic fields in massive dense core scales are either parallel or perpendicular to the parsec-scale magnetic fields. However, there are cases where this correlation at different scales does not hold (Girart et al., 2013; Hull et al., 2017a). Despite the overall trends where magnetic fields appear to be coherent with respect to larger scales and core orientation, there is no correlation with molecular outflow direction (Hull et al., 2013; Zhang et al., 2014). However, there are other works that found some correlation between the outflow direction and the magnetic field, although the alignment is far from being perfect (Galamez et al., 2020; Yen et al., 2021a). These two works show that, on one hand, the misalignment between the outflow and magnetic field direction appears to be correlated with the amount of angular momentum

(Galamez et al., 2020), and, on the other hand, the observed misalignment is not sufficient to reduce the efficiency of magnetic braking (Yen et al., 2021a).

Most of the observations have relied on indirect methods to derive the magnetic field strength from the (mostly dust) polarization observations (see Section 4.1). In spite of not being very accurate, these methods give a good approximation of the magnetic field strength. Thus, comparison between semi-analytical models or MHD simulations with polarization observations have found good agreement with the values obtained using different Davis-Chandrasekhar-Fermi approximations (Gonçalves et al., 2008; Frau et al., 2011; Juárez et al., 2017; Maury et al., 2018; Beltrán et al., 2019). Overall, the DCF shows that star forming cores appear to be supercritical by a factor of about 2, and that these cores are gravitationally bound (Myers and Basu, 2021). Measuring directly the (line-of-sight) strength of the magnetic field is very difficult, and there is a small amount of positive detection at core scales (Crutcher et al., 1999; Falgarone et al., 2008; Crutcher et al., 2009; Pillai et al., 2016; Nakamura et al., 2019). DR21(OH) is probably the only core where three different techniques have been used to derive the field strength (Crutcher et al., 1999; Hezareh et al., 2010; Girart et al., 2013). For the few sources with magnetic field strength derived from both (OH) Zeeman and dust polarization, the ratio of the plane-of-sky magnetic field component to its line-of-sight component, 4.7 ± 2.8 , is larger than the expected average value for random orientations (Myers and Basu, 2021). However, we should note that the OH Zeeman observations probably trace lower densities than (sub)mm dust observations. In any case, using both data sets, the magnetic fields appear to increase with volume density as $B \propto n^{2/3}$, indicating that magnetic field strength is significant but not enough to avoid the gravitational collapse (Myers and Basu, 2021). Finally, it is important to be aware that the interpretation of the observational data is sometimes a source of vivid debate (Mouschovias and Tassis, 2010; Crutcher et al., 2010; Tassis et al., 2014), and

the application at core scales should be taken with caution (Reissl et al., 2021; Liu et al., 2021).

5.5 Protostellar disks

One of the major predictions of magnetized models regards the properties of rotationally-supported disks: embedded young disks are expected to be compact and dust-rich. In this section, we briefly summarize recent constraints brought by observations of the sizes and masses of protostellar disks.

Maury et al. (2010, 2019) used the NOEMA CALYPSO survey, at 1.3 mm and 2.7 mm to characterize the disk properties in twenty-six Class 0 and I protostars. Modeling the millimeter dust continuum emission with a combination of envelope and disk contributions directly in the visibility space, they find an average disk size of < 50 au ± 10 au in the Class 0 objects, and 115 ± 15 au in the Class I objects. The VANDAM survey (Segura-Cox et al., 2018; Tobin et al., 2020) used VLA then ALMA observations of the mm dust continuum emission to characterize the radii of Class 0 and Class I disk sizes in Perseus and Orion. Their most recent results in Orion performing multi-wavelength analysis (25 Class 0 sources, 44 Class I sources) report smaller median dust disk radii than their preliminary analysis, with Class 0 disks having radii ~ 35 au in Orion (Sheehan et al., 2022), and no statistically significant difference between the properties of Class 0 and Class I disks. This later point may be specific to Orion, however, as our census of all embedded disks radii from the literature presented in Figure 4 does show a difference, with Class I disks being statistically more extended. Cox et al. (2017) and Encalada et al. (2021) used 2D Gaussian fits applied to the ALMA dust continuum images of Class I protostars in Ophiuchus and find respectively a median dust disk radius from 12.6 au to ~ 23.5 au. These measurements are also included in Figure 4.

These aforementioned studies rely mainly on the analysis of the thermal dust emission, but protostellar disks can also be identified thanks to

kinematic signatures. Inside the centrifugal radius, the gas rotates with nearly-Keplerian motions as the pressure and centrifugal acceleration balance the radial gravitational acceleration. Measuring the size of rotationally-supported disks in embedded protostars needs to distinguish the disk emission from that of the infalling envelope, kinematically. Identifying the transition from envelope kinematics dominated by infalling gas ($v_r \propto r^{-1/2}$ and $v_r > v_\phi$) to gas contained in a rotationally supported disk, with $v_\phi(r) \propto \sqrt{(G \times M_{\star+\text{disk}})/r}$ and $v_r \ll v_\phi$, is thus, in theory, a simple way of measuring disk gaseous sizes. In practice, the simultaneous contribution of gas kinematics from different origins, chemistry effects on molecular gas tracers, and projection effects of asymmetric gas motions make it a hard task to clearly measure the rotation velocity v_ϕ in protostellar envelopes down to the disk outer radius. Only few protostars show clear signatures of Keplerian motions that can be used to characterize their disk: in the few objects that have an estimate of the dusty disk sizes, the gaseous disk size and dusty disk sizes are similar, within the relatively large uncertainties associated (Ohashi et al., 2014; Yen et al., 2017; Bjerkeli et al., 2019; Maret et al., 2020; Harsono et al., 2014; Chou et al., 2014; Yen et al., 2014; Aso et al., 2015).

Protostellar disk masses are usually measured from the dust emission, estimating dust masses from a set of hypothesis on the dust properties then correcting by a gas-to-dust ratio to obtain gas masses. The choice of wavelength(s) for the dust observations is crucial: for example, in Perseus, Tychoniec et al. (2020) measure median dust masses of the embedded disks $\sim 5 \times 10^{-4} M_\odot$ for Class 0 and $2 \times 10^{-4} M_\odot$ for Class I from the VLA dust continuum emission at centimetre wavelengths. In comparison, dust masses from sub-millimetre dust emission in ALMA bands towards the same population of disks in Perseus are significantly lower, $1.4 \times 10^{-4} M_\odot$ and $4 \times 10^{-5} M_\odot$ for 38 Class 0 and 39 Class I respectively. These lower dust disk masses are in better agreement with the dust masses found in Orion embedded disks: it suggests that dust masses extrapolated

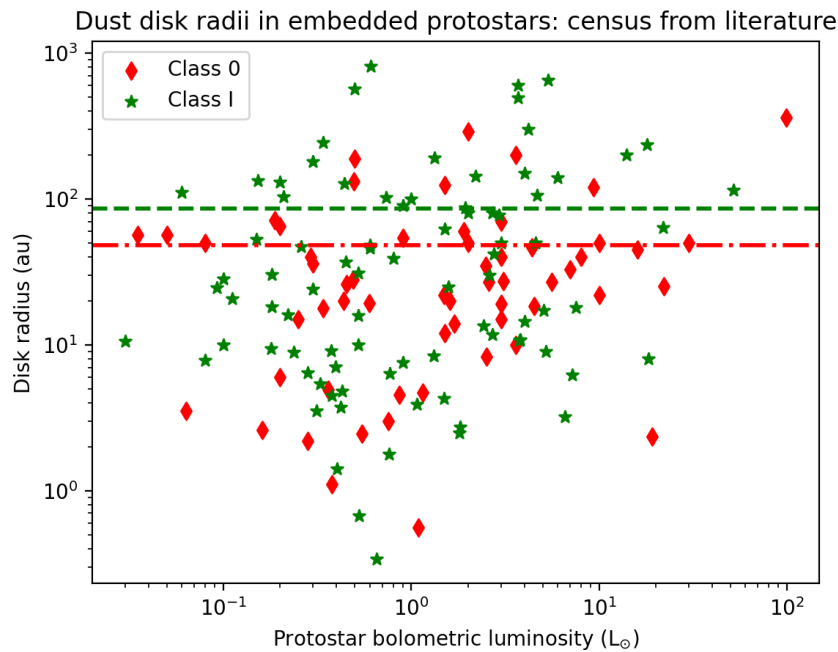


Figure 4. Class 0 (in red) and Class I (in green) protostellar disk radii observed, from the dust continuum emission at millimeter wavelengths ($\lambda < 2.7\text{mm}$). Most measurements stem from the CALYPSO survey (Maury et al., 2019) and the VANDAM survey (Sheehan et al., 2022). Other sources from Oya et al. (2014); Lee et al. (2018b); Yen et al. (2015b, 2017); Cox et al. (2017); Aso et al. (2015); Ohashi et al. (2014); Brinch and Jørgensen (2013); Harsono et al. (2014); Miotello et al. (2014); Sheehan and Eisner (2017); Encalada et al. (2021). The mean dust disk radii for each Class are indicated as horizontal lines (48 au for Class 0 and 86 au for Class I).

from long wavelengths may be significantly overestimated, due to the unknown emissivity and size distribution of dust grains in the dense environments that are disks. In Ophiuchus, the mean Class I disk dust mass is found to be significantly lower, $9 \times 10^{-6} M_{\odot}$ (Williams et al., 2019; Encalada et al., 2021): it is still about 5 times greater than the mean Class II disk mass in the same region, but the dispersion in each class is so high that there is a large overlap between the two distributions. Sheehan et al. (2022) used multi-wavelength analysis of the SED towards Orion protostars. These estimates are also associated to large error bars, but the multi-wavelength analysis they performed should allow to better discriminate the disk from the envelope contribution and hence provide more robust results. They find median dust mass $2 \times 10^{-5} M_{\odot}$ for the Class 0 protostars, and $1.5 \times 10^{-5} M_{\odot}$ for

the Class I protostars, pointing towards much smaller embedded disk masses and less clear mass differences between the evolutionary stages than suggested by previous simplistic estimates made from single wavelength analysis. Finally, when the temperature of embedded disks can be investigated, observational studies suggest these disks may be warmer than their older counterparts, with typical temperatures around 20-30 K (van't Hoff et al., 2020; Zamponi et al., 2021).

For the high mass stars, the rapid dynamical evolution and the larger distances make the detection of the rotationally supported disk more difficult, since they are in most cases surrounded by very massive molecular envelopes. This makes the identification of the disks more controversial. Resolving their velocity structures, masses, and sizes has been made possible only recently thanks

to ALMA. Relatively isolated disks are very rare, such as Orion I, which has unique features possibly related to a violent multiple star interaction event (Plambeck and Wright, 2016; Hirota et al., 2017; Ginsburg et al., 2019; Wright et al., 2022). Other clear cases of disks around massive stars, that appear to be a scaled up version of the ones around low-mass stars, are GGD MM1 (Girart et al., 2018; Añez-López et al., 2020b), G11.92-0.61 MM1 (Ilee et al., 2018), and G17.64+0.16 (Maud et al., 2019), with very massive ($2\text{--}5 M_{\odot}$), dense and hot ($\gtrsim 400$ K) disks. However, there are many cases reported in the literature where Keplerian velocity patterns can be fitted towards disk-like structures, which can extend from few hundreds to a thousand au (e.g. Sánchez-Monge et al., 2013; Johnston et al., 2015; Cesaroni et al., 2017; Beuther et al., 2017; Girart et al., 2017; Tanaka et al., 2020; Williams et al., 2022). In most cases, a detailed measurement of the gas temperature and surface density is needed to check the stability of such structures. The presence of disks around massive stars has also been found through near/mid-IR interferometry (Kraus et al., 2010; Frost et al., 2019).

These two works suggest that the observed massive disks are a scaled up version of low-mass disks, but need to be confirmed with larger samples.

5.6 Fragmentation into multiple systems

Measuring the multiplicity of Class 0 and I solar-type protostellar systems has been challenging and the focus of many observational works. Submillimetre/millimetre observations are the only reliable tool for characterizing Class 0 and I multiplicity, as near-infrared emission towards embedded protostars suffer from significant extinction due to the envelopes, and contamination by scattered light, while near-infrared observations are usually robust at characterizing multiplicity in more evolved YSOs (Duchêne and Kraus, 2013). The observed fraction of binary and multiple systems in low mass protostars are high, and similar to the multiplicity of main sequence stars in the field. On average, a multiplicity percentage of 64% is found

among Class 0 protostars with linear separations in the range 50 - 5000 au (e.g., Looney et al. 2000; Maury et al. 2010; Enoch et al. 2011; Tobin et al. 2013; Bouvier et al. 2021), whilst it is between 18% and 47% for Class I sources with linear separations in the range 45 - 5000 au (Haisch et al., 2004; Duchêne et al., 2004, 2007; Connelley et al., 2008a,b). For example, in the Orion molecular cloud, observations of 300 Class 0, I, or Flat Spectrum YSOs found a total of 85 multiple systems at separations $\lesssim 10000$ au, 58 multiples at separations $\lesssim 1000$ au, and only 47 multiples with maximum separations less than 500 au (Tobin et al., 2022). No statistically significant difference in the separations with evolutionary stages during the protostellar stages were found in the most complete studies so far, while tentative evidence is found that field stars and non-embedded YSOs may feature a lower number of wide (e.g., $a > 1000$ au) multiple systems than their embedded counterparts, in Orion (Tobin et al., 2022). Note that this result may be significantly driven by incompleteness at sampling wide systems around the most evolved YSOs and field stars: this limitation has now been partially lifted thanks to increasing astrometric precision and led, for example, to the discovery of a new large population of wide systems in Taurus within the range 1–60 kAU (Joncour et al., 2017). Finally, no statistically significant difference was found regarding the multiplicity fractions observed between regions of high and low YSO density, also in Orion.

Massive stars have a predilection for forming in clustered environments with other protostars, and their young embedded counterparts are thus often studied in cluster star-formation modes (Cyganowski et al., 2017). High mass star forming cores observed at high angular resolution appear to show different level of fragmentation (Beuther and Schilke, 2004; Rodón et al., 2012; Palau et al., 2013; Busquet et al., 2016; Sánchez-Monge et al., 2017; Liu et al., 2019; Sadaghiani et al., 2020). The process of fragmentation is hierarchical (Beuther and Schilke, 2004; Beuther et al., 2015) and appears to proceed down to disk scales (Beuther et al.,

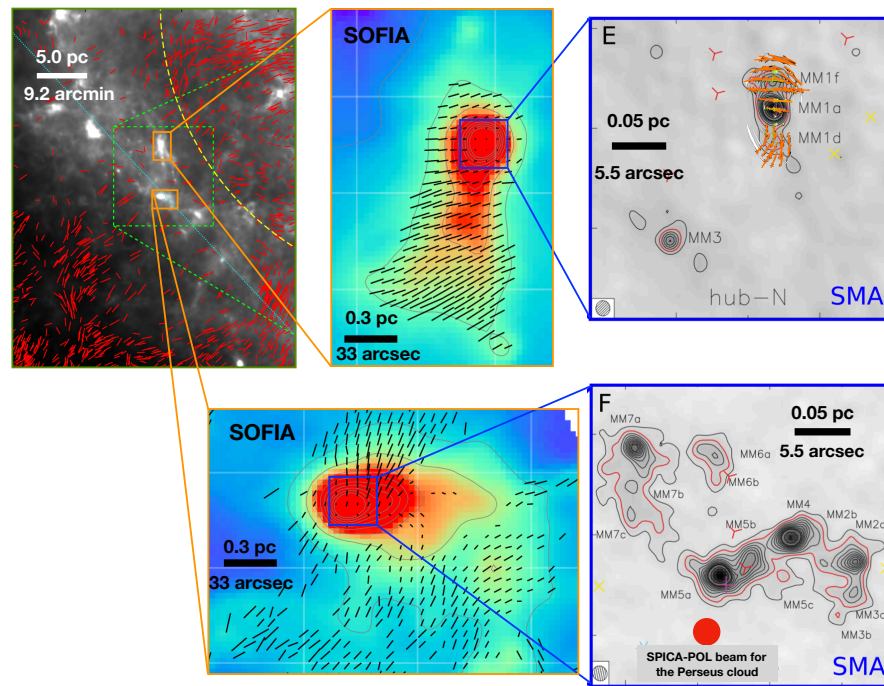


Figure 5. Composite images of the G14.225-0.506 massive star forming region (Busquet et al., 2016; Santos et al., 2016). Top left panel: R band optical polarization vectors (red segments) overlaid on Herschel $250\mu\text{m}$ image overlapped (from Santos et al. 2016). Central panels: SOFIA/HAWC+ $200\mu\text{m}$ images (beam $14''$) of the Northern (top) and Southern (bottom) hubs, with black segments showing the magnetic field direction (F. Santos, private communication). Right panels: Submillimeter Array (SMA) images of the 1.2 mm emission toward the centre of the Northern (top) and Southern (bottom) hubs (Busquet et al., 2016), with orange segments showing the magnetic field direction (Añez et al. in prep.).

2017; Busquet et al., 2019). The first systematic study of the level of fragmentation down to scales of ~ 1000 au suggested that this could be set by the initial magnetic field/turbulence balance (Palau et al., 2013). Subsequent studies found that the fragmentation level was only mildly correlated with the density profile, and that it is consistent with thermal or turbulent Jeans fragmentation (Palau et al., 2014, 2015, 2018; Beuther et al., 2018; Liu et al., 2019). However, in a more recent work when the fragmentation level is compared with the magnetic field properties derived from the dust polarization, there is a tentative correlation of the fragmentation level with the mass-to-flux-ratio (see Fig. 5, and Busquet et al., 2016; Añez-López et al., 2020a; Palau et al., 2021).

6 DISCUSSION: CONSTRAINTS ON MAGNETIZED MODELS FROM THE OBSERVATIONS

6.1 Magnetic fields

The observations of (sub-)millimeter polarized dust emission show that the magnetic field is detected in all dense environments producing stellar embryos. Assessing whether the observations can be trusted to infer statistically robust constraints on the magnetic fields threading protostellar cores, and compared to B-fields in models, requires the analysis of synthetic observations from magnetized models. Le Gouellec et al. (2020) and Valdivia et al. (2022) have post-processed outputs from non-ideal MHD models of protostellar evolution with the RAMSES code (Fromang et al., 2006) (see also the work of Kuffmeier et al. 2020 in Figure ??). Their work analyses the resulting synthetic polarized dust

emission maps, which are compared to the true B-field properties in the models and to observations. Valdivia et al. (2022) show that measurements of the line-of-sight averaged magnetic field line orientation using the polarized dust emission are precise enough to recover the mean field lines distribution with accuracy < 15 deg (typical of the error on polarization angles obtained with observations from large mm polarimetric facilities such as ALMA) in about 95% of the independent lines of sight peering through protostellar envelopes at all radii. When focusing on the smaller envelope radii < 500 au, where the magnetic field lines are more likely perturbed from the initially smooth configuration by infall and outflow and opacity effects kick in, 75% of the lines of sight still give robust results. Finally, Valdivia et al. (2022) and Le Gouellec et al. (2020) find that the polarization fraction is correlated to the degree of organization of the magnetic field along the line of sight, confirming that the behavior observed at larger scales, in less dense gas, holds true down to the scales of the envelopes of protostars. Le Gouellec et al. (2020) find that the dust alignment efficiency does not significantly vary with local gas density in their observations, and that the synthetic maps only can reproduce the observed polarimetric data when significant irradiation from the central protostar is included. Lam et al. (2021) have used numerical models compared to ALMA observations of the polarized dust emission by Cox et al. (2018): comparing polarization fractions they also conclude that dust polarization at ALMA wavelengths is most likely due to magnetically aligned grains in inner envelopes and dust scattering in disks.

Observationally, the correlation between outflow axis and the mean magnetic field direction has received a lot of attention because it is believed that the efficiency of magnetic braking to redistribute angular momentum and prevent the growth of disks to large radii depends on the configuration of the core's magnetic field with respect to the core's rotation axis when the collapse starts (Joos et al., 2012; Hirano et al., 2020), as portrayed

in Fig. 6. Using an SMA survey of twenty low-mass protostars, Galametz et al. (2018, 2020) has found that the protostellar envelopes tend to have a higher angular momentum associated to rotation on 5000 au scales if the mean envelope magnetic field measured at similar scales is misaligned with the rotational axis of the core, assumed to coincide with the outflow axis. On the other hand, observations analyzed in Yen et al. (2021b) have shown no correlation of the dust continuum protostellar disk radii with the misalignment between the magnetic fields and outflow axes in Orion A cores. Protostellar gas kinematics from the SMA MASSES (sample of 32 protostellar envelopes in Perseus) survey brings further support to the scenario proposed by Galametz et al. (2020), with a significant correlation between the rotational velocity gradients (at 1000 au, normalized by the infalling velocity gradients) and the misalignment angles between the magnetic fields and outflows (Gupta et al., 2022). At the very small envelope radii, the mean B-field direction are observed to be randomly aligned with respect to the outflow axis (Hull et al., 2013). However, as reported by Hull et al. (2014), there is evidence that cores with lower fractional polarization tend to have their outflows perpendicular to the mean B-field, which may suggest the existence of a non-negligible toroidal field morphology (caused by the core/disk rotation) in addition to the poloidal one caused by the envelope-disk accretion.

These results may be confronted to models where the magnetic field is efficient at reducing the amount of angular momentum transmitted to the inner envelope scales (< 1000 au), inhibiting the formation of large hydro-like disks. In some cases, numerical simulations have shown tentative evidence of better alignment of core-scale B fields and outflows in the more magnetized models (Lee et al., 2017). However, these observational results may also support the hypothesis that the angular momentum responsible for the formation and growth in size of protostellar disks has a more local origin, at a few hundreds of au scales, as discussed in recent theoretical studies

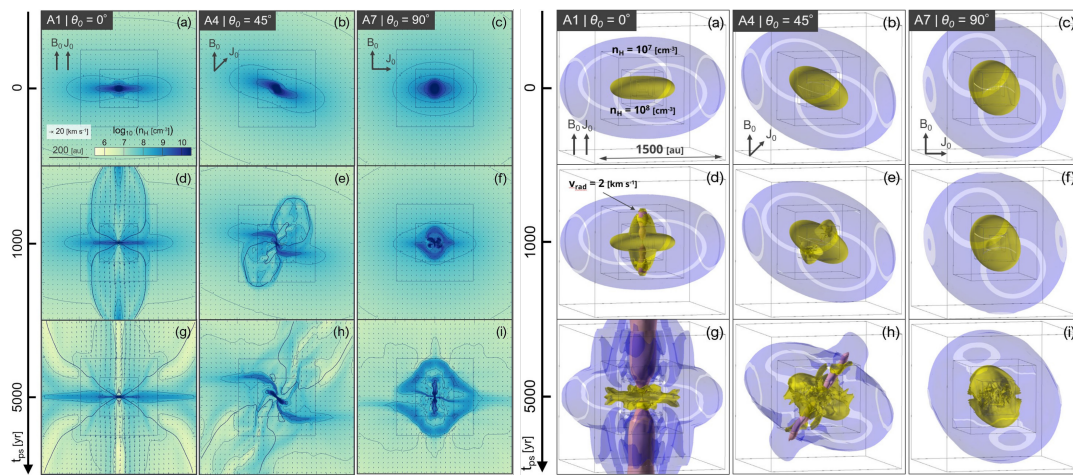


Figure 6. Left: Density (color and contours) and velocity (arrows) distributions in models from Hirano et al. (2020), implementing different angles between the magnetic field initial direction and the initial rotation axis of the core, at $t_{ps} = 0, 1000,$ and 5000 yr after protostar formation. The box size is 780 au. Right: Three-dimensional structures for the same models, highlighting two isodensity contours in purple and yellow, and one isovelocity contour of radial velocity $v_{rad} = 2 \text{ km s}^{-1}$ (in red). Note the absence of an outflow in the case of orthogonal configuration (third column): this case thus seems unrealistic considering the prevalence of outflows observed around low-mass protostars.

following the disk evolution and angular momentum evolution in star-forming cores (Verliat et al., 2020; Xu and Kunz, 2021; Lee et al., 2021b). Future observations will undoubtedly bring more constraints on the dynamical role of B-fields to regulate the protostellar collapse and set the pristine disk properties, with the upcoming large surveys thanks to the development of polarimetric capabilities and tools to model, e.g., polarized dust emission. Observations, with e.g. the large radio interferometers and next generation of mid-infrared facilities, of the small scale structures of these young disks, still largely unresolved spatially, will also shed light on this question.

6.2 Coupling the magnetic field to protostellar material

Observations of the low dust emissivities and high polarization fractions at mm wavelengths in embedded protostars suggest that partial grain growth, maybe up to grain sizes $> 100 \mu\text{m}$ could have already occurred during the first 0.1 Myr of the star formation process. If these low emissivities and high polarization fractions do indeed trace a population of large dust grains in the inner layers

of protostellar envelopes less than 0.1 Myrs old, the timescales to grow grains up to sizes $> 100 \mu\text{m}$ in dense star-forming material may need to be revised. For example, considering porous dust grains may help in growing grains to sub-millimeter sizes in a few dynamical timescales during the protostellar collapse (Ormel et al., 2009). Also, since small grains are not only coupled to the gas but also to the magnetic field, a magnetized collapse may also help segregating the grains with different charges, and ultimately shortening the grain coagulation timescale (Hoang, 2021). Also, the presence of rather large grains at early stages in the protostellar envelopes may increase the ability of protostellar disks to be efficient forges to build up even bigger dust grains, that are re-injected in envelopes thanks to protostellar winds and outflows (Wong et al., 2016; Bate and Lorén-Aguilar, 2017; Lebreuilly et al., 2020; Ohashi et al., 2021; Tsukamoto et al., 2021). Figure 7 shows an artist view of such circulation processes potentially affecting dust grains during the protostellar phase.

Moreover, observational evidences of grain growth during the embedded stages also bear strong consequences on the efficiency of magnetic fields to

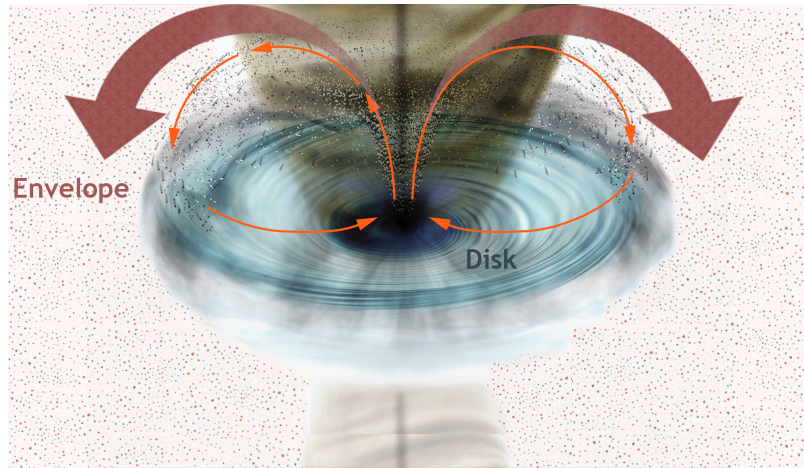


Figure 7. Artist impression of the dust growth and recycling from disk to envelope thanks to outflowing gas during the protostellar stage. Modified from an original illustration in Tsukamoto et al. (2021)

regulate the transport of angular momentum. Indeed, whereas in the diffuse interstellar medium, electric charges are carried by electrons and protons, in the dense cores and particularly at high densities, the small dust grains are the main charge carriers (Nishi et al., 1991; Nakano et al., 2002; Zhao et al., 2016). The disappearance of small dust grains while forming bigger grains increases magnetic resistivities (Nishi et al., 1991; Guillet et al., 2020a) and consequently let more B flux leak outwards during the collapse of the gas from the envelope onto the star-disk system (Zhao et al., 2021; Guillet et al., 2020b). Hence the disk properties may also depend strongly on the dust properties in the inner envelope.

The influence of the grain distribution on disk formation has been investigated through numerical simulations by Zhao et al. (2016). By removing the population of very small grains, the authors conclude that the ambipolar diffusion is enhanced by 1-2 orders of magnitude, see Figure 8. As expected the numerical simulations reveal that indeed the centrifugally supported disks, which form, sensitively depend on the presence of the very small grains. For instance, for a particular set of parameters (with a relatively strong field aligned with the rotation axis), no disk would form when a MRN grain distribution is assumed while disks of several tens of AU radius form when a

truncated MRN distribution is employed. Let us stress that the presence of very small grains in dense cores is presently poorly constraint. From a theoretical point of view, Guillet et al. (2020b) have shown that the latter may be efficiently removed by coagulation due to the drift between different dust species induced by ambipolar diffusion (see also Silsbee et al., 2020). To what extent this population could not be replaced, for instance by fragmentation of bigger grains, remains to be investigated. At disk scales, where the large densities are favorable for rapid dust growth, up to $a_d \sim 1$ mm, the magnetic resistivity can become many orders of magnitude bigger if small grains are rare, weakening ambipolar diffusion and recoupling the magnetic field and the gas.

Resistivities are also strongly dependent on the ionisation rate. Whereas most of the calculations assumed a value of a few $\zeta = 10^{-17} \text{ s}^{-1}$ inferred from typical cosmic ray galactic abundances (Padovani et al., 2009a), more extreme ionisation rates and their consequences on disk formation, have been recently explored. Wurster et al. (2018) performed simulation with ζ varying from 10^{-13} to 10^{-24} s^{-1} . They concluded that for $\zeta > 10^{-14} \text{ s}^{-1}$, the results are essentially identical to ideal MHD while for $\zeta < 10^{-24} \text{ s}^{-1}$, they are close to hydrodynamics. Kuffmeier et al. (2020) specifically explored the disk radius and mass dependence on

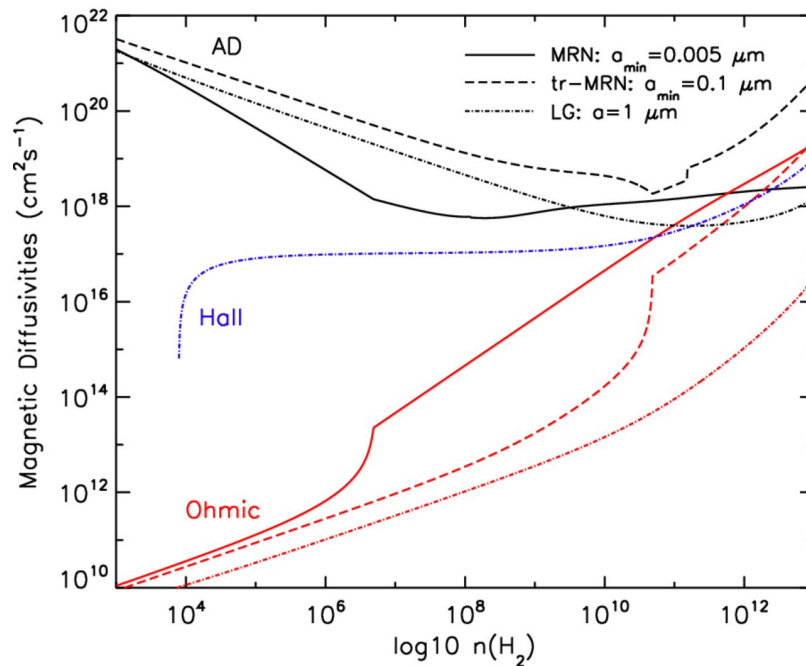


Figure 8. Change of MHD resistivities when removing the very small grains, from Zhao et al. (2016).

the ionisation rate, varying it by a factor of 10 from $\zeta = 10^{-17}$ to $\zeta = 10^{-16} \text{ s}^{-1}$. Performing bi-dimensional simulations with a mass-to-flux of 2.5, they found that with the highest ζ , no disk forms while a few tens of AU one forms with their smallest ζ . They further propose that cosmic ray abundances may control disk mass and size and explain the differences between disks observed in various regions (e.g. Cazzoletti et al., 2019).

6.3 Gas kinematics: rotation, mass infall and outflow rates

Observations do not suggest that cloud rotation is transmitted to star-forming cores (Tatematsu et al., 2016; Hsieh et al., 2021). At core scales, both hydrodynamical and magnetized models of core formation and evolution have shown that they do not produce rotating cores with the high angular momentum values measured by e.g. Goodman et al. (1998) at 0.1pc scales. Recent observations and models suggest that the angular momentum measured at core scales (e.g. $\sim 5000 \text{ au}$) could be due to non-axisymmetric motions associated to, e.g., turbulent and gravitational processes (Burkert and Bodenheimer, 2000; Offner et al., 2008; Dib

et al., 2010; Kuznetsova et al., 2019; Verliat et al., 2020). Hence, large scales velocity gradients in envelopes should not be interpreted automatically as organized rotation: for characterizing the motions responsible for the angular momentum observed, and as illustrated in Figure 9, resolved observations and their comparisons to model predictions are key. Finally, the angular momentum of the gas measured at envelope radii $< 1000 \text{ au}$ would predict disk whose sizes are broadly consistent with the observed ones, although observations reveal a tentative decrease of j_{spe} in inner envelopes, which may trace a decrease of angular momentum at small radii (Gaudel et al., 2020). Observations of complex gas kinematics in protostellar envelopes, from disturbed core-scale velocity gradients to localized streamers (see Figure 3) connecting the envelope to the disk scales confirm the wealth of observational evidence that the monolithic vision of collapse which prevailed in the past decades needs to be revised.

The rather high values of mass infall rates found in Class 0 protostars seem at first sight inconsistent with observed protostellar luminosities. While the bolometric luminosities of Class 0 protostars are

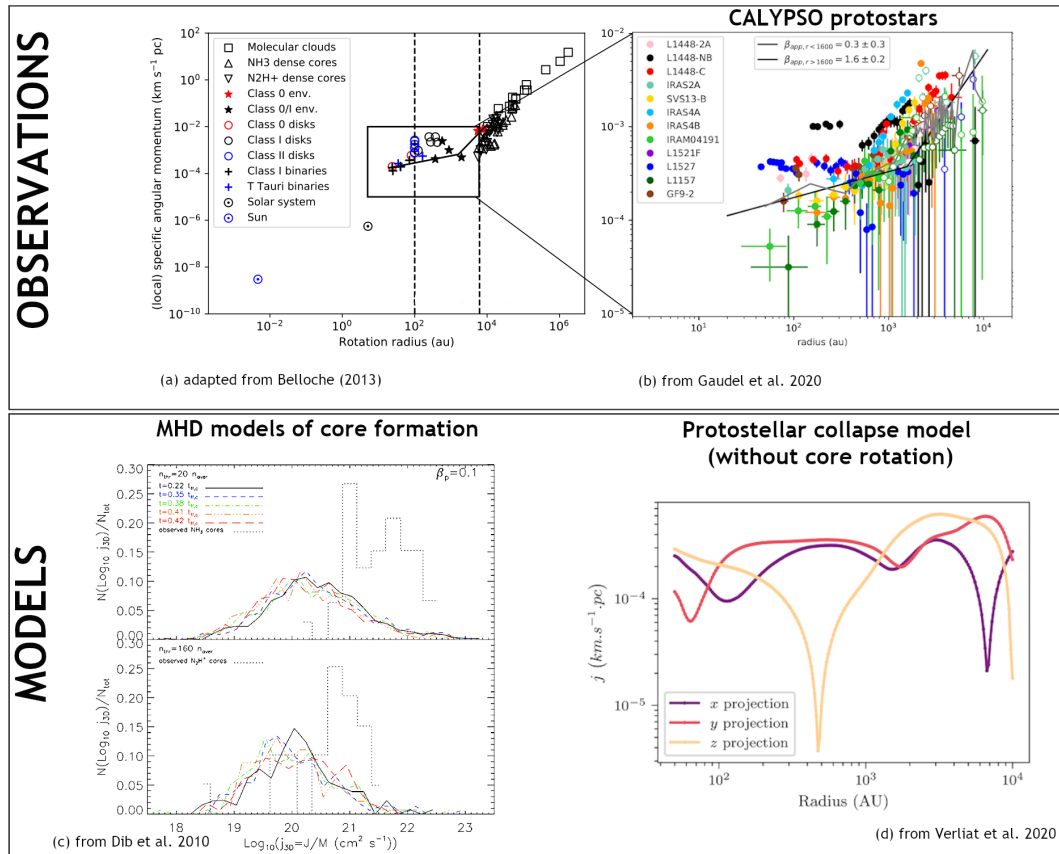


Figure 9. Observations and models of the angular momentum at core scales and disk scales, from Belloche (2013); Gaudel et al. (2020); Dib et al. (2010); Verliat et al. (2020).

typically a few L_{\odot} (with large variations from object to object), such accretion rates should produce a accretion luminosities a few tens of L_{\odot} . This is the well known luminosity problem (Dunham and Vorobyov, 2012), which was proposed to be solved with a scenario of quiet accretion including sporadic large accretion bursts. It remains unclear how such rare events could be captured so efficiently by observations measuring the gas accretion rates, as a recent ALMA survey of protostars in Perseus suggest the frequency of the bursts decrease with protostellar evolution, from a burst every 2400 yr in the Class 0 stage to 8000 yrs in the Class I stage (Hsieh et al., 2019). However, this scenario finds support in observations of molecular species: sudden temperature changes due to short but vigorous accretion bursts would explain why CO is observed where the current envelope temperature predicts it should be frozen onto dust grains (<

30K) for example (Anderl et al., 2016; Cieza et al., 2016; Frimann et al., 2017). It may also be that our lack of understanding of the physical conditions at the very small scales where most of the radiation is reprocessed to produce the observed luminosity, prevents us from properly model the expected luminosities, or that the gas mass infall rates measured at few hundreds of au in the envelopes are not representative of the true accretion rates at much smaller radii, onto the protostellar objects. Supporting this last hypothesis, it is interesting to note that MHD models following the evolution of low-mass cores find typical mass accretion rates $\sim 10^{-6} M_{\odot}$ per year, with large variations (Hennebelle et al., 2020; Kuznetsova et al., 2020). The global mass accretion rate from the disk to the central star is lower when the disk structure is properly modeled, and the short-term variation (bursts) of the mass accretion is also highly

attenuated with increased resolution (Kuffmeier et al., 2018; Lee et al., 2021b). It seems therefore that either the protostellar accretion rates obtained from observations are over-estimated, which could be due to sampling the inner envelope and not the disk-star connection, or the models predict slower mass accretion than protostars really do accrete. We stress that the existence of preferential directions along field lines, and the development of highly non-axisymmetric collapse may be responsible, in magnetized models, to regulate the mass accretion rate directly from the inner envelope to the central star, without the need to transit through the disk. In their MHD models of the evolution of massive cores into protostars Mignon-Risse et al. (2021) finds average mass accretion rates on the central object around $\sim 10^{-3} M_{\odot}$ per year, which is also about an order of magnitude lower than estimates from the observations towards similarly massive protostars.

6.4 The formation of disks

Recent observations benefiting from increased spatial resolution and sensitivities have firmly established that most disks around embedded protostars are compact and not as massive as early studies had suggested. The current disk radii estimates from the literature are shown in Figure 4. Such compact disks are difficult to produce in large fractions with purely hydrodynamical analytical models of disk formation conserving angular momentum, but could be a natural outcome of magnetized models of disk formation and models of anisotropic collapse (Hennebelle et al., 2020; Kuznetsova et al., 2022). Obtaining self-consistent disk populations from numerical simulations is quite challenging because it requires to be able to treat simultaneously spatial scales sufficiently small to resolve the protostellar disks while in the same time advance sufficiently the clump scales to allow the formation of a statistically significant number of disks. For this reason, only two studies have been reporting disk population self-consistently formed from numerical simulations. Bate (2018) presents Smooth particle hydrodynamical simulations of

a $500 M_{\odot}$ clump including radiative transfer, producing a disk population whose sizes ranges from about 10 to few 100 AU. The author compares the mass distribution inferred from simulations with several observational surveys and concludes that the disk formed in the simulations are up to 10 times more massive. Lebreuilly et al. (2021) present three adaptive mesh refinement simulations of $1000 M_{\odot}$ clump which treat radiative stellar feedback and both ideal and non-ideal MHD. The spatial resolution is up to 1 AU. Figure 10 shows for the three runs, the mass distribution and the radius distribution, respectively. For comparison, the data of VLA Class 0 disk mass distribution (purple, Tychoniec et al., 2020) have been reported, as well as the disk radius inferred by the Calypso (Maury et al., 2019) and VANDAM projects (Segura-Cox et al., 2018; Tobin et al., 2020). Altogether and as already suggested from individual studies that compared HD, MHD, and non-ideal MHD numerical models for single objects, the hydrodynamical disks appear to be bigger than the MHD ones and overall in less good agreement with observations than when magnetic field is included, particularly regarding the disk radius distribution. Whereas there is some scatter in the distributions, these first population studies, properly taking into account the initial conditions, appear to be promising tools for future comparisons to observations.

A local origin of the angular momentum building rotationally-supported disks has been proposed by some models: for example, Verliat et al. (2020) have shown that the observations of angular momentum in protostellar envelopes can be satisfactorily reproduced if the disk formation results from anisotropies in the local velocity field, and not a consequence of the transfer of angular momentum from organized large scale core rotation. As shown in Figure 9, some observational evidence may support that scenario, with a good agreement between those models and the observations of the specific angular momentum found in envelopes, or more recently for example the observations of the L1489 protostar suggesting only the inner part of

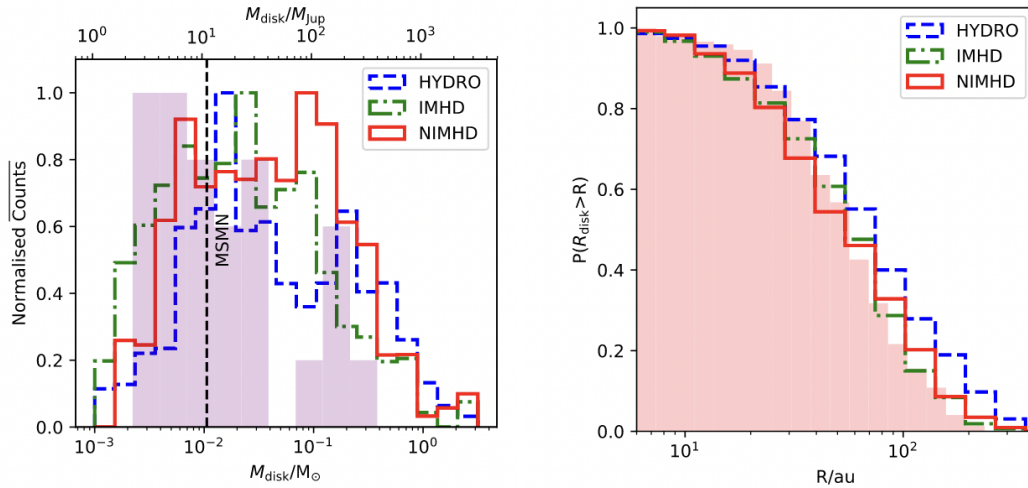


Figure 10. Left panel: Distributions of disk sizes obtained for the three disk population synthesis models presented in Lebreuilly et al. (2021) (note that the sizes are normalized so that their peak in the y-axis is 1). The mass of the minimum mass for the Solar nebula (MSMN) is indicated as a dashed line. Right: Cumulative distribution function of disk radius for the three models presented in Lebreuilly et al. (2021).

the envelope, at radii $< 4000 - 6000$, may be directly involved in forming the central star (Sai et al., 2022). This would imply that the material participating directly to building the disk and the star contains much less angular momentum than the values measured at core scales, lessening the angular momentum problem for star formation.

Although it was not shown observationally in the most embedded disks, models suggest it may be that the big dust drifts even during the early disk phases, leading to different apparent disk sizes recovered at different wavelengths. The uncertainties regarding dust properties in these specific conditions also affect the dust masses and hence the disk masses that are estimated in these objects. If observations suggesting young embedded disks are warm (20-30 K, van't Hoff et al. 2020; Zamponi et al. 2021) are confirmed, it could suggest gas kinematics within the disc play a significant role in heating the disk, as the protostellar radiation is expected to be highly extinct at such very high densities. For example, Zamponi et al. (2021) compare observations with synthetic observations of MHD protostellar disk models formed after the collapse of a dense core, and suggest that heating due

to gravitational instabilities in the disk is able to generate dust temperatures in agreement with observational constraints in the IRAS 16293 Class 0 disk.

The exact role of magnetic fields in setting the disks sizes and masses during the embedded phases can only be quantitatively addressed thanks to the comparison of observed properties to the outcomes of models. Maury et al. (2018) have shown that the B field geometry, small disk size and the kinematics of the B335 inner envelope can only be explained by a family of MHD models where the initially poloidal field in B335 is being pulled in the dominant direction of the collapse, but yet is strong enough ($\mu \sim 6$) to counteract partially the transfer of angular momentum inwards. In B335, they show the magnetic field is very likely to regulate the formation processes of the protostellar disk, constraining the size of the protostellar disk to < 20 au (see Figure 11). The role of the magnetic field in setting the disk size in B335 has also been discussed in subsequent studies (Yen et al., 2019; Bjerkele et al., 2019; Imai et al., 2019). However, new observations by Cabedo et al. (2022) suggest that the gas at small envelope radii is strongly

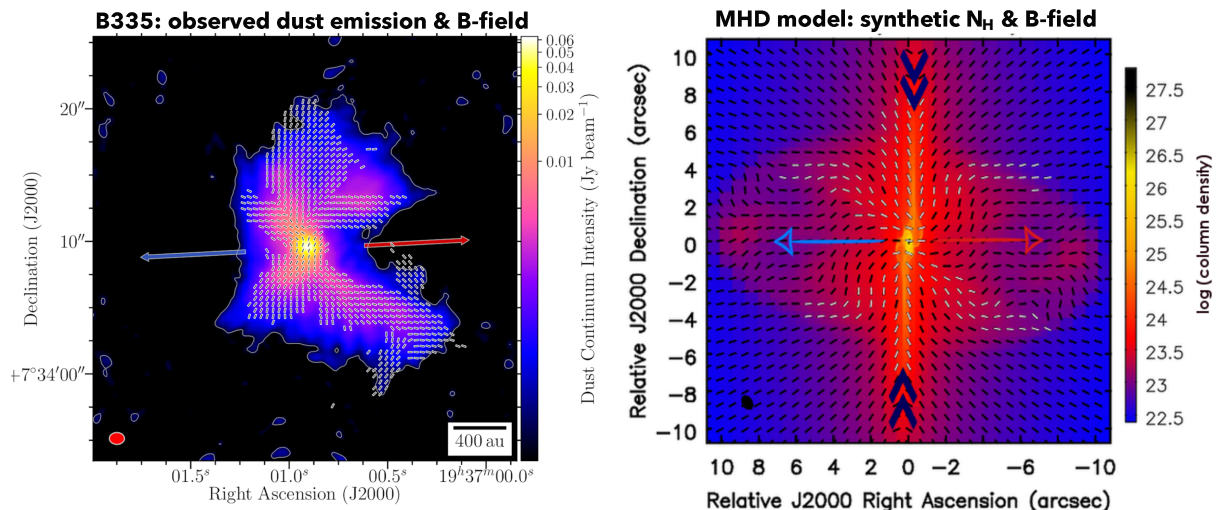


Figure 11. Observation and best model to match the properties in the B335 protostar, from Maury et al. (2018) and new ALMA observations (in prep.). The observed B field geometry shown in the left panel, the small disk size and the kinematics of the B335 inner envelope can only be explained by a family of MHD models where the initially poloidal field in B335 is being pulled in the dominant direction of the collapse, but yet is strong enough ($\mu \sim 6$) to counteract partially the transfer of angular momentum inwards and set the disk size in this Class 0 protostar: the best model is shown in the right panel.

ionized in B335, and points towards conditions typical of ideal MHD. It may very well be that the star-disk building phase consists in a succession of non-ideal and ideal MHD conditions in the “life of the protostar”. It would be possible to grow a quite large disk if it is formed before the onset of high ionization around the protostar (due to the protostar itself and the production of CR in the B-field lines around the protostar), while if the disks are still compact when the local ionization starts to increase at a fast pace, it may be more difficult to form large disks in the second half of the protostellar phase.

6.5 Influence of magnetic field on the formation of multiple systems

The fragmentation of low mass cores has been the subject of several studies (see e.g. Matsumoto and Hanawa, 2003; Goodwin et al., 2004). Several modes of fragmentation have been identified. Generally speaking, it is induced by the density fluctuations that are generated during the collapse on one hand by gravo-turbulence processes within the envelope and on the other hand through the formation of massive centrifugally supported unstable disks. The outcome of fragmentation

therefore entirely depends on the initial conditions, particularly rotation and turbulence initial values, but also on the amplitude of the initial density perturbations. It has been generally found however that under typical conditions and in the absence of magnetic field, a solar mass dense core tends to produce few fragments (say 2-10).

Several studies have been dedicated to the influence of magnetic field in this process (e.g. Machida et al., 2008; Hennebelle and Teyssier, 2008; Commerçon et al., 2010; Wurster et al., 2017; Wurster and Bate, 2019; Hennebelle et al., 2020), covering a broad range of parameters in terms of magnetic field intensity, rotation and initial turbulence. From these studies, clear trends can be inferred. First, the higher the rotational and/or turbulent energy, the more prone to fragmentation is the core. Numerical models of turbulent dense cores suggest that the directions of the specific angular momentum axis tends to vary as a function of envelope scales (Joos et al., 2013; Matsumoto et al., 2017), and that misaligned systems can form in turbulent conditions. Some numerical models also suggest that turbulent velocity fluctuations around protostellar cores may be responsible for

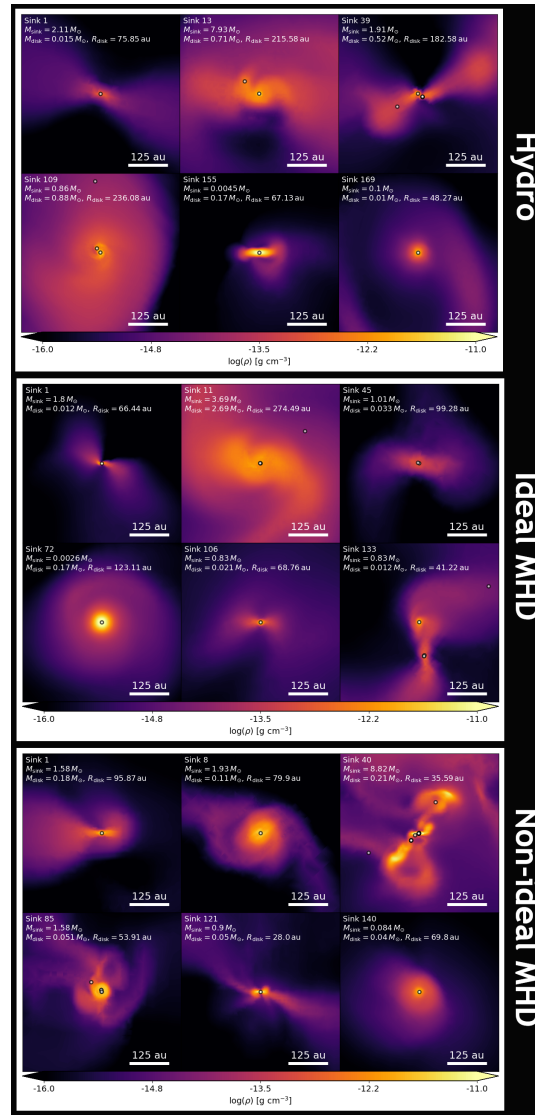


Figure 12. Lebreuilly et al. (2021): A sample of disks formed in three massive clump simulations, hydrodynamics, ideal MHD and non-ideal MHD (ambipolar diffusion). Hydrodynamical disks tend to be bigger and ideal MHD ones smaller than when ambipolar diffusion is included.

setting the rotational motions of these cores (Misugi et al., 2019). However, magnetic field has a drastic influence and in the case of low mass cores, mass-to-flux ratios as high as $\mu > 5 - 10$ may entirely suppress the formation of fragments. This is because in low mass cores, turbulence is at best trans-sonic and the density fluctuations induced by turbulence remain limited. Therefore, the dominant fragmentation mode is through the formation of massive disks. However, in the presence of magnetic field the disk sizes and masses are much smaller, and therefore they tend to be

stable. Another interesting trend is that the cores in which the magnetic field is initially perpendicular to the rotation axis are less prone to fragmentation than when it is aligned. One important fact to be taken into account however is that the amplitude of the density perturbations is also an important parameter, and the mentioned trends have been inferred for modest density fluctuations (typically below 10%). When the density fluctuations have a large amplitude, say of about 50%, they are sufficiently unstable to collapse individually even in the absence of rotation. In this case, magnetic field

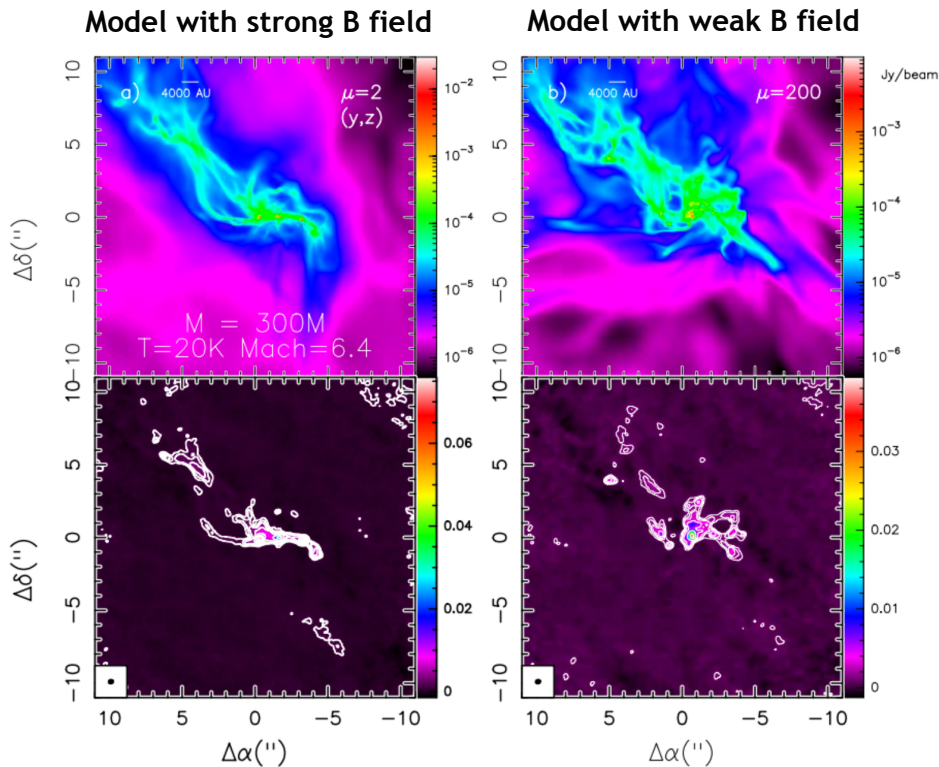


Figure 13. Models of the gravitational collapse of a $300 M_{\odot}$ clump, with gas temperature $T = 20$ K, and Mach number 6.4, from Fontani et al. (2018). Column density maps of two models are shown in the upper row, in the presence of a strong (left) magnetic field and a weak one (right). The lower row shows ALMA synthetic observations of the models using the 280 GHz dust continuum emission. Fewer fragments are seen in the more magnetized case.

is unable to impede fragmentation (Hennebelle and Teysier, 2008; Wurster et al., 2017). This would imply that the fragmentation is driven by the larger scales and the assembling process of the dense cores.

The influence of the magnetic field on the fragmentation of massive clumps has also been investigated. Because of the large amplitude of the density fluctuations, the impact of magnetic field on the fragmentation is relatively less important than that found in the case of low mass cores. For instance, Hennebelle et al. (2011) and Myers et al. (2013) found that in the presence of a significant magnetic field (e.g a few mG for mass-to-flux ratios around 2), the number of self-gravitating fragments is reduced by a factor of about 2. Fontani et al. (2016) and Fontani et al. (2018) have carried out observations and

simulations of massive clumps. They have studied and compared the fragmentation properties of the clumps from observations and simulations using synthetic images that mimic the observations as shown in Fig.13. They concluded that the fragmentation properties within the observations are better reproduced by the significantly magnetized models (typically $\mu = 2$) than by the weakly magnetized ones.

7 SUMMARY

Understanding how protostars and planet-forming disks form are cornerstone questions for us to understand both the stellar populations setting the evolution of our Universe and the conditions responsible for producing the planetary systems observed around most stars. The recent progresses made through observations and simulations suggest

that magnetic field is modifying in depth the outcome of the collapse and the formation of stars, by adding an extra support to the gas, by reducing the angular momentum available to build the disks, by launching outflows and even possibly favoring the dust grain coagulation into pebbles. Observations suggest that the so-called magnetic braking catastrophe is an issue that is solved, alleviated by implementing realistic physical conditions (turbulence, anisotropies of the density field, non-homogeneous initial B field due to conditions of core assembly and local environment, gas ionization and dust properties) in MHD models.

If the magnetized scenario we propose is common, recent work suggest that the angular momentum problem for star formation may be actually "solved" not by the formation of large disks but by the combination of (i) lack of organized rotation motions at large envelope radii, (ii) the inefficient angular momentum transport due to magnetic braking in the inner envelope (and angular momentum removed through rotating outflows generated by the presence of the magnetic field) and (iii) a local origin of the angular momentum incorporated in the star-disk system.

Major questions however remain to be solved for the next generations of astrophysicists. First, our understanding of the origin of the angular momentum that eventually build the disks is very incomplete. Whereas some of the gas momentum could obviously be inherited from larger scales, inertial processes naturally produce angular momentum in a non-axisymmetric system, opening the possibility to disks weakly related to large scale angular momentum. This possible scenario questions the effective role of magnetic braking at envelope scales to set the disk sizes, as local processes may be more important in shaping the outcome of star and disk formation. That means to better understand the transport of the magnetic field by processes like reconnection diffusion and ambipolar diffusion and their importance on regulating angular momentum transport and disk formation in the different stages. Characterizing

the properties of the compact protostellar disks, with very high angular resolution observations, will also be a key to set constraints and refine our models. Second, this scenario deeply relies on the efficiency of magnetic fields to couple to the gas reservoirs. This efficiency is driven by a complex set of physical conditions, which remain up to this day largely unconstrained. Our current knowledge of magnetic resistivities remains thus hampered by very large uncertainties. It is therefore key, in the future, that observations characterize both the gas and dust properties in embedded protostars, and are compared to models so we know whether magnetic braking is much more efficient in locations, and epochs, that are critical for setting the disk and stellar properties. Answering these questions will be a fascinating challenge that will require us to produce robust measurements of the magnetic intensity and topology in large samples of objects, but also find clever ways to access the gas ionisation fraction and dust grain properties in young embedded protostars.

ACKNOWLEDGMENTS

AM acknowledges support from the European Research Council (ERC) under Starting grant number 679937 – ‘MagneticYSOs’. This work was also partially supported by the program Unidad de Excelencia María de Maeztu CEX2020-001058-M. JMG also acknowledges support by the grant PID2020-117710GB-I00 (MCI-AEI-FEDER,UE). PH acknowledges support from the European Research Council synergy grant ECOGAL (Grant : 855130)

REFERENCES

- Añez-López, N., Busquet, G., Koch, P. M., Girart, J. M., Liu, H. B., Santos, F., et al. (2020a). Role of the magnetic field in the fragmentation process: the case of G14.225-0.506. *A&A* 644, A52. doi: 10.1051/0004-6361/202039152
- Añez-López, N., Osorio, M., Busquet, G., Girart, J. M., Macías, E., Carrasco-González, C., et al. (2020b). Modeling the Accretion Disk around

- the High-mass Protostar GGD 27-MM1. *ApJ* 888, 41. doi:10.3847/1538-4357/ab5dbc
- Allen, A., Li, Z.-Y., and Shu, F. H. (2003). Collapse of Magnetized Singular Isothermal Toroids. II. Rotation and Magnetic Braking. *ApJ* 599, 363–379. doi:10.1086/379243
- Alves, F. O., Caselli, P., Girart, J. M., Segura-Cox, D., Franco, G. A. P., Schmiedeke, A., et al. (2019). Gas flow and accretion via spiral streamers and circumstellar disks in a young binary protostar. *Science* 366, 90–93. doi:10.1126/science.aaw3491
- Alves, F. O., Cleeves, L. I., Girart, J. M., Zhu, Z., Franco, G. A. P., Zurlo, A., et al. (2020). A Case of Simultaneous Star and Planet Formation. *ApJ Letters* 904, L6. doi:10.3847/2041-8213/abc550
- Alves, F. O., Frau, P., Girart, J. M., Franco, G. A. P., Santos, F. P., and Wiesemeyer, H. (2014). On the radiation driven alignment of dust grains: Detection of the polarization hole in a starless core. *A&A* 569, L1. doi:10.1051/0004-6361/201424678
- Alves, F. O., Girart, J. M., Padovani, M., Galli, D., Franco, G. A. P., Caselli, P., et al. (2018). Magnetic field in a young circumbinary disk. *A&A* 616, A56. doi:10.1051/0004-6361/201832935
- Alves, F. O., Vlemmings, W. H. T., Girart, J. M., and Torrelles, J. M. (2012). The magnetic field of IRAS 16293-2422 as traced by shock-induced H₂O masers. *A&A* 542, A14. doi:10.1051/0004-6361/201118710
- Anderl, S., Maret, S., Cabrit, S., Belloche, A., Maury, A. J., André, P., et al. (2016). Probing the CO and methanol snow lines in young protostars. Results from the CALYPSO IRAM-PdBI survey. *A&A* 591, A3. doi:10.1051/0004-6361/201527831
- André, P., Ward-Thompson, D., and Barsony, M. (1993). Submillimeter continuum observations of Rho Ophiuchi A - The candidate protostar VLA 1623 and prestellar clumps. *ApJ* 406, 122–141. doi:10.1086/172425
- André, P., Ward-Thompson, D., and Barsony, M. (2000). From Prestellar Cores to Protostars: the Initial Conditions of Star Formation. *Protostars and Planets IV*, 59–+
- Artur de la Villarmois, E., Jørgensen, J. K., Kristensen, L. E., Bergin, E. A., Harsono, D., Sakai, N., et al. (2019). Physical and chemical fingerprint of protostellar disc formation. *A&A* 626, A71. doi:10.1051/0004-6361/201834877
- Aso, Y., Ohashi, N., Saigo, K., Koyamatsu, S., Aikawa, Y., Hayashi, M., et al. (2015). ALMA Observations of the Transition from Infall Motion to Keplerian Rotation around the Late-phase Protostar TMC-1A. *ApJ* 812, 27. doi:10.1088/0004-637X/812/1/27
- Bate, M. R. (2018). On the diversity and statistical properties of protostellar discs. *MNRAS* 475, 5618–5658. doi:10.1093/mnras/sty169
- Bate, M. R. and Lorén-Aguilar, P. (2017). On the dynamics of dust during protostellar collapse. *MNRAS* 465, 1089–1094. doi:10.1093/mnras/stw2853
- Bel, N. and Leroy, B. (1989). Zeeman splitting in interstellar molecules. *A&A* 224, 206–208
- Bel, N. and Leroy, B. (1998). Zeeman splitting in interstellar molecules. II. The ethynyl radical. *A&A* 335, 1025–1028
- Belloche, A. (2013). Observation of rotation in star forming regions: clouds, cores, disks, and jets. In *EAS Publications Series*, eds. P. Hennebelle and C. Charbonnel. vol. 62 of *EAS Publications Series*, 25–66. doi:10.1051/eas/1362002
- Beltrán, M. T., Cesaroni, R., Codella, C., Testi, L., Furuya, R. S., and Olmi, L. (2006). Infall of gas as the formation mechanism of stars up to 20 times more massive than the Sun. *Nature* 443, 427–429. doi:10.1038/nature05074
- Beltrán, M. T., Padovani, M., Girart, J. M., Galli, D., Cesaroni, R., Paladino, R., et al. (2019). ALMA resolves the hourglass magnetic field in G31.41+0.31. *A&A* 630, A54. doi:10.1051/0004-6361/201935701
- Beltrán, M. T., Rivilla, V. M., Cesaroni, R., Galli, D., Moscadelli, L., Ahmadi, A., et al. (2022). The sharp ALMA view of infall and outflow in the

- massive protocluster G31.41+0.31. *A&A* 659, A81. doi:10.1051/0004-6361/202142703
- Beuther, H., Henning, T., Linz, H., Feng, S., Ragan, S. E., Smith, R. J., et al. (2015). Hierarchical fragmentation and collapse signatures in a high-mass starless region. *A&A* 581, A119. doi:10.1051/0004-6361/201526759
- Beuther, H., Linz, H., Henning, T., Feng, S., and Teague, R. (2017). Multiplicity and disks within the high-mass core NGC 7538IRS1.. *A&A* 605, A61. doi:10.1051/0004-6361/201730575
- Beuther, H., Mottram, J. C., Ahmadi, A., Bosco, F., Linz, H., Henning, T., et al. (2018). Fragmentation and disk formation during high-mass star formation. IRAM NOEMA (Northern Extended Millimeter Array) large program CORE. *A&A* 617, A100. doi:10.1051/0004-6361/201833021
- Beuther, H. and Schilke, P. (2004). Fragmentation in MassiveStar Formation. *Science* 303, 1167–1169. doi:10.1126/science.1094014
- Beuther, H., Soler, J. D., Linz, H., Henning, T., Gieser, C., Kuiper, R., et al. (2020). Gravity and Rotation Drag the Magnetic Field in High-mass Star Formation. *ApJ* 904, 168. doi:10.3847/1538-4357/abc019
- Bjerkeli, P., Ramsey, J. P., Harsono, D., Calcutt, H., Kristensen, L. E., van der Wiel, M. H. D., et al. (2019). Kinematics around the B335 protostar down to au scales. *A&A* 631, A64. doi:10.1051/0004-6361/201935948
- Blandford, R. and Payne, D. (1982). Hydromagnetic flows from accretion discs and the production of radio jets. *MNRAS* 199, 883–903
- Bodenheimer, P. (1995). Angular Momentum Evolution of Young Stars and Disks. *ARA&A* 33, 199–238. doi:10.1146/annurev.aa.33.090195.001215
- Bouvier, M., López-Sepulcre, A., Ceccarelli, C., Sakai, N., Yamamoto, S., and Yang, Y. L. (2021). ORion Alma New GEneration Survey (ORANGES). I. Dust continuum and free-free emission of OMC-2/3 filament protostars. *A&A* 653, A117. doi:10.1051/0004-6361/202141157
- Bracco, A., Palmeirim, P., André, P., Adam, R., Ade, P., Bacmann, A., et al. (2017). Probing changes of dust properties along a chain of solar-type prestellar and protostellar cores in Taurus with NIKA. *A&A* 604, A52. doi:10.1051/0004-6361/201731117
- Braiding, C. R. and Wardle, M. (2012). The Hall effect in star formation. *MNRAS* 422, 261–281. doi:10.1111/j.1365-2966.2012.20601.x
- Brauer, R., Wolf, S., Reissl, S., and Ober, F. (2017). Magnetic fields in molecular clouds: Limitations of the analysis of Zeeman observations. *A&A* 601, A90. doi:10.1051/0004-6361/201629001
- Brinch, C. and Hogerheijde, M. R. (2010). LIME - a flexible, non-LTE line excitation and radiation transfer method for millimeter and far-infrared wavelengths. *A&A* 523, A25. doi:10.1051/0004-6361/201015333
- Brinch, C. and Jørgensen, J. K. (2013). Interplay between chemistry and dynamics in embedded protostellar disks. *A&A* 559, A82. doi:10.1051/0004-6361/201322463
- Brunngräber, R. and Wolf, S. (2019). Polarization reversal of scattered thermal dust emission in protoplanetary disks at submillimetre wavelengths. *A&A* 627, L10. doi:10.1051/0004-6361/201935169
- Brunngräber, R. and Wolf, S. (2021). Self-scattering on large, porous grains in protoplanetary disks with dust settling. *A&A* 648, A87. doi:10.1051/0004-6361/202040033
- Burkert, A. and Bodenheimer, P. (2000). Turbulent Molecular Cloud Cores: Rotational Properties. *ApJ* 543, 822–830. doi:10.1086/317122
- Busquet, G., Estalella, R., Palau, A., Liu, H. B., Zhang, Q., Girart, J. M., et al. (2016). What Is Controlling the Fragmentation in the Infrared Dark Cloud G14.225-0.506?: Different Levels of Fragmentation in Twin Hubs. *ApJ* 819, 139. doi:10.3847/0004-637X/819/2/139
- Busquet, G., Girart, J. M., Estalella, R., Fernández-López, M., Galván-Madrid, R., Anglada, G., et al. (2019). Unveiling a cluster of protostellar disks around the massive protostar GGD 27

- MM1. *A&A* 623, L8. doi:10.1051/0004-6361/201833687
- Cabedo, V., Maury, A., Girart, J. M., and Padovani, M. (2021). Structured velocity field in the inner envelope of B335: ALMA observations of rare CO isotopologues. *A&A* 653, A166. doi:10.1051/0004-6361/202140754
- Cabedo, V., Maury, A., Girart, J. M., Padovani, M., Hennebelle, P., Houde, M., et al. (2022). Magnetically regulated collapse in the B335 protostar? II. Observational constraints on gas ionization and magnetic field coupling. *arXiv e-prints*, arXiv:2204.10043
- Cazzoletti, P., Manara, C. F., Liu, H. B., van Dishoeck, E. F., Facchini, S., Alcalà, J. M., et al. (2019). ALMA survey of Class II protoplanetary disks in Corona Australis: a young region with low disk masses. *A&A* 626, A11. doi:10.1051/0004-6361/201935273
- Cazzoli, G., Lattanzi, V., Coriani, S., Gauss, J., Codella, C., Ramos, A. A., et al. (2017). Zeeman effect in sulfur monoxide. A tool to probe magnetic fields in star forming regions. *A&A* 605, A20. doi:10.1051/0004-6361/201730858
- Ceccarelli, C., Dominik, C., López-Sepulcre, A., Kama, M., Padovani, M., Caux, E., et al. (2014). Herschel Finds Evidence for Stellar Wind Particles in a Protostellar Envelope: Is This What Happened to the Young Sun? *ApJ Letters* 790, L1. doi:10.1088/2041-8205/790/1/L1
- Cesaroni, R., Sánchez-Monge, Á., Beltrán, M. T., Johnston, K. G., Maud, L. T., Moscadelli, L., et al. (2017). Chasing discs around O-type (proto)stars: Evidence from ALMA observations. *A&A* 602, A59. doi:10.1051/0004-6361/201630184
- Chamma, M. A., Houde, M., Girart, J. M., and Rao, R. (2018). Non-Zeeman circular polarization of molecular spectral lines in the ISM. *MNRAS* 480, 3123–3131. doi:10.1093/mnras/sty2068
- Chandrasekhar, S. and Fermi, E. (1953). Magnetic Fields in Spiral Arms. *ApJ* 118, 113–+. doi:10.1086/145731
- Chen, M. C.-Y., Di Francesco, J., Johnstone, D., Sadavoy, S., Hatchell, J., Mottram, J. C., et al. (2016). The JCMT Gould Belt Survey: Evidence for Dust Grain Evolution in Perseus Star-forming Clumps. *ApJ* 826, 95. doi:10.3847/0004-637X/826/1/95
- Chen, X., Ren, Z.-Y., Li, D.-L., Liu, T., Wang, K., Shen, Z.-Q., et al. (2021). Chemically Fresh Gas Inflows Detected in a Nearby High-mass Star-forming Region. *ApJ Letters* 923, L20. doi:10.3847/2041-8213/ac3ec8
- Chiang, H.-F., Looney, L. W., and Tobin, J. J. (2012). The Envelope and Embedded Disk around the Class 0 Protostar L1157-mm: Dual-wavelength Interferometric Observations and Modeling. *ApJ* 756, 168. doi:10.1088/0004-637X/756/2/168
- Ching, T.-C., Lai, S.-P., Zhang, Q., Yang, L., Girart, J. M., and Rao, R. (2016). Helical Magnetic Fields in the NGC 1333 IRAS 4A Protostellar Outflows. *ApJ* 819, 159. doi:10.3847/0004-637X/819/2/159
- Cho, J. and Yoo, H. (2016). A Technique for Constraining the Driving Scale of Turbulence and a Modified Chandrasekhar-Fermi Method. *ApJ* 821, 21. doi:10.3847/0004-637X/821/1/21
- Choi, M., Evans, I., Neal J., Gregersen, E. M., and Wang, Y. (1995). Modeling Line Profiles of Protostellar Collapse in B335 with the Monte Carlo Method. *ApJ* 448, 742. doi:10.1086/176002
- Chou, T.-L., Takakuwa, S., Yen, H.-W., Ohashi, N., and Ho, P. T. P. (2014). Transition from the Infalling Envelope to the Keplerian Disk around L1551 IRS 5. *ApJ* 796, 70. doi:10.1088/0004-637X/796/1/70
- Cieza, L. A., Casassus, S., Tobin, J., Bos, S. P., Williams, J. P., Perez, S., et al. (2016). Imaging the water snow-line during a protostellar outburst. *Nature* 535, 258–261. doi:10.1038/nature18612
- Commerçon, B., Hennebelle, P., Audit, E., Chabrier, G., and Teyssier, R. (2010). Protostellar collapse: radiative and magnetic feedbacks on small-scale fragmentation. *A&A* 510, L3. doi:10.1051/0004-6361/200913597
- Connelley, M. S., Reipurth, B., and Tokunaga, A. T. (2008a). The Evolution of the Multiplicity of Embedded Protostars. I. Sample Properties and

- Binary Detections. *AJ* 135, 2496–2525. doi:10.1088/0004-6256/135/6/2496
- Connelley, M. S., Reipurth, B., and Tokunaga, A. T. (2008b). The Evolution of the Multiplicity of Embedded Protostars. II. Binary Separation Distribution and Analysis. *AJ* 135, 2526–2536. doi:10.1088/0004-6256/135/6/2526
- Cortes, P. C., Crutcher, R. M., Shepherd, D. S., and Bronfman, L. (2008). Interferometric Mapping of Magnetic Fields: The Massive Star-forming Region G34.4+0.23 MM. *ApJ* 676, 464–471. doi:10.1086/524355
- Cortes, P. C., Crutcher, R. M., and Watson, W. D. (2005). Line Polarization of Molecular Lines at Radio Frequencies: The Case of DR 21(OH). *ApJ* 628, 780–788. doi:10.1086/430815
- Cortés, P. C., Sanhueza, P., Houde, M., Martín, S., Hull, C. L. H., Girart, J. M., et al. (2021). Magnetic Fields in Massive Star-forming Regions (MagMaR). II. Tomography through Dust and Molecular Line Polarization in NGC 6334I(N). *ApJ* 923, 204. doi:10.3847/1538-4357/ac28a1
- Cox, E. G., Harris, R. J., Looney, L. W., Chiang, H.-F., Chandler, C., Kratter, K., et al. (2017). Protoplanetary Disks in ρ Ophiuchus as Seen from ALMA. *ApJ* 851, 83. doi:10.3847/1538-4357/aa97e2
- Cox, E. G., Harris, R. J., Looney, L. W., Li, Z.-Y., Yang, H., Tobin, J. J., et al. (2018). ALMA's Polarized View of 10 Protostars in the Perseus Molecular Cloud. *ApJ* 855, 92. doi:10.3847/1538-4357/aaacd2
- Crutcher, R. (1999). Magnetic Fields in Molecular Clouds: Observations Confront Theory. *ApJ* 520, 706–713. doi:10.1086/307483
- Crutcher, R., Troland, T., Lazareff, B., Paubert, G., and Kazès, I. (1999). Detection of the CN Zeeman Effect in Molecular Clouds. *ApJ Letters* 514, L121–L124. doi:10.1086/311952
- Crutcher, R. M. (2012). Magnetic Fields in Molecular Clouds. *ARA&A* 50, 29–63. doi:10.1146/annurev-astro-081811-125514
- Crutcher, R. M., Hakobian, N., and Troland, T. H. (2009). Testing Magnetic Star Formation Theory. *ApJ* 692, 844–855. doi:10.1088/0004-637X/692/1/844
- Crutcher, R. M., Hakobian, N., and Troland, T. H. (2010). Self-consistent analysis of OH Zeeman observations. *MNRAS* 402, L64–L66. doi:10.1111/j.1745-3933.2009.00802.x
- Crutcher, R. M. and Kemball, A. J. (2019). Review of Zeeman Effect Observations of Regions of Star Formation K Zeeman Effect, Magnetic Fields, Star formation, Masers, Molecular clouds. *Frontiers in Astronomy and Space Sciences* 6, 66. doi:10.3389/fspas.2019.00066
- Cyganowski, C. J., Brogan, C. L., Hunter, T. R., Smith, R., Kruijssen, J. M. D., Bonnell, I. A., et al. (2017). Simultaneous low- and high-mass star formation in a massive protocluster: ALMA observations of G11.92-0.61. *MNRAS* 468, 3694–3708. doi:10.1093/mnras/stx043
- Dapp, W. B. and Basu, S. (2010). Averting the magnetic braking catastrophe on small scales: disk formation due to Ohmic dissipation. *A&A* 521, L56. doi:10.1051/0004-6361/201015700
- Dapp, W. B., Basu, S., and Kunz, M. W. (2012). Bridging the gap: disk formation in the Class 0 phase with ambipolar diffusion and Ohmic dissipation. *A&A* 541, A35. doi:10.1051/0004-6361/201117876
- Davis, J., Leverett and Greenstein, J. L. (1951). The Polarization of Starlight by Aligned Dust Grains. *ApJ* 114, 206. doi:10.1086/145464
- Deguchi, S. and Watson, W. D. (1984). Linear polarization of molecular lines at radio frequencies. *ApJ* 285, 126–133. doi:10.1086/162483
- Demyk, K., Meny, C., Leroux, H., Depecker, C., Brubach, J. B., Roy, P., et al. (2017a). Low-temperature MIR to submillimeter mass absorption coefficient of interstellar dust analogues. II. Mg and Fe-rich amorphous silicates. *A&A* 606, A50. doi:10.1051/0004-6361/201730944
- Demyk, K., Meny, C., Lu, X. H., Papatheodorou, G., Toplis, M. J., Leroux, H., et al. (2017b). Low temperature MIR to submillimeter mass absorption coefficient of interstellar dust

- analogues. I. Mg-rich glassy silicates. *A&A* 600, A123. doi:10.1051/0004-6361/201629711
- Dib, S., Hennebelle, P., Pineda, J. E., Csengeri, T., Bontemps, S., Audit, E., et al. (2010). The Angular Momentum of Magnetized Molecular Cloud Cores: A Two-dimensional-Three-dimensional Comparison. *ApJ* 723, 425–439. doi:10.1088/0004-637X/723/1/425
- Dirienzo, W. J., Brogan, C., Indebetouw, R., Chandler, C. J., Friesen, R. K., and Devine, K. E. (2015). Physical Conditions of the Earliest Phases of Massive Star Formation: Single-dish and Interferometric Observations of Ammonia and CCS in Infrared Dark Clouds. *AJ* 150, 159. doi:10.1088/0004-6256/150/5/159
- Donati, J.-F. and Landstreet, J. D. (2009). Magnetic Fields of Nondegenerate Stars. *ARA&A* 47, 333–370. doi:10.1146/annurev-astro-082708-101833
- Duchêne, G., Bontemps, S., Bouvier, J., André, P., Djupvik, A., and Ghez, A. (2007). Multiple protostellar systems. II. A high resolution near-infrared imaging survey in nearby star-forming regions. *A&A* 476, 229–242. doi:10.1051/0004-6361:20077270
- Duchêne, G., Bouvier, J., Bontemps, S., André, P., and Motte, F. (2004). Multiple protostellar systems. I. A deep near infrared survey of Taurus and Ophiuchus protostellar objects. *A&A* 427, 651–665. doi:10.1051/0004-6361:20041209
- Duchêne, G. and Kraus, A. (2013). Stellar Multiplicity. *ARA&A* 51, 269–310. doi:10.1146/annurev-astro-081710-102602
- Dunham, M. M. and Vorobyov, E. I. (2012). Resolving the Luminosity Problem in Low-mass Star Formation. *ApJ* 747, 52. doi:10.1088/0004-637X/747/1/52
- Encalada, F. J., Looney, L. W., Tobin, J. J., Sadavoy, S. I., Segura-Cox, D., Cox, E., et al. (2021). 870 μm Dust Continuum of the Youngest Protostars in Ophiuchus. *ApJ* 913, 149. doi:10.3847/1538-4357/abf4fd
- Enoch, M. L., Corder, S., Duchêne, G., Bock, D. C., Bolatto, A. D., Culverhouse, T. L., et al. (2011). Disk and Envelope Structure in Class 0 Protostars. II. High-resolution Millimeter Mapping of the Serpens Sample. *ApJS* 195, 21. doi:10.1088/0067-0049/195/2/21
- Eswaraiyah, C., Li, D., Furuya, R. S., Hasegawa, T., Ward-Thompson, D., Qiu, K., et al. (2021). The JCMT BISTRO Survey: Revealing the Diverse Magnetic Field Morphologies in Taurus Dense Cores with Sensitive Submillimeter Polarimetry. *ApJ Letters* 912, L27. doi:10.3847/2041-8213/abeb1c
- Evans, I., Neal J., Di Francesco, J., Lee, J.-E., Jørgensen, J. K., Choi, M., Myers, P. C., et al. (2015). Detection of Infall in the Protostar B335 with ALMA. *ApJ* 814, 22. doi:10.1088/0004-637X/814/1/22
- Evans, N. J., Dunham, M. M., Jørgensen, J. K., Enoch, M. L., Merín, B., van Dishoeck, E. F., et al. (2009). The Spitzer c2d Legacy Results: Star-Formation Rates and Efficiencies; Evolution and Lifetimes. *ApJS* 181, 321–350. doi:10.1088/0067-0049/181/2/321
- Ewertowski, B. and Basu, S. (2013). A Mathematical Model for an Hourglass Magnetic Field. *ApJ* 767, 33. doi:10.1088/0004-637X/767/1/33
- Eyink, G., Vishniac, E., Lalescu, C., Aluie, H., Kanov, K., Bürger, K., et al. (2013). Flux-freezing breakdown in high-conductivity magnetohydrodynamic turbulence. *Nature* 497, 466–469. doi:10.1038/nature12128
- Falceta-Gonçalves, D., Lazarian, A., and Houde, M. (2010). Damping of Magnetohydrodynamic Turbulence in Partially Ionized Gas and the Observed Difference of Velocities of Neutrals and Ions. *ApJ* 713, 1376–1385. doi:10.1088/0004-637X/713/2/1376
- Falceta-Gonçalves, D., Lazarian, A., and Kowal, G. (2008). Studies of Regular and Random Magnetic Fields in the ISM: Statistics of Polarization Vectors and the Chandrasekhar-Fermi Technique. *ApJ* 679, 537–551. doi:10.1086/587479
- Falgarone, E., Troland, T., Crutcher, R., and Paubert, G. (2008). CN Zeeman measurements in star formation regions. *A&A* 487, 247–252. doi:10.1051/0004-6361:200809577

- Favre, C., Ceccarelli, C., López-Sepulcre, A., Fontani, F., Neri, R., Manigand, S., et al. (2018). SOLIS IV. Hydrocarbons in the OMC-2 FIR4 Region, a Probe of Energetic Particle Irradiation of the Region. *ApJ* 859, 136. doi:10.3847/1538-4357/aabfd4
- Favre, C., López-Sepulcre, A., Ceccarelli, C., Dominik, C., Caselli, P., Caux, E., et al. (2017). The onset of energetic particle irradiation in Class 0 protostars. *A&A* 608, A82. doi:10.1051/0004-6361/201630177
- Fitz Axen, M., Offner, S. S. S., Gaches, B. A. L., Fryer, C. L., Hungerford, A., and Silsbee, K. (2021). Transport of Protostellar Cosmic Rays in Turbulent Dense Cores. *ApJ* 915, 43. doi:10.3847/1538-4357/abfc55
- Fontani, F., Commerçon, B., Giannetti, A., Beltrán, M. T., Sánchez-Monge, A., Testi, L., et al. (2016). Magnetically regulated fragmentation of a massive, dense, and turbulent clump. *A&A* 593, L14. doi:10.1051/0004-6361/201629442
- Fontani, F., Commerçon, B., Giannetti, A., Beltrán, M. T., Sánchez-Monge, Á., Testi, L., et al. (2018). Fragmentation properties of massive protocluster gas clumps: an ALMA study. *A&A* 615, A94. doi:10.1051/0004-6361/201832672
- Frau, P., Galli, D., and Girart, J. M. (2011). Comparing star formation models with interferometric observations of the protostar NGC 1333 IRAS 4A. I. Magnetohydrodynamic collapse models. *A&A* 535, A44. doi:10.1051/0004-6361/201117813
- Frimann, S., Jørgensen, J. K., Dunham, M. M., Bourke, T. L., Kristensen, L. E., Offner, S. S. R., et al. (2017). Protostellar accretion traced with chemistry. High-resolution C¹⁸O and continuum observations towards deeply embedded protostars in Perseus. *A&A* 602, A120. doi:10.1051/0004-6361/201629739
- Fromang, S., Hennebelle, P., and Teyssier, R. (2006). A high order Godunov scheme with constrained transport and adaptive mesh refinement for astrophysical magnetohydrodynamics. *A&A* 457, 371–384. doi:10.1051/0004-6361:20065371
- Frost, A. J., Oudmaijer, R. D., de Wit, W. J., and Lumsden, S. L. (2019). A multi-scale exploration of a massive young stellar object. A transition disk around G305.20+0.21? *A&A* 625, A44. doi:10.1051/0004-6361/201834583
- Galamez, M., Maury, A., Girart, J. M., Rao, R., Zhang, Q., Gaudel, M., et al. (2018). SMA observations of polarized dust emission in solar-type Class 0 protostars: Magnetic field properties at envelope scales. *A&A* 616, A139. doi:10.1051/0004-6361/201833004
- Galamez, M., Maury, A., Girart, J. M., Rao, R., Zhang, Q., Gaudel, M., et al. (2020). An observational correlation between magnetic field, angular momentum and fragmentation in the envelopes of Class 0 protostars? *A&A* 644, A47. doi:10.1051/0004-6361/202038854
- Galamez, M., Maury, A. J., Valdivia, V., Testi, L., Belloche, A., and André, P. (2019). Low dust emissivities and radial variations in the envelopes of Class 0 protostars: possible signature of early grain growth. *A&A* 632, A5. doi:10.1051/0004-6361/201936342
- Galli, D., Lizano, S., Shu, F. H., and Allen, A. (2006). Gravitational Collapse of Magnetized Clouds. I. Ideal Magnetohydrodynamic Accretion Flow. *ApJ* 647, 374–381. doi:10.1086/505257
- Gaudel, M., Maury, A. J., Belloche, A., Maret, S., André, P., Hennebelle, P., et al. (2020). Angular momentum profiles of Class 0 protostellar envelopes. *A&A* 637, A92. doi:10.1051/0004-6361/201936364
- Ginsburg, A., McGuire, B., Plambeck, R., Bally, J., Goddi, C., and Wright, M. (2019). Orion SrcI's Disk Is Salty. *ApJ* 872, 54. doi:10.3847/1538-4357/aafb71
- Girart, J. M., Crutcher, R. M., and Rao, R. (1999). Detection of Polarized CO Emission from the Molecular Outflow in NGC 1333 IRAS 4A. *ApJ Letters* 525, L109–L112. doi:10.1086/312345
- Girart, J. M., Estalella, R., Fernández-López, M., Curiel, S., Frau, P., Galvan-Madrid, R., et al. (2017). The Circumstellar Disk of the B0

- Protostar Powering the HH 80-81 Radio Jet. *ApJ* 847, 58. doi:10.3847/1538-4357/aa81c9
- Girart, J. M., Fernández-López, M., Li, Z. Y., Yang, H., Estalella, R., Anglada, G., et al. (2018). Resolving the Polarized Dust Emission of the Disk around the Massive Star Powering the HH 80-81 Radio Jet. *ApJ Letters* 856, L27. doi:10.3847/2041-8213/aab76b
- Girart, J. M., Frau, P., Zhang, Q., Koch, P. M., Qiu, K., Tang, Y.-W., et al. (2013). DR 21(OH): A Highly Fragmented, Magnetized, Turbulent Dense Core. *ApJ* 772, 69. doi:10.1088/0004-637X/772/1/69
- Girart, J. M., Greaves, J. S., Crutcher, R. M., and Lai, S. P. (2004). BIMA and JCMT Spectropolarimetric Observations of the CO J = 2 - 1 Line Towards Orion KL/IRc2. *Ap&SS* 292, 119–125. doi:10.1023/B:ASTR.0000045007.35868.17
- Girart, J. M., Rao, R., and Estalella, R. (2009). The L723 Low-Mass Star Forming Protostellar System: Resolving a Double Core. *ApJ* 694, 56–68. doi:10.1088/0004-637X/694/1/56
- Girart, J. M., Rao, R., and Marrone, D. P. (2006). Magnetic Fields in the Formation of Sun-Like Stars. *Science* 313, 812–814. doi:10.1126/science.1129093
- Girart, J. M., Viti, S., Estalella, R., and Williams, D. A. (2005). The molecular condensations ahead of Herbig-Haro objects. III. Radiative and dynamical perturbations of the HH 2 condensation. *A&A* 439, 601–612. doi:10.1051/0004-6361:20041720
- Goldreich, P. and Kylafis, N. D. (1981). On mapping the magnetic field direction in molecular clouds by polarization measurements. *ApJ Letters* 243, L75–L78. doi:10.1086/183446
- Goldreich, P. and Kylafis, N. D. (1982). Linear polarization of radio frequency lines in molecular clouds and circumstellar envelopes. *ApJ* 253, 606–621. doi:10.1086/159663
- Gonçalves, J., Galli, D., and Girart, J. M. (2008). Modeling the magnetic field in the protostellar source NGC 1333 IRAS 4A. *A&A* 490, L39–L42. doi:10.1051/0004-6361:200810861
- Goodman, A., Barranco, J., Wilner, D., and Heyer, M. (1998). Coherence in Dense Cores. II. The Transition to Coherence. *ApJ* 504, 223–+. doi:10.1086/306045
- Goodman, A., Benson, P., Fuller, G., and Myers, P. (1993). Dense cores in dark clouds. VIII - Velocity gradients. *ApJ* 406, 528–547. doi:10.1086/172465
- Goodwin, S. P., Whitworth, A. P., and Ward-Thompson, D. (2004). Simulating star formation in molecular cores. II. The effects of different levels of turbulence. *A&A* 423, 169–182. doi:10.1051/0004-6361:20040285
- Gray, W. J., McKee, C. F., and Klein, R. I. (2018). Effect of angular momentum alignment and strong magnetic fields on the formation of protostellar discs. *MNRAS* 473, 2124–2143. doi:10.1093/mnras/stx2406
- Grenier, I. A., Black, J. H., and Strong, A. W. (2015). The Nine Lives of Cosmic Rays in Galaxies. *ARA&A* 53, 199–246. doi:10.1146/annurev-astro-082214-122457
- Guillet, V., Girart, J. M., Maury, A. J., and Alves, F. O. (2020a). Polarized emission by aligned grains in the Mie regime: Application to protoplanetary disks observed by ALMA. *A&A* 634, L15. doi:10.1051/0004-6361/201937314
- Guillet, V., Hennebelle, P., Pineau des Forêts, G., Marcowith, A., Commerçon, B., and Marchand, P. (2020b). Dust coagulation feedback on magnetohydrodynamic resistivities in protostellar collapse. *A&A* 643, A17. doi:10.1051/0004-6361/201937387
- Gupta, A., Yen, H.-W., Koch, P., Bastien, P., Bourke, T. L., Chung, E. J., et al. (2022). Effects of magnetic field orientations in dense cores on gas kinematics in protostellar envelopes. *arXiv e-prints*, arXiv:2204.05636
- Haisch, J., Karl E., Greene, T. P., Barsony, M., and Stahler, S. W. (2004). A Near-Infrared Multiplicity Survey of Class I/Flat-Spectrum Systems in Six Nearby Molecular Clouds. *AJ* 127, 1747–1754. doi:10.1086/381952
- Harrison, R. E., Looney, L. W., Stephens, I. W., Li, Z.-Y., Teague, R., Crutcher, R. M., et al.

- (2021). ALMA CN Zeeman Observations of AS 209: Limits on Magnetic Field Strength and Magnetically Driven Accretion Rate. *ApJ* 908, 141. doi:10.3847/1538-4357/abd94e
- Harsono, D., Bjerkeli, P., van der Wiel, M. H. D., Ramsey, J. P., Maud, L. T., Kristensen, L. E., et al. (2018). Evidence for the start of planet formation in a young circumstellar disk. *Nature Astronomy* 2, 646–651. doi:10.1038/s41550-018-0497-x
- Harsono, D., Jørgensen, J. K., van Dishoeck, E. F., Hogerheijde, M. R., Bruderer, S., Persson, M. V., et al. (2014). Rotationally-supported disks around Class I sources in Taurus: disk formation constraints. *A&A* 562, A77. doi:10.1051/0004-6361/201322646
- Harsono, D., van der Wiel, M. H. D., Bjerkeli, P., Ramsey, J. P., Calcutt, H., Kristensen, L. E., et al. (2021). Resolved molecular line observations reveal an inherited molecular layer in the young disk around TMC1A. *A&A* 646, A72. doi:10.1051/0004-6361/202038697
- He, Y.-X., Zhou, J.-J., Esimbek, J., Ji, W.-G., Wu, G., Tang, X.-D., et al. (2015). Infall motions in massive star-forming regions: results from years 1 and 2 of the MALT90 survey. *MNRAS* 450, 1926–1936. doi:10.1093/mnras/stv732
- Heimsoth, D. J., Stephens, I. W., Arce, H. G., Bourke, T. L., Myers, P. C., and Dunham, M. M. (2021). Evolution and Kinematics of Protostellar Envelopes in the Perseus Molecular Cloud. *arXiv e-prints*, arXiv:2112.09848
- Heitsch, F., Zweibel, E. G., Mac Low, M.-M., Li, P., and Norman, M. L. (2001). Magnetic Field Diagnostics Based on Far-Infrared Polarimetry: Tests Using Numerical Simulations. *ApJ* 561, 800–814. doi:10.1086/323489
- Hennebelle, P. and Ciardi, A. (2009). Disk formation during collapse of magnetized protostellar cores. *ArXiv e-prints*
- Hennebelle, P., Commerçon, B., Chabrier, G., and Marchand, P. (2016). Magnetically Self-regulated Formation of Early Protoplanetary Disks. *ApJ Letters* 830, L8. doi:10.3847/2041-8205/830/1/L8
- Hennebelle, P., Commerçon, B., Joos, M., Klessen, R. S., Krumholz, M., Tan, J. C., et al. (2011). Collapse, outflows and fragmentation of massive, turbulent and magnetized prestellar barotropic cores. *A&A* 528, A72. doi:10.1051/0004-6361/201016052
- Hennebelle, P., Commerçon, B., Lee, Y.-N., and Charnoz, S. (2020). What determines the formation and characteristics of protoplanetary discs? *A&A* 635, A67. doi:10.1051/0004-6361/201936714
- Hennebelle, P. and Fromang, S. (2008). Magnetic processes in a collapsing dense core. I. Accretion and ejection. *A&A* 477, 9–24. doi:10.1051/0004-6361:20078309
- Hennebelle, P. and Teyssier, R. (2008). Magnetic processes in a collapsing dense core. II. Fragmentation. Is there a fragmentation crisis? *A&A* 477, 25–34. doi:10.1051/0004-6361:20078310
- Hezareh, T., Csengeri, T., Houde, M., Herpin, F., and Bontemps, S. (2014). Probing the turbulent ambipolar diffusion scale in molecular clouds with spectroscopy. *MNRAS* 438, 663–671. doi:10.1093/mnras/stt2237
- Hezareh, T., Houde, M., McCoe, C., and Li, H.-b. (2010). Observational Determination of the Turbulent Ambipolar Diffusion Scale and Magnetic Field Strength in Molecular Clouds. *ApJ* 720, 603–607. doi:10.1088/0004-637X/720/1/603
- Hezareh, T., Wiesemeyer, H., Houde, M., Gusdorf, A., and Siringo, G. (2013). Non-Zeeman circular polarization of CO rotational lines in SNR IC 443. *A&A* 558, A45. doi:10.1051/0004-6361/201321900
- Hildebrand, R. H. and Dragovan, M. (1995). The Shapes and Alignment Properties of Interstellar Dust Grains. *ApJ* 450, 663. doi:10.1086/176173
- Hildebrand, R. H., Kirby, L., Dotson, J. L., Houde, M., and Vaillancourt, J. E. (2009). Dispersion of Magnetic Fields in Molecular Clouds. I. *ApJ* 696, 567–573. doi:10.1088/0004-637X/696/1/567
- Hily-Blant, P., Walmsley, M., Pineau Des Forêts, G., and Flower, D. (2008). CN in prestellar cores.

- A&A* 480, L5–L8. doi:10.1051/0004-6361:20079296
- Hirano, S., Tsukamoto, Y., Basu, S., and Machida, M. N. (2020). The Effect of Misalignment between the Rotation Axis and Magnetic Field on the Circumstellar Disk. *ApJ* 898, 118. doi:10.3847/1538-4357/ab9f9d
- Hirota, T., Machida, M. N., Matsushita, Y., Motogi, K., Matsumoto, N., Kim, M. K., et al. (2017). Disk-driven rotating bipolar outflow in Orion Source I. *Nature Astronomy* 1, 0146. doi:10.1038/s41550-017-0146
- Hoang, T. (2021). Effects of grain alignment with magnetic fields on grain growth and the structure of dust aggregates. *arXiv e-prints*, arXiv:2109.07669
- Hoang, T. and Lazarian, A. (2014). Grain alignment by radiative torques in special conditions and implications. *MNRAS* 438, 680–703. doi:10.1093/mnras/stt2240
- Houde, M., Bastien, P., Peng, R., Phillips, T. G., and Yoshida, H. (2000). Probing the Magnetic Field with Molecular Ion Spectra. *ApJ* 536, 857–864. doi:10.1086/308980
- Houde, M., Hezareh, T., Jones, S., and Rajabi, F. (2013). Non-Zeeman Circular Polarization of Molecular Rotational Spectral Lines. *ApJ* 764, 24. doi:10.1088/0004-637X/764/1/24
- Houde, M., Hull, C. L. H., Plambeck, R. L., Vaillancourt, J. E., and Hildebrand, R. H. (2016). Dispersion of Magnetic Fields in Molecular Clouds. IV. Analysis of Interferometry Data. *ApJ* 820, 38. doi:10.3847/0004-637X/820/1/38
- Houde, M., Lankhaar, B., Rajabi, F., and Chamma, M. A. (2022). The generation and transformation of polarization signals in molecular lines through collective anisotropic resonant scattering. *MNRAS* 511, 295–315. doi:10.1093/mnras/stab3806
- Houde, M., Rao, R., Vaillancourt, J. E., and Hildebrand, R. H. (2011). Dispersion of Magnetic Fields in Molecular Clouds. III. *ApJ* 733, 109. doi:10.1088/0004-637X/733/2/109
- Houde, M., Vaillancourt, J. E., Hildebrand, R. H., Chitsazzadeh, S., and Kirby, L. (2009). Dispersion of Magnetic Fields in Molecular Clouds. II. *ApJ* 706, 1504–1516. doi:10.1088/0004-637X/706/2/1504
- Hsieh, C.-H., Arce, H. G., Mardones, D., Kong, S., and Plunkett, A. (2021). Rotating Filament in Orion B: Do Cores Inherit Their Angular Momentum from Their Parent Filament? *ApJ* 908, 92. doi:10.3847/1538-4357/abd034
- Hsieh, T.-H., Murillo, N. M., Belloche, A., Hirano, N., Walsh, C., van Dishoeck, E. F., et al. (2019). Chronology of Episodic Accretion in Protostars—An ALMA Survey of the CO and H₂O Snowlines. *ApJ* 884, 149. doi:10.3847/1538-4357/ab425a
- Hull, C. L. H., Girart, J. M., Tychoniec, Ł., Rao, R., Cortés, P. C., Pokhrel, R., et al. (2017a). ALMA Observations of Dust Polarization and Molecular Line Emission from the Class 0 Protostellar Source Serpens SMM1. *ApJ* 847, 92. doi:10.3847/1538-4357/aa7fe9
- Hull, C. L. H., Le Gouellec, V. J. M., Girart, J. M., Tobin, J. J., and Bourke, T. L. (2020). Understanding the Origin of the Magnetic Field Morphology in the Wide-binary Protostellar System BHR 71. *ApJ* 892, 152. doi:10.3847/1538-4357/ab5809
- Hull, C. L. H., Mocz, P., Burkhart, B., Goodman, A. A., Girart, J. M., Cortés, P. C., et al. (2017b). Unveiling the Role of the Magnetic Field at the Smallest Scales of Star Formation. *ApJ Letters* 842, L9. doi:10.3847/2041-8213/aa71b7
- Hull, C. L. H., Plambeck, R. L., Bolatto, A. D., Bower, G. C., Carpenter, J. M., Crutcher, R. M., et al. (2013). Misalignment of Magnetic Fields and Outflows in Protostellar Cores. *ApJ* 768, 159. doi:10.1088/0004-637X/768/2/159
- Hull, C. L. H., Plambeck, R. L., Kwon, W., Bower, G. C., Carpenter, J. M., Crutcher, R. M., et al. (2014). TADPOL: A 1.3 mm Survey of Dust Polarization in Star-forming Cores and Regions. *ApJS* 213, 13. doi:10.1088/0067-0049/213/1/13
- Hull, C. L. H. and Zhang, Q. (2019). Interferometric observations of magnetic fields in forming stars. *Frontiers in Astronomy and Space Sciences* 6, 3. doi:10.3389/fspas.2019.00003

- Ilee, J. D., Cyganowski, C. J., Brogan, C. L., Hunter, T. R., Forgan, D. H., Haworth, T. J., et al. (2018). G11.92-0.61 MM 1: A Fragmented Keplerian Disk Surrounding a Proto-O Star. *ApJ Letters* 869, L24. doi:10.3847/2041-8213/aaeffc
- Imai, M., Oya, Y., Sakai, N., López-Sepulcre, A., Watanabe, Y., and Yamamoto, S. (2019). Unveiling a Few Astronomical Unit Scale Rotation Structure around the Protostar in B335. *ApJ Letters* 873, L21. doi:10.3847/2041-8213/ab0c20
- Johnston, K. G., Robitaille, T. P., Beuther, H., Linz, H., Boley, P., Kuiper, R., et al. (2015). A Keplerian-like Disk around the Forming O-type Star AFGL 4176. *ApJ Letters* 813, L19. doi:10.1088/2041-8205/813/1/L19
- Joncour, I., Duchêne, G., and Moraux, E. (2017). Multiplicity and clustering in Taurus star-forming region. I. Unexpected ultra-wide pairs of high-order multiplicity in Taurus. *A&A* 599, A14. doi:10.1051/0004-6361/201629398
- Jones, A. P., Köhler, M., Ysard, N., Bocchio, M., and Verstraete, L. (2017). The global dust modelling framework THEMIS. *A&A* 602, A46. doi:10.1051/0004-6361/201630225
- Jones, T. J., Bagley, M., Krejny, M., Andersson, B. G., and Bastien, P. (2015). Grain Alignment in Starless Cores. *AJ* 149, 31. doi:10.1088/0004-6256/149/1/31
- Joos, M., Hennebelle, P., and Ciardi, A. (2012). Protostellar disk formation and transport of angular momentum during magnetized core collapse. *A&A* 543, A128. doi:10.1051/0004-6361/201118730
- Joos, M., Hennebelle, P., Ciardi, A., and Fromang, S. (2013). The influence of turbulence during magnetized core collapse and its consequences on low-mass star formation. *A&A* 554, A17. doi:10.1051/0004-6361/201220649
- Jørgensen, J. K., Johnstone, D., Kirk, H., and Myers, P. C. (2007). Current Star Formation in the Perseus Molecular Cloud: Constraints from Unbiased Submillimeter and Mid-Infrared Surveys. *ApJ* 656, 293–305. doi:10.1086/510150
- Jørgensen, J. K., Schöier, F. L., and van Dishoeck, E. F. (2004). Molecular inventories and chemical evolution of low-mass protostellar envelopes. *A&A* 416, 603–622. doi:10.1051/0004-6361:20034440
- Juárez, C., Girart, J. M., Frau, P., Palau, A., Estalella, R., Morata, O., et al. (2017). A correlation between chemistry, polarization, and dust properties in the Pipe nebula starless core FeSt 1-457. *A&A* 597, A74. doi:10.1051/0004-6361/201628608
- Kandori, R., Tamura, M., Tomisaka, K., Nakajima, Y., Kusakabe, N., Kwon, J., et al. (2017). Distortion of Magnetic Fields in a Starless Core II: 3D Magnetic Field Structure of FeSt 1-457. *ApJ* 848, 110. doi:10.3847/1538-4357/aa8d18
- Kataoka, A., Muto, T., Momose, M., Tsukagoshi, T., Fukagawa, M., Shibai, H., et al. (2015). Millimeter-wave Polarization of Protoplanetary Disks due to Dust Scattering. *ApJ* 809, 78. doi:10.1088/0004-637X/809/1/78
- Kataoka, A., Okuzumi, S., and Tazaki, R. (2019). Millimeter-wave Polarization Due to Grain Alignment by the Gas Flow in Protoplanetary Disks. *ApJ Letters* 874, L6. doi:10.3847/2041-8213/ab0c9a
- Kirchschlager, F. and Bertrang, G. H. M. (2020). Self-scattering of non-spherical dust grains. The limitations of perfect compact spheres. *A&A* 638, A116. doi:10.1051/0004-6361/202037943
- Ko, C.-L., Liu, H. B., Lai, S.-P., Ching, T.-C., Rao, R., and Girart, J. M. (2020). Resolving Linear Polarization due to Emission and Extinction of Aligned Dust Grains on NGC 1333 IRAS4A with JVL A and ALMA. *ApJ* 889, 172. doi:10.3847/1538-4357/ab5e79
- Koch, P. M., Tang, Y.-W., and Ho, P. T. P. (2013). Interpreting the Role of the Magnetic Field from Dust Polarization Maps. *ApJ* 775, 77. doi:10.1088/0004-637X/775/1/77
- Koch, P. M., Tang, Y.-W., Ho, P. T. P., Zhang, Q., Girart, J. M., Chen, H.-R. V., et al. (2014). The Importance of the Magnetic Field from an SMA-CSO-combined Sample of Star-forming Regions. *ApJ* 797, 99. doi:10.1088/0004-637X/797/2/99

- Köhler, R., Neuhäuser, R., Krämer, S., Leinert, C., Ott, T., and Eckart, A. (2008). Multiplicity of young stars in and around R Coronae Australis. *A&A* 488, 997–1006. doi:10.1051/0004-6361:200809897
- Kowal, G., Lazarian, A., Vishniac, E. T., and Otmianowska-Mazur, K. (2009). Numerical Tests of Fast Reconnection in Weakly Stochastic Magnetic Fields. *ApJ* 700, 63–85. doi:10.1088/0004-637X/700/1/63
- Kraus, S., Hofmann, K.-H., Menten, K. M., Schertl, D., Weigelt, G., Wyrowski, F., et al. (2010). A hot compact dust disk around a massive young stellar object. *Nature* 466, 339–342. doi:10.1038/nature09174
- Kuffmeier, M., Frimann, S., Jensen, S. S., and Haugbølle, T. (2018). Episodic accretion: the interplay of infall and disc instabilities. *MNRAS* 475, 2642–2658. doi:10.1093/mnras/sty024
- Kuffmeier, M., Zhao, B., and Caselli, P. (2020). Ionization: a possible explanation for the difference of mean disk sizes in star-forming regions. *A&A* 639, A86. doi:10.1051/0004-6361/201937328
- Kunze, K. E. (2013). Cosmological magnetic fields. *Plasma Physics and Controlled Fusion* 55, 124026. doi:10.1088/0741-3335/55/12/124026
- Kuznetsova, A., Bae, J., Hartmann, L., and Low, M.-M. M. (2022). Anisotropic Infall and Substructure Formation in Embedded Disks. *ApJ* 928, 92. doi:10.3847/1538-4357/ac54a8
- Kuznetsova, A., Hartmann, L., and Heitsch, F. (2019). The Origins of Protostellar Core Angular Momenta. *ApJ* 876, 33. doi:10.3847/1538-4357/ab12ce
- Kuznetsova, A., Hartmann, L., and Heitsch, F. (2020). Angular Momenta, Magnetization, and Accretion of Protostellar Cores. *ApJ* 893, 73. doi:10.3847/1538-4357/ab7eac
- Kwon, W., Looney, L. W., Mundy, L. G., Chiang, H.-F., and Kemball, A. J. (2009). Grain Growth and Density Distribution of the Youngest Protostellar Systems. *ApJ* 696, 841–852. doi:10.1088/0004-637X/696/1/841
- Kwon, W., Stephens, I. W., Tobin, J. J., Looney, L. W., Li, Z.-Y., van der Tak, F. F. S., et al. (2019). Highly Ordered and Pinched Magnetic Fields in the Class 0 Protobinary System L1448 IRS 2. *ApJ* 879, 25. doi:10.3847/1538-4357/ab24c8
- Lai, S.-P., Girart, J. M., and Crutcher, R. M. (2003a). Interferometric Mapping of Magnetic Fields in Star-forming Regions. III. Dust and CO Polarization in DR 21(OH). *ApJ* 598, 392–399. doi:10.1086/378769
- Lai, S.-P., Velusamy, T., and Langer, W. D. (2003b). The High Angular Resolution Measurement of Ion and Neutral Spectra as a Probe of the Magnetic Field Structure in DR 21(OH). *ApJ Letters* 596, L239–L242. doi:10.1086/379502
- Lam, K. H., Chen, C.-Y., Li, Z.-Y., Yang, H., Cox, E. G., Looney, L. W., et al. (2021). The transition of polarized dust thermal emission from the protostellar envelope to the disc scale. *MNRAS* 507, 608–620. doi:10.1093/mnras/stab2105
- Lam, K. H., Li, Z.-Y., Chen, C.-Y., Tomida, K., and Zhao, B. (2019). Disc formation in magnetized dense cores with turbulence and ambipolar diffusion. *MNRAS* 489, 5326–5347. doi:10.1093/mnras/stz2436
- Lankhaar, B. and Vlemmings, W. (2020a). Collisional polarization of molecular ions: a signpost of ambipolar diffusion. *A&A* 638, L7. doi:10.1051/0004-6361/202038196
- Lankhaar, B. and Vlemmings, W. (2020b). PORTAL: Three-dimensional polarized (sub)millimeter line radiative transfer. *A&A* 636, A14. doi:10.1051/0004-6361/202037509
- Lankhaar, B., Vlemmings, W., and Bjerkeli, P. (2022). Tracing the large-scale magnetic field morphology in protoplanetary disks using molecular line polarization. *A&A* 657, A106. doi:10.1051/0004-6361/202141285
- Lazarian, A., Andersson, B. G., and Hoang, T. (2015). Grain alignment: Role of radiative torques and paramagnetic relaxation. In *Polarimetry of Stars and Planetary Systems*. 81

- Lazarian, A. and Vishniac, E. T. (1999). Reconnection in a Weakly Stochastic Field. *ApJ* 517, 700–718. doi:10.1086/307233
- Le Gouellec, V. J. M., Hull, C. L. H., Maury, A. J., Girart, J. M., Tychoniec, Ł., Kristensen, L. E., et al. (2019). Characterizing Magnetic Field Morphologies in Three Serpens Protostellar Cores with ALMA. *ApJ* 885, 106. doi:10.3847/1538-4357/ab43c2
- Le Gouellec, V. J. M., Maury, A. J., Guillet, V., Hull, C. L. H., Girart, J. M., Verliat, A., et al. (2020). A statistical analysis of dust polarization properties in ALMA observations of Class 0 protostellar cores. *A&A* 644, A11. doi:10.1051/0004-6361/202038404
- Lebreuilly, U., Commerçon, B., and Laibe, G. (2020). Protostellar collapse: the conditions to form dust-rich protoplanetary disks. *A&A* 641, A112. doi:10.1051/0004-6361/202038174
- Lebreuilly, U., Hennebelle, P., Colman, T., Commerçon, B., Klessen, R., Maury, A., et al. (2021). Protoplanetary Disk Birth in Massive Star-forming Clumps: The Essential Role of the Magnetic Field. *ApJ Letters* 917, L10. doi:10.3847/2041-8213/ac158c
- Lee, C.-F., Hwang, H.-C., Ching, T.-C., Hirano, N., Lai, S.-P., Rao, R., et al. (2018a). Unveiling a magnetized jet from a low-mass protostar. *Nature Communications* 9, 4636. doi:10.1038/s41467-018-07143-8
- Lee, C.-F., Kwon, W., Jhan, K.-S., Hirano, N., Hwang, H.-C., Lai, S.-P., et al. (2019). A Pseudodisk Threaded with a Toroidal and Pinched Poloidal Magnetic Field Morphology in the HH 211 Protostellar System. *ApJ* 879, 101. doi:10.3847/1538-4357/ab2458
- Lee, C.-F., Li, Z.-Y., Hirano, N., Shang, H., Ho, P. T. P., and Zhang, Q. (2018b). ALMA Observations of the Very Young Class 0 Protostellar System HH211-mm: A 30 au Dusty Disk with a Disk Wind Traced by SO? *ApJ* 863, 94. doi:10.3847/1538-4357/aad2da
- Lee, C.-F., Li, Z.-Y., Yang, H., Daniel Lin, Z.-Y., Ching, T.-C., and Lai, S.-P. (2021a). What Produces Dust Polarization in the HH 212 Protostellar Disk at 878 μm : Dust Self-scattering or Dichroic Extinction? *ApJ* 910, 75. doi:10.3847/1538-4357/abe53a
- Lee, J. W. Y., Hull, C. L. H., and Offner, S. S. R. (2017). Synthetic Observations of Magnetic Fields in Protostellar Cores. *ApJ* 834, 201. doi:10.3847/1538-4357/834/2/201
- Lee, Y.-N., Charnoz, S., and Hennebelle, P. (2021b). Protoplanetary disk formation from the collapse of a prestellar core. *A&A* 648, A101. doi:10.1051/0004-6361/202038105
- Lee, Y.-N., Marchand, P., Liu, Y.-H., and Hennebelle, P. (2021c). Universal Protoplanetary Disk Size under Complete Nonideal Magnetohydrodynamics: The Interplay between Ion-neutral Friction, Hall Effect, and Ohmic Dissipation. *ApJ* 922, 36. doi:10.3847/1538-4357/ac235d
- Levin, S. M., Langer, W. D., Velusamy, T., Kuiper, T. B. H., and Crutcher, R. M. (2001). Measuring the Magnetic Field Strength in L1498 with Zeeman-splitting Observations of CCS. *ApJ* 555, 850–854. doi:10.1086/321518
- Li, H.-b. and Houde, M. (2008). Probing the Turbulence Dissipation Range and Magnetic Field Strengths in Molecular Clouds. *ApJ* 677, 1151–1156. doi:10.1086/529581
- Li, J. I.-H., Liu, H. B., Hasegawa, Y., and Hirano, N. (2017). Systematic Analysis of Spectral Energy Distributions and the Dust Opacity Indices for Class 0 Young Stellar Objects. *ApJ* 840, 72. doi:10.3847/1538-4357/aa6f04
- Li, Z.-Y., Krasnopolsky, R., and Shang, H. (2013). Does Magnetic-field-Rotation Misalignment Solve the Magnetic Braking Catastrophe in Protostellar Disk Formation? *ApJ* 774, 82. doi:10.1088/0004-637X/774/1/82
- Li, Z.-Y. and Shu, F. (1996). Magnetized Singular Isothermal Toroids. *ApJ* 472, 211–+. doi:10.1086/178056
- Liu, H. B., Chen, H.-R. V., Román-Zúñiga, C. G., Galván-Madrid, R., Ginsburg, A., Ho, P. T. P., et al. (2019). Investigating Fragmentation of Gas Structures in OB Cluster-forming Molecular Clump G33.92+0.11 with 1000 au Resolution

- Observations of ALMA. *ApJ* 871, 185. doi:10.3847/1538-4357/aaf6b4
- Liu, H. B., Lai, S.-P., Hasegawa, Y., Hirano, N., Rao, R., Li, I. H., et al. (2016). Detection of Linearly Polarized 6.9 mm Continuum Emission from the Class 0 Young Stellar Object NGC 1333 IRAS4A. *ApJ* 821, 41. doi:10.3847/0004-637X/821/1/41
- Liu, J., Zhang, Q., Commerçon, B., Valdivia, V., Maury, A., and Qiu, K. (2021). Calibrating the Davis-Chandrasekhar-Fermi Method with Numerical Simulations: Uncertainties in Estimating the Magnetic Field Strength from Statistics of Field Orientations. *ApJ* 919, 79. doi:10.3847/1538-4357/ac0cec
- Liu, S.-Y., Su, Y.-N., Zinchenko, I., Wang, K.-S., Meyer, D. M. A., Wang, Y., et al. (2020). ALMA View of the Infalling Envelope around a Massive Protostar in S255IR SMA1. *ApJ* 904, 181. doi:10.3847/1538-4357/abc0ec
- Liu, T., Wu, Y., and Zhang, H. (2013). Uniform Infall toward the Cometary H II Region in the G34.26+0.15 Complex? *ApJ* 776, 29. doi:10.1088/0004-637X/776/1/29
- Looney, L., Mundy, L., and Welch, W. (2000). Unveiling the Circumstellar Envelope and Disk: A Subarcsecond Survey of Circumstellar Structures. *ApJ* 529, 477–498. doi:10.1086/308239
- Machida, M. N., Tomisaka, K., Matsumoto, T., and Inutsuka, S.-i. (2008). Formation Scenario for Wide and Close Binary Systems. *ApJ* 677, 327–347. doi:10.1086/529133
- Marchand, P., Tomida, K., Commerçon, B., and Chabrier, G. (2019). Impact of the Hall effect in star formation, improving the angular momentum conservation. *A&A* 631, A66. doi:10.1051/0004-6361/201936215
- Mardones, D., Myers, P. C., Tafalla, M., Wilner, D. J., Bachiller, R., and Garay, G. (1997). A Search for Infall Motions toward Nearby Young Stellar Objects. *ApJ* 489, 719–733. doi:10.1086/304812
- Maret, S., Maury, A. J., Belloche, A., Gaudel, M., André, P., Cabrit, S., et al. (2020). Searching for kinematic evidence of Keplerian disks around Class 0 protostars with CALYPSO. *A&A* 635, A15. doi:10.1051/0004-6361/201936798
- Martin, P. G., Roy, A., Bontemps, S., Miville-Deschênes, M.-A., Ade, P. A. R., Bock, J. J., et al. (2012). Evidence for Environmental Changes in the Submillimeter Dust Opacity. *ApJ* 751, 28. doi:10.1088/0004-637X/751/1/28
- Masson, J., Chabrier, G., Hennebelle, P., Vaytet, N., and Commerçon, B. (2016). Ambipolar diffusion in low-mass star formation. I. General comparison with the ideal magnetohydrodynamic case. *A&A* 587, A32. doi:10.1051/0004-6361/201526371
- Mathis, J. S., Rumpl, W., and Nordsieck, K. H. (1977). The size distribution of interstellar grains. *ApJ* 217, 425–433. doi:10.1086/155591
- Matsumoto, T. and Hanawa, T. (2003). Fragmentation of a Molecular Cloud Core versus Fragmentation of the Massive Protoplanetary Disk in the Main Accretion Phase. *ApJ* 595, 913–934. doi:10.1086/377367
- Matsumoto, T., Machida, M. N., and Inutsuka, S.-i. (2017). Circumstellar Disks and Outflows in Turbulent Molecular Cloud Cores: Possible Formation Mechanism for Misaligned Systems. *ApJ* 839, 69. doi:10.3847/1538-4357/aa6a1c
- Matsumoto, T. and Tomisaka, K. (2004). Directions of Outflows, Disks, Magnetic Fields, and Rotation of Young Stellar Objects in Collapsing Molecular Cloud Cores. *ApJ* 616, 266–282. doi:10.1086/424897
- Matthews, B. C., McPhee, C. A., Fissel, L. M., and Curran, R. L. (2009). The Legacy of SCUPOL: 850 μm Imaging Polarimetry from 1997 to 2005. *ApJS* 182, 143–204. doi:10.1088/0067-0049/182/1/143
- Maud, L. T., Cesaroni, R., Kumar, M. S. N., Rivilla, V. M., Ginsburg, A., Klaassen, P. D., et al. (2019). Substructures in the Keplerian disc around the O-type (proto-)star G17.64+0.16. *A&A* 627, L6. doi:10.1051/0004-6361/201935633
- Maureira, M. J., Arce, H. G., Offner, S. S. R., Dunham, M. M., Pineda, J. E., Fernández-López, M., et al. (2017). A Turbulent Origin for the

- Complex Envelope Kinematics in the Young Low-mass Core Per-bolo 58. *ApJ* 849, 89. doi:10.3847/1538-4357/aa91ce
- Maury, A. J., André, P., Hennebelle, P., Motte, F., Stamatellos, D., Bate, M., et al. (2010). Toward understanding the formation of multiple systems. A pilot IRAM-PdBI survey of Class 0 objects. *A&A* 512, A40. doi:10.1051/0004-6361/200913492
- Maury, A. J., André, P., Men'shchikov, A., Könyves, V., and Bontemps, S. (2011). The formation of active protoclusters in the Aquila rift: a millimeter continuum view. *A&A* 535, A77. doi:10.1051/0004-6361/201117132
- Maury, A. J., André, P., Testi, L., Maret, S., Belloche, A., Hennebelle, P., et al. (2019). Characterizing young protostellar disks with the CALYPSO IRAM-PdBI survey: large Class 0 disks are rare. *A&A* 621, A76. doi:10.1051/0004-6361/201833537
- Maury, A. J., Girart, J. M., Zhang, Q., Hennebelle, P., Keto, E., Rao, R., et al. (2018). Magnetically regulated collapse in the B335 protostar? I. ALMA observations of the polarized dust emission. *MNRAS* 477, 2760–2765. doi:10.1093/mnras/sty574
- Maury, A. J., Wiesemeyer, H., and Thum, C. (2012). CN Zeeman observations of the NGC 2264-C protocluster. *A&A* 544, A69. doi:10.1051/0004-6361/201219148
- Mazzei, R., Cleaves, L. I., and Li, Z.-Y. (2020). Untangling Magnetic Complexity in Protoplanetary Disks with the Zeeman Effect. *ApJ* 903, 20. doi:10.3847/1538-4357/abb67a
- Mellon, R. R. and Li, Z.-Y. (2008). Magnetic braking and protostellar disk formation: The ideal mhd limit. *The Astrophysical Journal* 681, 1356–1376
- Mignon-Risse, R., González, M., Commerçon, B., and Rosdahl, J. (2021). Collapse of turbulent massive cores with ambipolar diffusion and hybrid radiative transfer. I. Accretion and multiplicity. *A&A* 652, A69. doi:10.1051/0004-6361/202140617
- Miotello, A., Testi, L., Lodato, G., Ricci, L., Rosotti, G., Brooks, K., et al. (2014). Grain growth in the envelopes and disks of Class I protostars. *A&A* 567, A32. doi:10.1051/0004-6361/201322945
- Misugi, Y., Inutsuka, S.-i., and Arzoumanian, D. (2019). An Origin for the Angular Momentum of Molecular Cloud Cores: A Prediction from Filament Fragmentation. *ApJ* 881, 11. doi:10.3847/1538-4357/ab2382
- Mottram, J. C., van Dishoeck, E. F., Kristensen, L. E., Karska, A., San José-García, I., Khanna, S., et al. (2017). Outflows, infall and evolution of a sample of embedded low-mass protostars. The William Herschel Line Legacy (WILL) survey. *A&A* 600, A99. doi:10.1051/0004-6361/201628682
- Mottram, J. C., van Dishoeck, E. F., Schmalzl, M., Kristensen, L. E., Visser, R., Hogerheijde, M. R., et al. (2013). Waterfalls around protostars. Infall motions towards Class 0/I envelopes as probed by water. *A&A* 558, A126. doi:10.1051/0004-6361/201321828
- Mouschovias, T. and Spitzer, L., Jr. (1976). Note on the collapse of magnetic interstellar clouds. *ApJ* 210, 326–+. doi:10.1086/154835
- Mouschovias, T. C. (1979). Magnetic braking of self-gravitating, oblate interstellar clouds. *ApJ* 228, 159–162. doi:10.1086/156832
- Mouschovias, T. C. and Morton, S. A. (1985). The Angular Momentum Problem during Star Formation - Magnetically Linked Aligned Rotators - Part Two - Results. *ApJ* 298, 205. doi:10.1086/163599
- Mouschovias, T. C. and Paleologou, E. V. (1980). The angular momentum problem and magnetic braking during star formation - Exact solutions for an aligned and a perpendicular rotator. *Moon and Planets* 22, 31–45. doi:10.1007/BF00896865
- Mouschovias, T. C. and Tassis, K. (2010). Self-consistent analysis of OH-Zeeman observations: too much noise about noise. *MNRAS* 409, 801–807. doi:10.1111/j.1365-2966.2010.17345.x

- Myers, A. T., McKee, C. F., Cunningham, A. J., Klein, R. I., and Krumholz, M. R. (2013). The Fragmentation of Magnetized, Massive Star-forming Cores with Radiative Feedback. *ApJ* 766, 97. doi:10.1088/0004-637X/766/2/97
- Myers, P. C. and Basu, S. (2021). Magnetic Properties of Star-forming Dense Cores. *ApJ* 917, 35. doi:10.3847/1538-4357/abf4c8
- Myers, P. C., Basu, S., and Auddy, S. (2018). Magnetic Field Structure in Spheroidal Star-forming Clouds. *ApJ* 868, 51. doi:10.3847/1538-4357/aae695
- Nakamura, F., Kameno, S., Kusune, T., Mizuno, I., Dobashi, K., Shimoikura, T., et al. (2019). First clear detection of the CCS Zeeman splitting toward the pre-stellar core, Taurus Molecular Cloud 1. *PASJ* 71, 117. doi:10.1093/pasj/psz102
- Nakano, T., Nishi, R., and Umebayashi, T. (2002). Mechanism of Magnetic Flux Loss in Molecular Clouds. *ApJ*
- Nakatani, R., Liu, H. B., Ohashi, S., Zhang, Y., Hanawa, T., Chandler, C., et al. (2020). Substructure Formation in a Protostellar Disk of L1527 IRS. *ApJ Letters* 895, L2. doi:10.3847/2041-8213/ab8eaa
- Nishi, R., Nakano, T., and Umebayashi, T. (1991). Magnetic Flux Loss from Interstellar Clouds with Various Grain-Size Distributions. *ApJ* 368, 181. doi:10.1086/169682
- Ober, F., Wolf, S., Uribe, A. L., and Klahr, H. H. (2015). Tracing planet-induced structures in circumstellar disks using molecular lines. *A&A* 579, A105. doi:10.1051/0004-6361/201526117
- Offner, S. S. R., Klein, R. I., and McKee, C. F. (2008). Driven and Decaying Turbulence Simulations of Low-Mass Star Formation: From Clumps to Cores to Protostars. *ApJ* 686, 1174–1194. doi:10.1086/590238
- Ohashi, N., Saigo, K., Aso, Y., Aikawa, Y., Koyamatsu, S., Machida, M. N., et al. (2014). Formation of a Keplerian Disk in the Infalling Envelope around L1527 IRS: Transformation from Infalling Motions to Kepler Motions. *ApJ* 796, 131. doi:10.1088/0004-637X/796/2/131
- Ohashi, S., Kobayashi, H., Nakatani, R., Okuzumi, S., Tanaka, H., Murakawa, K., et al. (2021). Ring Formation by Coagulation of Dust Aggregates in the Early Phase of Disk Evolution around a Protostar. *ApJ* 907, 80. doi:10.3847/1538-4357/abd0fa
- Ormel, C. W., Paszun, D., Dominik, C., and Tielens, A. G. G. M. (2009). Dust coagulation and fragmentation in molecular clouds. I. How collisions between dust aggregates alter the dust size distribution. *A&A* 502, 845–869. doi:10.1051/0004-6361/200811158
- Ostriker, E. C., Stone, J. M., and Gammie, C. F. (2001). Density, Velocity, and Magnetic Field Structure in Turbulent Molecular Cloud Models. *ApJ* 546, 980–1005. doi:10.1086/318290
- Oya, Y., Sakai, N., Sakai, T., Watanabe, Y., Hirota, T., Lindberg, J. E., et al. (2014). A Substellar-mass Protostar and its Outflow of IRAS 15398-3359 Revealed by Subarcsecond-resolution Observations of H₂CO and CCH. *ApJ* 795, 152. doi:10.1088/0004-637X/795/2/152
- Padovani, M., Brinch, C., Girart, J. M., Jørgensen, J. K., Frau, P., Hennebelle, P., et al. (2012). Adaptable radiative transfer innovations for submillimetre telescopes (ARTIST). Dust polarisation module (DustPol). *A&A* 543, A16. doi:10.1051/0004-6361/201219028
- Padovani, M., Galli, D., and Glassgold, A. E. (2009a). Cosmic-ray ionization of molecular clouds. *A&A* 501, 619–631. doi:10.1051/0004-6361/200911794
- Padovani, M., Hennebelle, P., Marcowith, A., and Ferrière, K. (2015). Cosmic-ray acceleration in young protostars. *A&A* 582, L13. doi:10.1051/0004-6361/201526874
- Padovani, M., Ivlev, A. V., Galli, D., and Caselli, P. (2018). Cosmic-ray ionisation in circumstellar discs. *A&A* 614, A111. doi:10.1051/0004-6361/201732202
- Padovani, M., Marcowith, A., Galli, D., Hunt, L. K., and Fontani, F. (2021). The double signature of local cosmic-ray acceleration in star-forming regions. *A&A* 649, A149. doi:10.1051/0004-6361/202039918

- Padovani, M., Walmsley, C. M., Tafalla, M., Galli, D., and Müller, H. S. P. (2009b). C₂H in prestellar cores. *A&A* 505, 1199–1211. doi:10.1051/0004-6361/200912547
- Palau, A., Ballesteros-Paredes, J., Vázquez-Semadeni, E., Sánchez-Monge, Á., Estalella, R., Fall, S. M., et al. (2015). Gravity or turbulence? - III. Evidence of pure thermal Jeans fragmentation at ~ 0.1 pc scale. *MNRAS* 453, 3785–3797. doi:10.1093/mnras/stv1834
- Palau, A., Estalella, R., Girart, J. M., Fuente, A., Fontani, F., Commerçon, B., et al. (2014). Fragmentation of Massive Dense Cores Down to ~ 1000 AU: Relation between Fragmentation and Density Structure. *ApJ* 785, 42. doi:10.1088/0004-637X/785/1/42
- Palau, A., Fuente, A., Girart, J. M., Estalella, R., Ho, P. T. P., Sánchez-Monge, Á., et al. (2013). Early Stages of Cluster Formation: Fragmentation of Massive Dense Cores down to ~ 1000 AU. *ApJ* 762, 120. doi:10.1088/0004-637X/762/2/120
- Palau, A., Zapata, L. A., Román-Zúñiga, C. G., Sánchez-Monge, Á., Estalella, R., Busquet, G., et al. (2018). Thermal Jeans Fragmentation within ~ 1000 au in OMC-1S. *ApJ* 855, 24. doi:10.3847/1538-4357/aaad03
- Palau, A., Zhang, Q., Girart, J. M., Liu, J., Rao, R., Koch, P. M., et al. (2021). Does the Magnetic Field Suppress Fragmentation in Massive Dense Cores? *ApJ* 912, 159. doi:10.3847/1538-4357/abee1e
- Paron, S., Ortega, M. E., Marinelli, A., Areal, M. B., and Martínez, N. C. (2021). Cyano radical emission at small spatial scales towards massive protostars. *A&A* 653, A77. doi:10.1051/0004-6361/202141424
- Pattle, K., Fissel, L., Tahani, M., Liu, T., and Ntormousi, E. (2022). Magnetic fields in star formation: from clouds to cores. *arXiv e-prints*, arXiv:2203.11179
- Pattle, K., Ward-Thompson, D., Berry, D., Hatchell, J., Chen, H.-R., Pon, A., et al. (2017). The JCMT BISTRO Survey: The Magnetic Field Strength in the Orion A Filament. *ApJ* 846, 122. doi:10.3847/1538-4357/aa80e5
- Pillai, T., Kauffmann, J., Wiesemeyer, H., and Menten, K. M. (2016). CN Zeeman and dust polarization in a high-mass cold clump. *A&A* 591, A19. doi:10.1051/0004-6361/201527803
- Pineda, J. E., Maury, A. J., Fuller, G. A., Testi, L., García-Appadoo, D., Peck, A. B., et al. (2012). The first ALMA view of IRAS 16293-2422. Direct detection of infall onto source B and high-resolution kinematics of source A. *A&A* 544, L7. doi:10.1051/0004-6361/201219589
- Pineda, J. E., Schmiedeke, A., Caselli, P., Stahler, S. W., Frayer, D. T., Church, S. E., et al. (2021). Neutral versus Ion Line Widths in Barnard 5: Evidence for Penetration by Magnetohydrodynamic Waves. *ApJ* 912, 7. doi:10.3847/1538-4357/abebdd
- Pineda, J. E., Segura-Cox, D., Caselli, P., Cunningham, N., Zhao, B., Schmiedeke, A., et al. (2020). A protostellar system fed by a streamer of 10,500 au length. *Nature Astronomy* 4, 1158–1163. doi:10.1038/s41550-020-1150-z
- Pineda, J. E., Zhao, B., Schmiedeke, A., Segura-Cox, D. M., Caselli, P., Myers, P. C., et al. (2019). The Specific Angular Momentum Radial Profile in Dense Cores: Improved Initial Conditions for Disk Formation. *ApJ* 882, 103. doi:10.3847/1538-4357/ab2cd1
- Plambeck, R. L. and Wright, M. C. H. (2016). ALMA Observations of Orion Source I at 350 and 660 GHz. *ApJ* 833, 219. doi:10.3847/1538-4357/833/2/219
- Planck Collaboration, Ade, P. A. R., Aghanim, N., Arnaud, M., Ashdown, M., Aumont, J., et al. (2011). Planck early results. XX. New light on anomalous microwave emission from spinning dust grains. *A&A* 536, A20. doi:10.1051/0004-6361/201116470
- Podio, L., Lefloch, B., Ceccarelli, C., Codella, C., and Bachiller, R. (2014). Molecular ions in the protostellar shock L1157-B1. *A&A* 565, A64. doi:10.1051/0004-6361/201322928
- Pratap, P., Dickens, J. E., Snell, R. L., Miralles, M. P., Bergin, E. A., Irvine, W. M., et al. (1997). A Study of the Physics and Chemistry of TMC-1. *ApJ* 486, 862–885. doi:10.1086/304553

- Price, D. J. and Bate, M. R. (2007). The impact of magnetic fields on single and binary star formation. *MNRAS* 377, 77–90. doi:10.1111/j.1365-2966.2007.11621.x
- Qiu, K., Zhang, Q., and Menten, K. M. (2011). Outflows, Accretion, and Clustered Protostellar Cores Around a Forming O Star. *ApJ* 728, 6. doi:10.1088/0004-637X/728/1/6
- Qiu, K., Zhang, Q., Menten, K. M., Liu, H. B., Tang, Y.-W., and Girart, J. M. (2014). Submillimeter Array Observations of Magnetic Fields in G240.31+0.07: An Hourglass in a Massive Cluster-forming Core. *ApJ Letters* 794, L18. doi:10.1088/2041-8205/794/1/L18
- Redaelli, E., Alves, F. O., Santos, F. P., and Caselli, P. (2019). Magnetic properties of the protostellar core IRAS 15398-3359. *A&A* 631, A154. doi:10.1051/0004-6361/201936271
- Reissl, S., Stutz, A. M., Klessen, R. S., Seifried, D., and Walch, S. (2021). Magnetic fields in star-forming systems - II: Examining dust polarization, the Zeeman effect, and the Faraday rotation measure as magnetic field tracers. *MNRAS* 500, 153–176. doi:10.1093/mnras/staa3148
- Reissl, S., Wolf, S., and Brauer, R. (2016). Radiative transfer with POLARIS. I. Analysis of magnetic fields through synthetic dust continuum polarization measurements. *A&A* 593, A87. doi:10.1051/0004-6361/201424930
- Rodón, J. A., Beuther, H., and Schilke, P. (2012). Fragmentation in the massive star-forming region IRAS 19410+2336. *A&A* 545, A51. doi:10.1051/0004-6361/200912994
- Russell, C. T. (1991). The magnetosphere. *Annual Review of Earth and Planetary Sciences* 19, 169–182. doi:10.1146/annurev.earth.19.050191.001125
- Sadaghiani, M., Sánchez-Monge, Á., Schilke, P., Liu, H. B., Clarke, S. D., Zhang, Q., et al. (2020). Physical properties of the star-forming clusters in NGC 6334. A study of the continuum dust emission with ALMA. *A&A* 635, A2. doi:10.1051/0004-6361/201935699
- Sadavoy, S. I., Stutz, A. M., Schnee, S., Mason, B. S., Di Francesco, J., and Friesen, R. K. (2016). Dust emissivity in the star-forming filament OMC 2/3. *A&A* 588, A30. doi:10.1051/0004-6361/201527364
- Sai, J., Ohashi, N., Maury, A. J., Maret, S., Yen, H.-W., Aso, Y., et al. (2022). Which Part of Dense Cores Feeds Material to Protostars? The Case of L1489 IRS. *ApJ* 925, 12. doi:10.3847/1538-4357/ac341d
- Sánchez-Monge, Á., Cesaroni, R., Beltrán, M. T., Kumar, M. S. N., Stanke, T., Zinnecker, H., et al. (2013). A candidate circumbinary Keplerian disk in G35.20-0.74 N: A study with ALMA. *A&A* 552, L10. doi:10.1051/0004-6361/201321134
- Sánchez-Monge, Á., Schilke, P., Schmiedeke, A., Ginsburg, A., Cesaroni, R., Lis, D. C., et al. (2017). The physical and chemical structure of Sagittarius B2. II. Continuum millimeter emission of Sgr B2(M) and Sgr B2(N) with ALMA. *A&A* 604, A6. doi:10.1051/0004-6361/201730426
- Sanhueza, P., Girart, J. M., Padovani, M., Galli, D., Hull, C. L. H., Zhang, Q., et al. (2021). Gravity-driven Magnetic Field at 1000 au Scales in High-mass Star Formation. *ApJ Letters* 915, L10. doi:10.3847/2041-8213/ac081c
- Santos, F. P., Busquet, G., Franco, G. A. P., Girart, J. M., and Zhang, Q. (2016). Magnetically Dominated Parallel Interstellar Filaments in the Infrared Dark Cloud G14.225-0.506. *ApJ* 832, 186. doi:10.3847/0004-637X/832/2/186
- Santos-Lima, R., de Gouveia Dal Pino, E. M., and Lazarian, A. (2012). The Role of Turbulent Magnetic Reconnection in the Formation of Rotationally Supported Protostellar Disks. *ApJ* 747, 21. doi:10.1088/0004-637X/747/1/21
- Santos-Lima, R., de Gouveia Dal Pino, E. M., and Lazarian, A. (2013). Disc formation in turbulent cloud cores: is magnetic flux loss necessary to stop the magnetic braking catastrophe or not? *MNRAS* 429, 3371–3378. doi:10.1093/mnras/sts597
- Santos-Lima, R., Guerrero, G., de Gouveia Dal Pino, E. M., and Lazarian, A. (2021). Diffusion of large-scale magnetic fields by reconnection

- in MHD turbulence. *MNRAS* 503, 1290–1309. doi:10.1093/mnras/stab470
- Schleuning, D. A. (1998). Far-Infrared and Submillimeter Polarization of OMC-1: Evidence for Magnetically Regulated Star Formation. *ApJ* 493, 811–825. doi:10.1086/305139
- Segura-Cox, D. M., Looney, L. W., Tobin, J. J., Li, Z.-Y., Harris, R. J., Sadavoy, S., et al. (2018). The VLA Nascent Disk and Multiplicity Survey of Perseus Protostars (VANDAM). V. 18 Candidate Disks around Class 0 and I Protostars in the Perseus Molecular Cloud. *ApJ* 866, 161. doi:10.3847/1538-4357/aaddf3
- Seifried, D., Banerjee, R., Pudritz, R. E., and Klessen, R. S. (2012). Disc formation in turbulent massive cores: circumventing the magnetic braking catastrophe. *MNRAS* 423, L40–L44. doi:10.1111/j.1745-3933.2012.01253.x
- Seo, Y. M., Majumdar, L., Goldsmith, P. F., Shirley, Y. L., Willacy, K., Ward-Thompson, D., et al. (2019). An Ammonia Spectral Map of the L1495-B218 Filaments in the Taurus Molecular Cloud. II. CCS and HC₇N Chemistry and Three Modes of Star Formation in the Filaments. *ApJ* 871, 134. doi:10.3847/1538-4357/aaf887
- Sheehan, P. D. and Eisner, J. A. (2017). Disk Masses for Embedded Class I Protostars in the Taurus Molecular Cloud. *ApJ* 851, 45. doi:10.3847/1538-4357/aa9990
- Sheehan, P. D., Tobin, J. J., Looney, L. W., and Megeath, S. T. (2022). The VLA/ALMA Nascent Disk and Multiplicity (VANDAM) Survey of Orion Protostars. VI. Insights from Radiative Transfer Modeling. *ApJ* 929, 76. doi:10.3847/1538-4357/ac574d
- Shinnaga, H. and Yamamoto, S. (2000). Zeeman Effect on the Rotational Levels of CCS and SO in the ³Σ⁻ Ground State. *ApJ* 544, 330–335. doi:10.1086/317212
- Shu, F. (1977). Self-similar collapse of isothermal spheres and star formation. *ApJ* 214, 488–497. doi:10.1086/155274
- Silsbee, K., Ivlev, A. V., Padovani, M., and Caselli, P. (2018). Magnetic Mirroring and Focusing of Cosmic Rays. *ApJ* 863, 188. doi:10.3847/1538-4357/aad3cf
- Silsbee, K., Ivlev, A. V., Sipilä, O., Caselli, P., and Zhao, B. (2020). Rapid elimination of small dust grains in molecular clouds. *A&A* 641, A39. doi:10.1051/0004-6361/202038063
- Skalidis, R. and Tassis, K. (2021). High-accuracy estimation of magnetic field strength in the interstellar medium from dust polarization. *A&A* 647, A186. doi:10.1051/0004-6361/202039779
- Stephens, I. W., Fernández-López, M., Li, Z.-Y., Looney, L. W., and Teague, R. (2020). Low-level Carbon Monoxide Line Polarization in Two Protoplanetary Disks: HD 142527 and IM Lup. *ApJ* 901, 71. doi:10.3847/1538-4357/abaef7
- Su, Y.-N., Liu, S.-Y., Li, Z.-Y., Lee, C.-F., Hirano, N., Takakuwa, S., et al. (2019). The Infall Motion in the Low-mass Protostellar Binary NGC 1333 IRAS 4A1/4A2. *ApJ* 885, 98. doi:10.3847/1538-4357/ab4818
- Tafalla, M., Santiago-García, J., Myers, P., Caselli, P., Walmsley, C., and Crapsi, A. (2006). On the internal structure of starless cores. II. A molecular survey of L1498 and L1517B. *A&A* 455, 577–593. doi:10.1051/0004-6361:20065311
- Takahashi, S., Machida, M. N., Tomisaka, K., Ho, P. T. P., Fomalont, E. B., Nakanishi, K., et al. (2019). ALMA High Angular Resolution Polarization Study: An Extremely Young Class 0 Source, OMC-3/MMS 6. *ApJ* 872, 70. doi:10.3847/1538-4357/aaf6ed
- Tanaka, K. E. I., Zhang, Y., Hirota, T., Sakai, N., Motogi, K., Tomida, K., et al. (2020). Salt, Hot Water, and Silicon Compounds Tracing Massive Twin Disks. *ApJ Letters* 900, L2. doi:10.3847/2041-8213/abadfc
- Tassis, K., Willacy, K., Yorke, H. W., and Turner, N. J. (2014). Effect of OH depletion on measurements of the mass-to-flux ratio in molecular cloud cores. *MNRAS* 445, L56–L59. doi:10.1093/mnras/slu130
- Tatematsu, K., Ohashi, S., Sanhueza, P., Nguyen Luong, Q., Umemoto, T., and Mizuno, N. (2016). Angular momentum of the N₂H⁺ cores in the

- Orion A cloud. *PASJ* 68, 24. doi:10.1093/pasj/psw002
- Tazaki, R., Lazarian, A., and Nomura, H. (2017). Radiative Grain Alignment In Protoplanetary Disks: Implications for Polarimetric Observations. *ApJ* 839, 56. doi:10.3847/1538-4357/839/1/56
- Teague, R., Hull, C. L. H., Guilloteau, S., Bergin, E. A., Dutrey, A., Henning, T., et al. (2021). Discovery of Molecular-line Polarization in the Disk of TW Hya. *ApJ* 922, 139. doi:10.3847/1538-4357/ac2503
- Terebey, S., Shu, F., and Cassen, P. (1984). The collapse of the cores of slowly rotating isothermal clouds. *ApJ* 286, 529–551. doi:10.1086/162628
- Tobin, J. J., Hartmann, L., Chiang, H.-F., Wilner, D. J., Looney, L. W., Loinard, L., et al. (2013). Modeling the Resolved Disk around the Class 0 Protostar L1527. *ApJ* 771, 48. doi:10.1088/0004-637X/771/1/48
- Tobin, J. J., Offner, S. S. R., Kratter, K. M., Megeath, S. T., Sheehan, P. D., Looney, L. W., et al. (2022). The VLA/ALMA Nascent Disk And Multiplicity (VANDAM) Survey of Orion Protostars. V. A Characterization of Protostellar Multiplicity. *ApJ* 925, 39. doi:10.3847/1538-4357/ac36d2
- Tobin, J. J., Sheehan, P. D., Megeath, S. T., Díaz-Rodríguez, A. K., Offner, S. S. R., Murillo, N. M., et al. (2020). The VLA/ALMA Nascent Disk and Multiplicity (VANDAM) Survey of Orion Protostars. II. A Statistical Characterization of Class 0 and Class I Protostellar Disks. *ApJ* 890, 130. doi:10.3847/1538-4357/ab6f64
- Tomida, K., Okuzumi, S., and Machida, M. N. (2015). Radiation Magnetohydrodynamic Simulations of Protostellar Collapse: Nonideal Magnetohydrodynamic Effects and Early Formation of Circumstellar Disks. *ApJ* 801, 117. doi:10.1088/0004-637X/801/2/117
- Tomida, K., Tomisaka, K., Matsumoto, T., Hori, Y., Okuzumi, S., Machida, M. N., et al. (2013). Radiation Magnetohydrodynamic Simulations of Protostellar Collapse: Protostellar Core Formation. *ApJ* 763, 6. doi:10.1088/0004-637X/763/1/6
- Tsukamoto, Y., Iwasaki, K., Okuzumi, S., Machida, M. N., and Inutsuka, S. (2015). Bimodality of Circumstellar Disk Evolution Induced by the Hall Current. *ApJ Letters* 810, L26. doi:10.1088/2041-8205/810/2/L26
- Tsukamoto, Y., Machida, M. N., and Inutsuka, S.-i. (2021). “Ashfall” Induced by Molecular Outflow in Protostar Evolution. *ApJ Letters* 920, L35. doi:10.3847/2041-8213/ac2b2f
- Tsukamoto, Y., Okuzumi, S., Iwasaki, K., Machida, M. N., and Inutsuka, S. (2018). Does Misalignment between Magnetic Field and Angular Momentum Enhance or Suppress Circumstellar Disk Formation? *ApJ* 868, 22. doi:10.3847/1538-4357/aae4dc
- Tsukamoto, Y., Okuzumi, S., Iwasaki, K., Machida, M. N., and Inutsuka, S.-i. (2017). The impact of the Hall effect during cloud core collapse: Implications for circumstellar disk evolution. *PASJ* 69, 95. doi:10.1093/pasj/psx113
- Turner, B. E. and Heiles, C. (2006). The C₄H Zeeman Effect in TMC-1: Understanding Low-Mass Star Formation. *ApJS* 162, 388–400. doi:10.1086/498431
- Tychoniec, Ł., Manara, C. F., Rosotti, G. P., van Dishoeck, E. F., Cridland, A. J., Hsieh, T.-H., et al. (2020). Dust masses of young disks: constraining the initial solid reservoir for planet formation. *A&A* 640, A19. doi:10.1051/0004-6361/202037851
- Uchida, K. I., Fiebig, D., and Güsten, R. (2001). Zeeman line splitting measurements sampling dense gas in dark cloud and star-forming cores. *A&A* 371, 274–286. doi:10.1051/0004-6361:20010329
- Valdivia, V., Maury, A., Brauer, R., Hennebelle, P., Galametz, M., Guillet, V., et al. (2019). Indirect evidence of significant grain growth in young protostellar envelopes from polarized dust emission. *MNRAS* 488, 4897–4904. doi:10.1093/mnras/stz2056
- Valdivia, V., Maury, A., and Hennebelle, P. (2022). Is the mm/sub-mm dust polarization

- a robust tracer of the magnetic field topology in protostellar envelopes? A model exploration. [arXiv e-prints](#), arXiv:2203.14505
- Van De Putte, D., Gordon, K. D., Roman-Duval, J., Williams, B. F., Baes, M., Tchernyshyov, K., et al. (2020). Evidence of Dust Grain Evolution from Extinction Mapping in the IC 63 Photodissociation Region. *ApJ* 888, 22. doi:10.3847/1538-4357/ab557f
- van 't Hoff, M. L. R., Leemker, M., Tobin, J. J., Harsono, D., Jørgensen, J. K., and Bergin, E. A. (2022). The young embedded disk L1527 IRS: constraints on the water snowline and cosmic ray ionization rate from HCO⁺ observations. [arXiv e-prints](#), arXiv:2204.08622
- van't Hoff, M. L. R., Harsono, D., Tobin, J. J., Bosman, A. D., van Dishoeck, E. F., Jørgensen, J. K., et al. (2020). Temperature Structures of Embedded Disks: Young Disks in Taurus Are Warm. *ApJ* 901, 166. doi:10.3847/1538-4357/abb1a2
- Verlat, A., Hennebelle, P., Maury, A. J., and Gaudel, M. (2020). Protostellar disk formation by a nonrotating, nonaxisymmetric collapsing cloud: model and comparison with observations. *A&A* 635, A130. doi:10.1051/0004-6361/201936394
- Vlemmings, W. H. T., Lankhaar, B., Cazzoletti, P., Ceccobello, C., Dall'Olio, D., van Dishoeck, E. F., et al. (2019). Stringent limits on the magnetic field strength in the disc of TW Hya. ALMA observations of CN polarisation. *A&A* 624, L7. doi:10.1051/0004-6361/201935459
- Wielebinski, R. (2005). Magnetic Fields in the Milky Way, Derived from Radio Continuum Observations and Faraday Rotation Studies. In *Cosmic Magnetic Fields*, eds. R. Wielebinski and R. Beck. vol. 664 of *Lecture Notes in Physics*, Berlin Springer Verlag, 89. doi:10.1007/11369875_5
- Williams, G. M., Cyganowski, C. J., Brogan, C. L., Hunter, T. R., Ilee, J. D., Nazari, P., et al. (2022). ALMA observations of the Extended Green Object G19.01-0.03 - I. A Keplerian disc in a massive protostellar system. *MNRAS* 509, 748–762. doi:10.1093/mnras/stab2973
- Williams, J. P., Cieza, L., Hales, A., Ansdell, M., Ruiz-Rodriguez, D., Casassus, S., et al. (2019). The Ophiuchus DISK Survey Employing ALMA (ODISEA): Disk Dust Mass Distributions across Protostellar Evolutionary Classes. *ApJ Letters* 875, L9. doi:10.3847/2041-8213/ab1338
- Wong, Y. H. V., Hirashita, H., and Li, Z.-Y. (2016). Millimeter-sized grains in the protostellar envelopes: Where do they come from? *PASJ* 68, 67. doi:10.1093/pasj/psw066
- Wright, M., Bally, J., Hirota, T., Miller, K., Harding, T., Colletuori, K., et al. (2022). Structure of the Source I Disk in Orion-KL. *ApJ* 924, 107. doi:10.3847/1538-4357/ac391b
- Wurster, J. (2016). NICIL: A Stand Alone Library to Self-Consistently Calculate Non-Ideal Magnetohydrodynamic Coefficients in Molecular Cloud Cores. *PASA* 33, e041. doi:10.1017/pasa.2016.34
- Wurster, J. and Bate, M. R. (2019). Disc formation and fragmentation using radiative non-ideal magnetohydrodynamics. *MNRAS* 486, 2587–2603. doi:10.1093/mnras/stz1023
- Wurster, J., Bate, M. R., and Price, D. J. (2018). The effect of extreme ionization rates during the initial collapse of a molecular cloud core. *MNRAS* 476, 2063–2074. doi:10.1093/mnras/sty392
- Wurster, J. and Lewis, B. T. (2020). Non-ideal magnetohydrodynamics versus turbulence - I. Which is the dominant process in protostellar disc formation? *MNRAS* 495, 3795–3806. doi:10.1093/mnras/staa1339
- Wurster, J., Price, D. J., and Bate, M. R. (2017). The impact of non-ideal magnetohydrodynamics on binary star formation. *MNRAS* 466, 1788–1804. doi:10.1093/mnras/stw3181
- Wyrowski, F., Güsten, R., Menten, K. M., Wiesemeyer, H., and Klein, B. (2012). Terahertz ammonia absorption as a probe of infall in high-mass star forming clumps. *A&A* 542, L15. doi:10.1051/0004-6361/201218927
- Xu, W. and Kunz, M. W. (2021). Formation and evolution of protostellar accretion discs - I.

- Angular-momentum budget, gravitational self-regulation, and numerical convergence. *MNRAS* 502, 4911–4929. doi:10.1093/mnras/stab314
- Yang, H., Li, Z.-Y., Looney, L. W., Girart, J. M., and Stephens, I. W. (2017). Scattering-produced (sub)millimetre polarization in inclined discs: optical depth effects, near-far side asymmetry and dust settling. *MNRAS* 472, 373–388. doi:10.1093/mnras/stx1951
- Yang, Y., Jiang, Z., Chen, Z., Ao, Y., and Yu, S. (2021). In Search of Infall Motion in Molecular Clumps. III. HCO⁺ (1-0) and H₁₃CO⁺ (1-0) Mapping Observations toward Confirmed Infall Sources. *ApJ* 922, 144. doi:10.3847/1538-4357/ac22ab
- Yen, H.-W., Gu, P.-G., Hirano, N., Koch, P. M., Lee, C.-F., Liu, H. B., et al. (2019). HL Tau Disk in HCO⁺ (3-2) and (1-0) with ALMA: Gas Density, Temperature, Gap, and One-arm Spiral. *ApJ* 880, 69. doi:10.3847/1538-4357/ab29f8
- Yen, H.-W., Koch, P. M., Hull, C. L. H., Ward-Thompson, D., Bastien, P., Hasegawa, T., et al. (2021a). The JCMT BISTRO Survey: Alignment between Outflows and Magnetic Fields in Dense Cores/Clumps. *ApJ* 907, 33. doi:10.3847/1538-4357/abca99
- Yen, H.-W., Koch, P. M., Takakuwa, S., Ho, P. T. P., Ohashi, N., and Tang, Y.-W. (2015a). Observations of Infalling and Rotational Motions on a 1000 AU Scale around 17 Class 0 and 0/I Protostars: Hints of Disk Growth and Magnetic Braking? *ApJ* 799, 193. doi:10.1088/0004-637X/799/2/193
- Yen, H.-W., Koch, P. M., Takakuwa, S., Krasnopolsky, R., Ohashi, N., and Aso, Y. (2017). Signs of Early-stage Disk Growth Revealed with ALMA. *ApJ* 834, 178. doi:10.3847/1538-4357/834/2/178
- Yen, H.-W., Takakuwa, S., Koch, P. M., Aso, Y., Koyamatsu, S., Krasnopolsky, R., et al. (2015b). No Keplerian Disk \lesssim 10 AU Around the Protostar B335: Magnetic Braking or Young Age? *ApJ* 812, 129. doi:10.1088/0004-637X/812/2/129
- Yen, H.-W., Takakuwa, S., Ohashi, N., Aikawa, Y., Aso, Y., Koyamatsu, S., et al. (2014). ALMA Observations of Infalling Flows toward the Keplerian Disk around the Class I Protostar L1489 IRS. *ApJ* 793, 1. doi:10.1088/0004-637X/793/1/1
- Yen, H.-W., Zhao, B., Koch, P. M., and Gupta, A. (2021b). No Impact of Core-scale Magnetic Field, Turbulence, or Velocity Gradient on Sizes of Protostellar Disks in Orion A. *ApJ* 916, 97. doi:10.3847/1538-4357/ac0723
- Yen, H.-W., Zhao, B., Koch, P. M., Krasnopolsky, R., Li, Z.-Y., Ohashi, N., et al. (2018). Constraint on ion-neutral drift velocity in the Class 0 protostar B335 from ALMA observations. *A&A* 615, A58. doi:10.1051/0004-6361/201732195
- Ysard, N., Koehler, M., Jimenez-Serra, I., Jones, A. P., and Verstraete, L. (2019). From grains to pebbles: the influence of size distribution and chemical composition on dust emission properties. *A&A* 631, A88. doi:10.1051/0004-6361/201936089
- Zamponi, J., Maureira, M. J., Zhao, B., Liu, H. B., Ilee, J. D., Forgan, D., et al. (2021). The young protostellar disc in IRAS 16293-2422 B is hot and shows signatures of gravitational instability. *MNRAS* 508, 2583–2599. doi:10.1093/mnras/stab2657
- Zelko, I. A. and Finkbeiner, D. P. (2020). Implications of Grain Size Distribution and Composition for the Correlation between Dust Extinction and Emissivity. *ApJ* 904, 38. doi:10.3847/1538-4357/abbb8d
- Zhang, C.-P., Launhardt, R., Liu, Y., Tobin, J. J., and Henning, T. (2021). Pebbles in an embedded protostellar disk: the case of CB 26. *A&A* 646, A18. doi:10.1051/0004-6361/202039536
- Zhang, Q., Qiu, K., Girart, J. M., Liu, H. B., Tang, Y.-W., Koch, P. M., et al. (2014). Magnetic Fields and Massive Star Formation. *ApJ* 792, 116. doi:10.1088/0004-637X/792/2/116
- Zhao, B., Caselli, P., Li, Z.-Y., Krasnopolsky, R., Shang, H., and Lam, K. H. (2020). Hall effect in protostellar disc formation and evolution. *MNRAS* 492, 3375–3395. doi:10.1093/mnras/staa041

- Zhao, B., Caselli, P., Li, Z.-Y., Krasnopolsky, R., Shang, H., and Lam, K. H. (2021). The interplay between ambipolar diffusion and Hall effect on magnetic field decoupling and protostellar disc formation. *MNRAS* 505, 5142–5163. doi:10.1093/mnras/stab1295
- Zhao, B., Caselli, P., Li, Z.-Y., Krasnopolsky, R., Shang, H., and Nakamura, F. (2016). Protostellar disc formation enabled by removal of small dust grains. *MNRAS* 460, 2050–2076. doi:10.1093/mnras/stw1124
- Zinchenko, I., Caselli, P., and Pirogov, L. (2009). Chemical differentiation in regions of high-mass star formation - II. Molecular multiline and dust continuum studies of selected objects. *MNRAS* 395, 2234–2247. doi:10.1111/j.1365-2966.2009.14687.x